2012

Constitutive modeling of dense granular flow based on discrete element method simulations

Vidyapati Vidyapati
Iowa State University

Constitutive modeling of dense granular flow based on discrete element method simulations

by

Vidyapati

A dissertation submitted to the graduate faculty

in partial fulfillment of the requirements for the degree of

DOCTOR OF PHILOSOPHY

Major: Mechanical Engineering

Program of Study Committee:

Shankar Subramaniam, Major Professor

Rodney O. Fox

Pranav Shrotriya

Monica H. Lamm

Xinwei Wang

Iowa State University

Ames, Iowa

2012

DEDICATION

I would like to dedicate this dissertation to my parents for their support, encouragement and never ending love.

TABLE OF CONTENTS

LIST OF TABLES

LIST OF FIGURES

ACKNOWLEDGEMENTS

It gives me immense pleasure to express my sincere thanks and deep appreciations to those who have helped me with various aspects of conducting this research and supported me through this journey in graduate school. With sincerest gratitude, I would like to thank my major professor Dr. Shankar Subramaniam for his constant guidance, encouragement, patience and support throughout this research and writing of this dissertation. I could not have finished this task without his help. He has been very responsive and was always willing to work with me whenever I got stuck. His depth of technical knowledge and enlightened views on the whole research process has left deep impression for my lifetime. His sincere advice and support has been invaluable on both academic and personal fronts.

Thanks to all the committee members: Dr. Rodney Fox, Dr. Pranav Shrotriya, Dr. Xinwei Wang and Dr. Monica Lamm for their valuable comments on this dissertation, which helped me improve it. This work would not have been possible without their feedback and constructive comments. In addition, many thanks to all the Iowa State University teachers who have taught me invaluable skills while my stay here at Iowa State. I would also like to thank Dr. Sankaran Sundaresan at Princeton University for reading and giving thoughtful comments on many of my research articles.

Even though I have been away from my family, I never felt that during my stay here ISU. Many thanks goes to all my fellow lab mates: Sudheer Tenneti, Ravi Kolakaluri, Bo Sun, Mohammad Mehrabadi and Eric Murphy. I would also like to thanks Dr. Madhusudan Pai, Dr. Rahul Garg, Dr. Ying Xu and Dr. Sergiy Markutsya for answering

my naive questions during my initial days in the lab. A special thank goes to Dr. Jin Sun with whom I have worked very closely during my initial PhD days. He taught and helped me setting up many simulations and problems using LAMMPS code. At Iowa State I have been fortunate enough to have many good friends with whom I enjoyed both technical and personal interactions; thanks to Hari Krishna Kodali, Varun Vikas, Sunil Kumar Arolla, Kaustubh Kaluskar, Praveen Kumar and Karthik Devendran.

I would also like to acknowledge the financial support from the US Department of Energy, National Energy Technology Laboratory (Grant Number: DE–FG26–07NT43070), administered under advanced coal research at US colleges and universities. I also acknowledge partial financial support from department of Mechanical Engineering at Iowa State University and giving me an opportunity to work as a teaching assistant for undergraduate fluid mechanics course.

Last but not the least, words cannot describe the love, support, and encouragement I have received from my family during my graduate studies at Iowa State University.

ABSTRACT

The vision of this research study is to exploit physical insights obtained through microscale simulations to develop better and accurate macroscale constitutive models in different regimes of granular flow. Development of these constitutive models at macroscale that incorporates microscale particle interactions, need tools such as, DEM (discrete element method) simulations, to probe microscale behavior. These DEM simulations are helpful in understanding the granular physics and mesoscale descriptors that link microscale particle interaction to macroscopic constitutive behavior.

In order to attain the primary goal of development of constitutive models, DEM simulations are validated with the experiments in a Couette shear device. It is found that DEM simulations are capable of capturing the regime transition from quasi–static to the intermediate behavior as observed in the experiments. Influence of microscale parameters on granular rheology is demonstrated using comprehensive regime map established using DEM data. Existence of a third stable granular phase is discovered that is neither completely solid–like nor completely fluid–like. A new modified form of the free energy density function is proposed to capture this third stable granular phase observed in the DEM simulations. Further, a constitutive model based on the order parameter (OP) framework is refined, and a linear model with new model coefficient extracted from data of 3D DEM simulations of homogeneously sheared granular flows is proposed, which is denoted as refined order parameter (ROP) model. Performance of this ROP model along with other existing constitutive models is assessed in the different regimes of granular flow. It is found that the intermediate regime poses significant challenge

to predictive capability of the constitutive models. In order to capture this complex rheological behavior of the intermediate regime a constitutive model based on mesoscale descriptors (such as the coordination number and the fabric tensor) that links microscale particle interactions to the macroscale behavior is developed. It is shown that the proposed contact stress model is capable of capturing the correct scaling of the stress with the shear rate even in the intermediate and dense regime of granular flow.

CHAPTER 1. INTRODUCTION

1.1 Background

Granular flows are fundamental particle systems found in solid processing and Nature. For example, solid processing is a multi-billion dollar industry that remains a critical part of the pharmaceutical (e.g., capsule, tablet solids), agriculture (e.g., fruit, soil), consumer product (e.g., cereal, detergent, can goods), and bioenergy (e.g., biomass, biofuels) industries. Understanding the behavior of granular matter is a topic of active research that continues to yield exciting and often surprising results. Granular flow is important in many applications such as silos, pebble–bed nuclear reactors (Rycroft et al., 2006), and clean coal technology devices (Syamlal et al., 2009). Rheology of granular flows remains difficult to predict in both Nature and technological application (Fenistein and Hecke, 2003). This is due to the fact that granular media are highly complex materials that typically exhibit nonlinear constitutive behavior under shear (Campbell, 2002), with different regimes that depend on microscale properties (e.g., particle friction and coefficient of restitution) as well as macroscale properties (e.g., solid volume fraction and the shear rate).

The current research is focused on incorporating microscale particle interactions into a constitutive modeling framework at the macroscale, using mesoscale descriptors that link microscale interactions to macroscopic constitutive behavior, as shown in Fig. 1.1. Further, these microscale particle interactions are correlated with the constitutive behavior of granular flows in different regimes. These different regimes are classified based

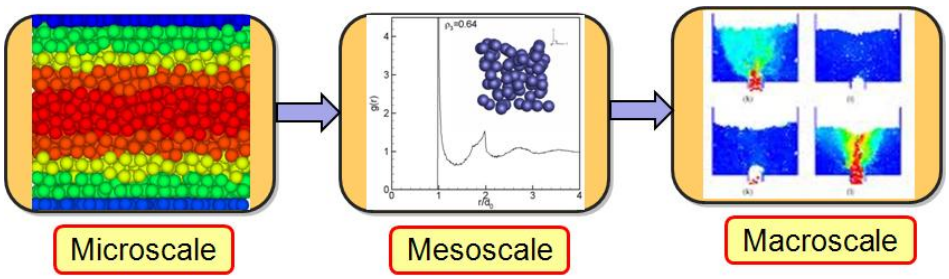

Figure 1.1 Connection between microscale particle interactions and macroscale constitutive behavior.

on the scaling of shear stress σ with the strain rate $\dot{\gamma}$ as described below:

1. Inertial regime: Characteristic scale of stress increases as square of the strain rate ($\sigma \propto \dot{\gamma}^2$) (Bagnold, 1954).

2. Intermediate regime: Stress is related to the strain rate in the form of a power law ($\sigma \propto \dot{\gamma}^n$), where n takes values between 0 to 2 based on particle (friction coefficient) and flow (shear rate) properties (Tardos et al., 2003).

3. Quasi–static regime: Stress remains independent of the strain rate ($\sigma \neq f(\dot{\gamma})$) (Campbell, 2002).

Figure 1.2 shows the regime map for granular flows with their corresponding constitutive behavior in each regime (inertial, intermediate and quasi–static). As seen in Fig. 1.2, the kinetic theory for rapid granular flow (inertial regime) (Goldhirsch, 2003) predicts a constitutive behavior in which stress scales as square of the strain rate. In the other extreme regime, plasticity models applied to soil mechanics for slow quasi–static flow (Nedderman, 1992; Schaeffer, 1987) result in a stress that is independent of the applied shear rate. However, experiments performed by Tardos et al. (2003) reveal the existence of a third intermediate (transitional) regime that is characterized by $\sigma \propto \dot{\gamma}^n$, where $0 < n < 2$. These experiments also indicate that the intermediate regime is

broad enough in the parameter space of solid volume fraction and shear rate to require a continuum model to capture its constitutive behavior. The continuum description of granular flows is obtained by a statistical averaging procedure that results in averaged conservation equations for mass, momentum and energy. The granular stress tensor that appears in the solid phase mean momentum equation is closed using a constitutive model, that relates average stress to average strain rate.

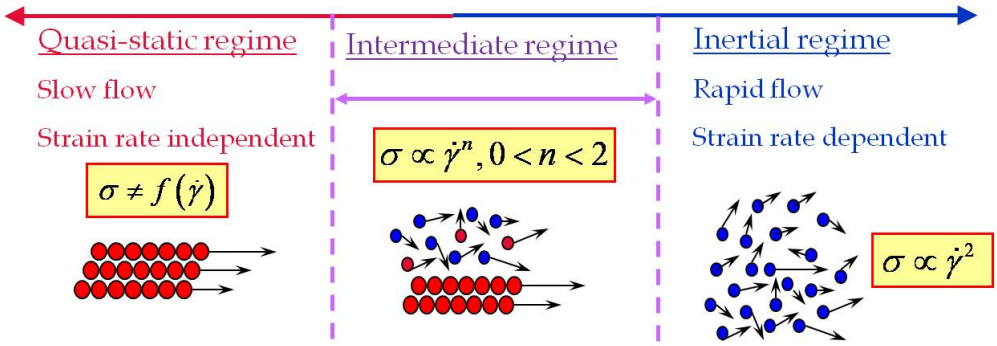

Figure 1.2 Regime map for granular flows and their corresponding constitutive behavior.

From an engineering perspective, one of the most interesting phenomena in granular flow is the regime transition from the quasi–static to inertial (rapid flow) regime. This phenomenon of regime transition has been observed in many industrial and practical applications such as discharge of granular particles from silos or hoppers. It also affects the discharge rate from these devices (Vidyapati and Subramaniam, 2012b). However, the mechanisms of regime transition have not been fully understood in spite of many studies in both engineering and physics communities. Regime transition is governed by a combination of mechanisms, which themselves depend on particle and flow properties. For example, particle properties that influence the regime transition in granular flows are: particle–particle friction coefficient, particle inelasticity, and shape of the particle. The flow property that influences the regime transition is shear rate. In the quasi–static

regime, slowly sheared granular assemblies with enduring frictional contacts between the grains behave like a solid, exhibiting constitutive behavior analogous to plasticity. However, granular material can also behave like a liquid when poured from a hopper or silo, or like a gas when rapidly sheared with the grains experiencing binary, instantaneous collisions at sufficiently low solid volume fraction (Jaeger et al., 1996).

The importance of understanding regime transition in granular flows, and modeling it accurately, motivates the current research to characterize the constitutive behavior of granular flow in different regimes. However, the focus here is on dense granular flows, because many common materials such as sand, require large shear rates to reach the rapid flow regime that is unattainable for all practical purposes; such material will demonstrate either slow flow or a quasi–static regime behavior depending upon the solid volume fraction and particle friction coefficient. The continuum models can be then used in Computational Fluid Dynamics (CFD) tools to better capture the regime transition, and to assist in design and optimization of processes involving granular flows in the intermediate regime.

1.2 Research objectives and approaches

This study addresses the following questions:

1. How to incorporate the nature of grain contacts (enduring or instantaneous) into a constitutive modeling framework at macroscale?

2. How successful are these constitutive models in predicting constitutive behavior in different regimes of granular flow?

3. How successful will these models be in addressing practical engineering problems, such as discharge from silo, where all three different regimes (inertial, intermediate and quasi–static) of granular flow co–exist?

4. Are DEM (discrete element method) simulations capable of capturing the regime transition in granular rheology that is observed in experiments?

In order to attain the aforementioned objectives, at the microscale level discrete element method (DEM) is employed to simulate dry granular flows. DEM simulates individual particle dynamics and computes the contact forces between particles based on a contact mechanics model. The microscale information obtained from DEM simulations will give physical insights into collective particle behaviors, such as flow and microstructure formation, and will guide the continuum model development. These microscale simulations can further be used to develop closure models for the granular stress in a given constitutive model. The data obtained from these microscale simulations can also be used to validate constitutive models. Whereas, at the other end, reliable and accurate continuum model plays an important role in predicting granular rheology at larger or industrial scale (Sundaresan, 2001). The main goal of this research is to investigate the solid particle behavior from the microscale and incorporate more relevant modeling information into a constitutive model at the macroscale.

1.3 Original contribution of this dissertation

The original and significant contributions of this research work are summarized in the following.

1.3.1 Granular flow physics from DEM simulations

1. Established a comprehensive regime map (including the intermediate regime) based on the scaling of shear stress σ with the strain rate $\dot{\gamma}$. This regime map is built using DEM data of homogeneously sheared granular assembly for wide range of solid volume fractions, particle friction coefficients and shear rates.

2. Discovered existence of a third stable granular phase, that is neither completely fluid–like nor completely solid–like. Proposed a modified form of the free energy density function to capture this third stable granular phase.

1.3.2 Development of constitutive models

1. A constitutive model is developed based on the original order parameter (OP) concept proposed by Volfson et al. (2003a). Performance of this refined order parameter (ROP) model is assessed in different regimes and results are explained by analyzing granular stress data from DEM simulations.

2. A constitutive model based on mesoscale descriptors (the coordination number, the fabric tensor and the pair correlation function) is developed from first principles to capture the complex rheology of granular flow in the intermediate and dense regimes. The predictive capability of the proposed contact stress model is verified for homogeneous shear flow using DEM data.

1.3.3 Validation of DEM with experiments

1. Established a computational method to simulate Couette shear cell device using DEM (discrete element method). Verified the hypothesis of regime transition from quasi–static to intermediate behavior in the presence of a secondary vertical flow as observed in experiments (Kheiripour Langroudi et al., 2010b).

1.3.4 Device–scale simulations

1. Established accuracy of different continuum models for a silo discharge problem using DEM simulations. It is shown that all three different regimes (inertial, intermediate and the quasi–static) co–exist in the silo discharge problem.

1.4 Outline of dissertation

Chapter 2 provides some background information on rheology of granular flows along with a brief review of macroscopic constitutive modeling.

Chapter 3 describes the contact model used in DEM (discrete element method) simulations and role of microscale modeling of granular flows is discussed.

Chapter 4 presents a comparison between DEM and experimental study of dense granular flow in a Couette shear cell device. It will be shown that DEM is a useful tool to qualitative predict the regime transition in the granular flows (transition from the quasi–static to intermediate behavior when secondary vertical flow is induced). However, there are quantitative differences in the predictions.

In chapter 5, DEM simulations are used to characterize granular rheology and granular phase transition by studying the order parameter (OP) dynamics. Existence of a new third stable granular 'phase' is observed and a modified form of the free energy density function is proposed to capture this third stable granular 'phase'. Further, a linear OP based continuum model is proposed and assessed in different regimes of granular flows.

In chapter 6, discharge dynamics of granular particles from a flat–bottomed silo is studied using both continuum modeling and DEM simulations. A quantitative comparison between results of continuum and DEM simulations is performed by comparing discharge rates, solid velocities and solid stresses for a three–dimensional (3D) flat–bottomed silo.

Chapter 7 presents a constitutive model developed from first principle to capture the complex rheology of granular flows in the intermediate and dense regime. In this proposed model, the contact stress is linked to the mesoscale descriptors such as the coordination number, the fabric tensor and the pair correlation function. Further model predictive capabilities is assessed in the intermediate and dense regime of granular flows with DEM data.

Chapter 8 summaries the main conclusions from the research work in this dissertation. Possible extension to this research work are discussed from the microscale and macroscale modeling prospective.

CHAPTER 2. RHEOLOGY OF GRANULAR FLOWS

This chapter presents a brief review of existing theories and constitutive models for predicting the rheology of granular flow in different regimes.

2.1 Classification of granular rheology in different regimes

Granular rheology in different regimes is classified as follows:

1. Inertial regime: Stress follows Bagnold's scaling ($\sigma \propto \dot{\gamma}^2$) with the strain rate. Constitutive models based on kinetic theory for rapid granular flow (Lun et al., 1984; Jenkins and Savage, 1983; Goldhirsch, 2003) have been reasonably successful in describing the granular rheology of inertial regime. In this regime stress is dominated by binary or instantaneous collisions.

2. Intermediate regime: Stress shows a power law behavior ($\sigma \propto \dot{\gamma}^n$, $0 < n < 2$) with the strain rate. The intermediate regime still lacks a predictive constitutive model (Jop et al., 2006; G.D.R. MiDi, 2004; Vidyapati et al., 2012; Vidyapati and Subramaniam, 2012a). In this regime both collisional and frictional interactions between particles are important in capturing the correct granular rheology.

3. Quasi–static regime: Stress remains independent of the strain rate ($\sigma \neq f(\dot{\gamma})$). Models based on plasticity theory and soil mechanics (Nedderman, 1992; Schaeffer, 1987) are used to capture this rate independent behavior of stress. In this regime

external force is supported by force chains within the granular material (Jaeger et al., 1996).

A quantitative description of the macroscale behavior of granular flow in industrial devices require a reliable constitutive model for the stress tensor in different regimes (Sundaresan, 2001). However, even a seemingly simple practical device for the storage and discharge of granular material such as a flat–bottomed silo poses a surprisingly difficult challenge for continuum models (Srivastava and Sundaresan, 2003; Benyahia, 2008). Figure 2.1(b) shows that the discharge rate predicted from continuum simulations deviates considerably (more than 80%) from the Beverloo correlation (Beverloo et al., 1961) and DEM data. The discharge rate from a silo is controlled by the complex rheology of granular flow due to co–existence of different flow regimes (Vidyapati and Subramaniam, 2012b). This complex behavior makes it very difficult to formulate a comprehensive macroscale theory for granular stress tensor, which can describe all the flow regimes.

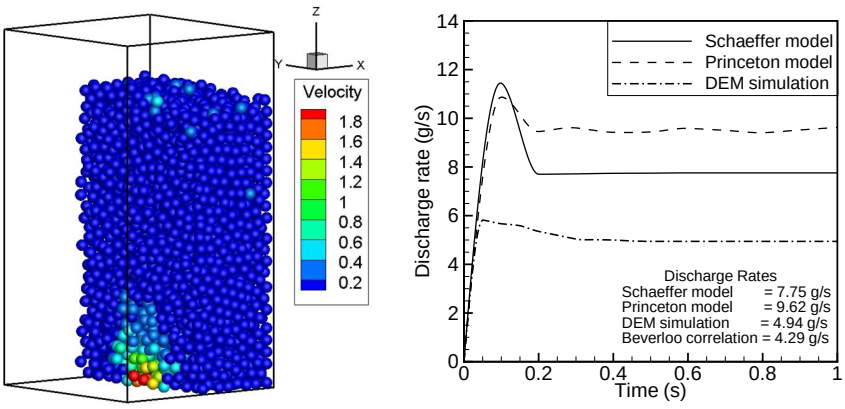

(a) (b)

Figure 2.1 (a) DEM simulation of granular discharge from a flat–bottomed silo with a circular orifice ($d_{orifice}/d_p = 6$), and (b) Dependence of discharge rate of granular material from a flat–bottomed silo on the constitutive model for the solid–phase stress tensor.

The stress tensor in the granular material is a function of both particle and flow level properties which corresponds to different scales of the problem, e.g., macroscale,

mesoscale and microscale. Hence, the granular stress tensor can be represented as,

$$\sigma_{ij} = f(\text{macroscale parameters}, \text{mesoscale parameters}, \text{microscale parameters}). \quad (2.1)$$

Parameters like solid volume fraction and shear rate belong to macroscale in Eq. 2.1. Similarly, interparticle friction coefficient and coefficient of restitution belongs to microscale parameters. The mesoscale parameters can be described by quantities such as the order parameter (OP), the pair correlation function, the fabric tensor and the coordination number. The functional form of the stress tensor in Eq. 2.1, can be further probed using the following approaches:

1. Classical continuum theories.
2. Statistical mechanics (e.g., kinetic theory for granular flows).
3. Micromechanical approach.
4. Phenomenological models based on experiments or computer simulations.

2.2 Review of constitutive modeling of granular flows

Most of the constitutive models (Johnson and Jackson, 1987; Srivastava and Sundaresan, 2003) used to predict the behavior of granular flows are based on an additive decomposition of the total granular stress as a weighted sum of kinetic and frictional contributions ($\sigma_{ij} = \sigma^k_{ij} + \sigma^f_{ij}$), with the weight factor specified solely as a function of the solid volume fraction. Existing models for the particle pressure at the packing limit are inadequate, although a recently proposed model (Sun and Sundaresan, 2011) for granular stress in the quasi–static regime that is based on the evolution of the fabric tensor promises to remedy this deficiency. Both experiments in a 2D granular shear cell (GSC) (McCarthy et al., 2010; Jasti and Higgs, 2008) and DEM simulations (Volfson et al., 2003b) reveal that grain contact in the intermediate regime are in a "phase

transition" characterized by a mix of enduring solidlike contacts and transient fluidlike contacts. While most constitutive models in use are phenomenological, this observation motivates the development of a constitutive model for the intermediate regime based on microscale physical interactions between the grains. In particular, these grains interactions are not determined by the solid volume fraction alone, but are dependent on particle properties (such as particle friction coefficient, inelasticity) and the local shear rate. Consequently, the simple additive models are not capable of capturing this complex constitutive behavior, these models also assume that the stress and strain rate are coaxial (Savage, 1998), but this assumption is not verified in the intermediate regime.

Savage (1998) proposed a continuum theory based on associated flow rule that relates the strain rate and the shear stress in plastic frictional systems. Averaging strain rate fluctuations yields a Bingham–like constitutive relation, in which the shear stress and strain rate tensors are always coaxial. Furthermore, it also postulates that the viscosity diverges as the density approaches the close–packing limit. The problem of slow granular flow in rough–walled vertical chute was studied by this model. A concentration boundary layer being thicker than the velocity boundary layer was obtained, which was consistent with the experimental observations.

Aranson and co–workers (Aranson and Tsimring, 2002; Volfson et al., 2003a,b) proposed an alternative additive model that attempts to characterize the granular "phase transition" in the intermediate regime using an approach analogous to the Landau theory of phase transitions (Landau and Lifshitz, 1980) by introducing a scalar order parameter, that is used to determine, the relative contribution of kinetic and frictional stresses. The order parameter (OP) is defined as the ratio of space–times averaged number of "solid" contacts to all contacts within a sampling volume,

$$\rho = \frac{\overline{\langle Z_s \rangle}}{\overline{\langle Z \rangle}}. \tag{2.2}$$

The stress was decomposed into a "fluid" and "static" part,

$$\sigma_{ij} = \sigma_{ij}^{f} + \sigma_{ij}^{s}. \tag{2.3}$$

The value of the order parameter specifies the ratio between the static and fluid part of the stress tensor. The order parameter was assumed to obey dissipative dynamics governed by a free energy functional with two local minima. This description was based on the separation of static and fluid components of the shear stress and assumed Newtonian friction law for the fluid components. The viscosity coefficient is expected to remain finite at the fluidization threshold. This model yields a good qualitative description of many phenomena occurring in granular flows. However, the model is limited to two dimensions and the correlation of the order parameter with the model coefficients was fitted from only 2D molecular simulations. The stress tensor in this model was correctly generalized to an objective form that is independent of the coordinate system by Gao et al. (2005). This objective representation correctly models the isotropic and anisotropic parts of the stress tensor. This general objective form of the model also relaxes the assumption in the original model that the principal axes of the granular stress tensor be coaxial with that of the fluid stress tensor.

In summary, existing constitutive models for granular flow should take into account different parameters at different scales, e.g., macroscale, mesoscale and microscale. However, it is found that most of the constitutive models for granular flow take into account the parameters which belongs to, two extreme scales (macroscale and microscale) of the problem. Nevertheless very few model (such as OP model proposed by Volfson et al. (2003b)) take into account the intermediate scale (mesoscale) of the problem in the framework of a constitutive model. This review also guides the research to determine the capabilities and limitations of the state–of–art models and to contribute to the new understanding and development of constitutive models.

CHAPTER 3. MIRCOSCALE MODELING OF GRANULAR FLOWS

An alternative approach to macroscopic constitutive modeling is the microscale model of granular flow that treats the granular material as a collection of discrete particles and resolves particle interactions at the scale of individual particles. This chapter presents a background information on microscale DEM (discrete element method) simulations of granular flow. These microscale DEM simulations are a tool to probe microscale physics and give insights about mesoscale descriptors which are useful in connecting microscale behavior to constitutive models at macroscale. The microscale simulations also serve to validate the continuum models by testing the validation of their underlying assumptions and range of their applications in terms of all the simulation parameters (e.g., particle volume fractions, interparticle friction coefficients, shear rates etc.). The following section describes the contact model used in these microscale DEM simulations.

3.1 Description of contact model in DEM

A contact mechanics model is used in the DEM algorithm to capture multiparticle contacts. The idea of DEM is to numerically integrate the equations of motion for all the particles in the system (Allen and Tildesley, 1989). Soft sphere DEM for granular flows is to supply contact force models for solid particles. Pioneering work in this field was done by Cundall and Strack (1979). Since the realistic modeling of the deformations of the particles is such too complicated, a simplified contact force and the overlap

relation (Silbert et al., 2001), the so called spring–dashpot model, is used in this work which is shown in Fig. 3.1. The basic principles of the spring–dashpot model are briefly described in the following.

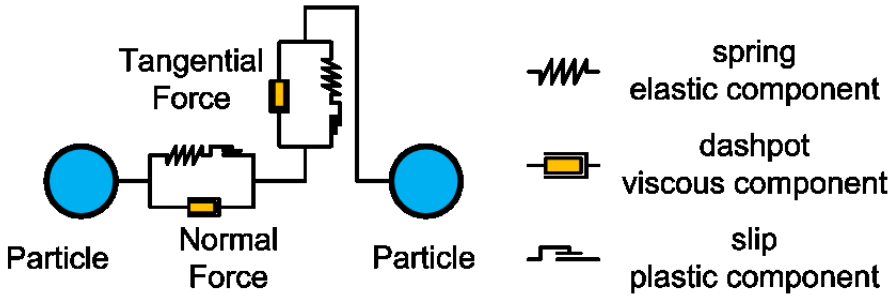

Figure 3.1 Standard contact law in DEM.

For two contacting particle $\{i,j\}$, with radii $\{a_i,a_j\}$ at positions $\{\mathbf{r}_i,\mathbf{r}_j\}$, with velocities $\{\mathbf{v}_i,\mathbf{v}_j\}$ and angular velocities $\{\boldsymbol{\omega}_i,\ \boldsymbol{\omega}_j\}$ (see Fig. 3.2), the normal compression δ_{ij}, relative normal velocity $\mathbf{v}_{n_{ij}}$, and relative tangential velocity $\mathbf{v}_{t_{ij}}$ are (Silbert et al., 2001):

$$\delta_{ij} = d_0 - r_{ij}, \tag{3.1}$$

$$\mathbf{v}_{n_{ij}} = (\mathbf{v}_{ij} \cdot \mathbf{n}_{ij})\,\mathbf{n}_{ij}, \tag{3.2}$$

$$\mathbf{v}_{t_{ij}} = \mathbf{v}_{ij} - \mathbf{v}_{n_{ij}} - (a_i\boldsymbol{\omega}_i + a_j\boldsymbol{\omega}_j) \times \mathbf{n}_{ij}, \tag{3.3}$$

where $d_0 = a_i + a_j$, $\mathbf{r}_{ij} = \mathbf{r}_i - \mathbf{r}_j$, $\mathbf{n}_{ij} = \mathbf{r}_{ij}/r_{ij}$, with $r_{ij} = |\mathbf{r}_{ij}|$ and $\mathbf{v}_{ij} = \mathbf{v}_i - \mathbf{v}_j$. Note that there is no sum over repeated indices. The rate of change of the elastic tangential displacement $\mathbf{u}_{t_{ij}}$, set to zero at the initiation of a contact is,

$$\frac{d\mathbf{u}_{t_{ij}}}{dt} = \mathbf{v}_{t_{ij}} - \frac{\left(\mathbf{u}_{t_{ij}} \cdot \mathbf{v}_{ij}\right)\mathbf{r}_{ij}}{r_{ij}^2}. \tag{3.4}$$

The last term in Eq. 3.4 arises from rigid body rotation around the contact point and ensures that $\mathbf{u}_{t_{ij}}$ always lies in the local tangent plane of contact. Normal and tangential

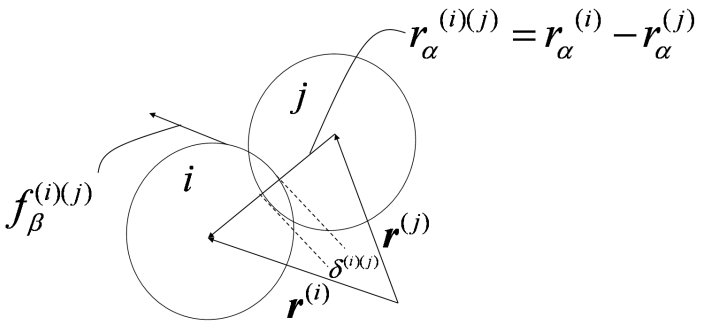

Figure 3.2 Schematic of two particles i and j contact with normal overlap $\delta^{(i)(j)}$ and position vectors $\mathbf{r}^{(i)}$ and $\mathbf{r}^{(j)}$, respectively.

forces acting on particle i are:

$$\mathbf{F}_{n_{ij}} = f\left(\delta_{ij}/d\right)\left(k_n \delta_{ij}\mathbf{n}_{ij} - \gamma_n m_{eff}\mathbf{v}_{n_{ij}}\right), \tag{3.5}$$

$$\mathbf{F}_{t_{ij}} = f\left(\delta_{ij}/d\right)\left(-k_t \mathbf{u}_{t_{ij}} - \gamma_t m_{eff}\mathbf{v}_{t_{ij}}\right), \tag{3.6}$$

where $k_{n,t}$ and $\gamma_{n,t}$ are the spring stiffness and viscoelastic constants, respectively, and $m_{eff} = m_i m_j / \left(m_i + m_j\right)$ is the reduced mass of spheres with masses m_i and m_j. The corresponding contact force on particle j is simply given by Newton's third law, i.e., $\mathbf{F}_{ji} = -\mathbf{F}_{ij}$. The function $f\left(\delta_{ij}/d\right) = 1$ is for the linear spring–dashpot model, and $f\left(\delta_{ij}/d\right) = \sqrt{\delta_{ij}/d}$ is for Hertzian contacts with viscoelastic damping between spheres.

Static friction is implemented by keeping track of the elastic shear displacement throughout the lifetime of a contact. The static yield criterion, characterized by a local particle friction coefficient μ, is modeled by truncating the magnitude of $\mathbf{u}_{t_{ij}}$ as necessary to satisfy $|\mathbf{F}_{t_{ij}}| < |\mu \mathbf{F}_{n_{ij}}|$. Thus, the contact surfaces are treated as "sticking"

when $|\mathbf{F}_{t_{ij}}| < |\mu \mathbf{F}_{n_{ij}}|$, and as "slipping" when the yield criterion is satisfied.

The amount of energy lost in collisions is characterized by the value of the coefficient of restitution, which is defined as the negative ratio of the particle normal velocity after collision to the velocity before collision. For the linear spring-dashpot model, the coefficient of normal restitution and contact time can be analytically obtained:

$$e_n = \exp\left(-\gamma_n t_c/2\right), \tag{3.7}$$

where the contact time t_c is given by

$$t_c = \pi\left(k_n/m_{\text{eff}} - \gamma_n^2/4\right)^{-1/2}. \tag{3.8}$$

The value of the spring constant should be large enough to avoid particle interpenetration, yet not so large as to require an unreasonably small simulation time step Δt, since an accurate simulation typically requires $\Delta t \sim t_c/50$ (Campbell, 2002). After the contact force is calculated, the equations of motion, which are ordinary differential equations, can be numerically integrated to get the particle trajectories.

3.2 Review of microscale modeling of granular flows

Microscale DEM simulations have been successfully used to quantify the constitutive behavior of granular flow in different regimes (Campbell, 2002; Aarons and Sundaresan, 2006). A quantitative understanding of the different regimes of flow for monodisperse, cohesionless, frictional particles has emerged from DEM simulations performed by Campbell (2002). Using DEM simulations of homogeneously sheared flow of cohesionless particles in periodic domains Campbell (2002) identified different regimes of granular flow mainly inertial (rapid flow), quasi–static and the intermediate. Campbell (2002) confirmed that DEM reproduces the qualitative constitutive behavior that is observed in the experiments namely, that in the inertial regime stress increases as the

square of the strain rate, in the quasi–static regime the stress did not vary appreciably with the applied shear rate, and in the intermediate regime the stress varies with the applied shear rate, but this relation takes different forms that depends on the solid volume fraction, interparticle friction coefficient and the shear rate.

Aarons and Sundaresan (2006) performed DEM simulations of cohesive particles in order to investigate the effect of interparticle attractive forces on the regime of rheology manifested by dense assemblies. They (Aarons and Sundaresan, 2006) showed that with the addition of interparticle attractive forces the regime boundaries shift in a systematic manner, and that the quasi–static regime expands. McCarthy et al. (2010) used detailed particle level experimental measurements to quantitatively validate DEM simulations in an annular shear cell. The velocity, granular temperature and solid volume fraction profiles was extracted by using particle tracking velocimetry (DPIV) and compared with the computational data. They also studied the influence of the contact mechanics model and performed sensitivity analysis on device and particle geometry and material properties employed.

Vidyapati et al. (2012) studied the rheology of dense granular material using an annular Couette cell by experiments and computations. It is shown that DEM simulations are capable of capturing the regime transition from quasi–static to intermediate regime when a secondary vertical flow is induced, which is also observed in the experiments. Ketterhagen et al. (2009) used DEM to assess powder flow from hoppers and results were compared to widely used hopper design charts. A Mass Flow Index (MFI) based on velocity profile data is used to quantitatively characterize the nature of the flow pattern as mass–flow, funnel–flow or some intermediate. In a recent work, Vidyapati and Subramaniam (2012a) used DEM simulations to characterize granular rheology and granular phase transition by studying the order parameter (OP) dynamics. DEM simulations performed in this study reveal existence of a third stable granular phase that is neither completely fluid–like nor completely solid–like. Further, a modified form

of the free energy density function is proposed to account for this third stable granular phase observed in these DEM simulations.

In summary, the qualitative predictions and detailed information about the granular microstructure obtained through these microscale DEM simulations, make it a valuable complement to experiments to develop constitutive models in different regimes of granular flows.

CHAPTER 4. EXPERIMENTAL AND COMPUTATIONAL STUDIES OF DENSE GRANULAR FLOW: TRANSITION FROM QUASI–STATIC TO INTERMEDIATE REGIME IN A COUETTE SHEAR DEVICE

A paper published in *Powder Technology* [1]

Vidyapati, M. Kheiripour Langroudi, J. Sun, S. Sundaresan, G. I. Tardos and S. Subramaniam

Abstract

Rheology of dense granular material in an annular Couette cell is studied by experimentation and simulation. A transition from quasi-static to intermediate behavior is identified when a secondary vertical flow is induced. This secondary flow-induced transition and a power-law relation between stress and shear rate in the intermediate regime are verified to be robust rheological features by simulation using discrete element method (DEM). The insensitivity of this transition to certain particle and operational parameters is also shown by the simulation. The transitional and intermediate behavior is modeled by an order parameter (OP) based model with the fluidlike stress calculated using a constitutive relation from the kinetic theory for granular flows (KTGF). The suitability of this approach is discussed.

[1] *Powder Technology*, vol. 220, pp. 7–14, 2012.

Notation for section 4.1 to section 4.5

$\triangle t$ Time step for simulation

$\hat{t}$ Nondimensional time based on gravity scaling

d_0 Particle diameter

e Particle restitution coefficient

F_0 Scaling factor for force

F_n Normal force

F_t Tangential force

g Acceleration due to gravity

k^* Nondimensional shear rate

k_0 Scaling factor for stiffness

k_n Particle normal stiffness coefficient

k_t Particle tangential stiffness coefficient

L Side length of the domain

m_0 Particle mass

t Time

t^* Typical time of collisional for solid contacts

t_0 Scaling factor for time

t_c Binary collision time

$\mathbf{v}'$ Fluctuating velocity of particle

v_0 Scaling factor for velocity

Z Total number of contacts

Z_s Number of solidlike (enduring) contacts

Greek symbols

α, β Model coefficients of the ROP model

$\dot{\gamma}$ Shear rate

$\dot{\gamma}_{max}$ Maximum shear rate

γ^* Nondimensional shear rate based on elastic scaling

γ_n Particle normal damping coefficient

γ_t Particle tangential damping coefficient

$\hat{\gamma}$ Nondimensional shear rate based on gravity scaling

μ_p Particle friction coefficient

μ_t Tangential coefficient of friction

μ_w Wall friction coefficient

ν Solid volume fraction

ρ Particle density

σ_0 Scaling factor for stress

σ_{ij} Total granular stress

σ_{ij}^f Fluidlike contribution to the total granular stress

σ_{ij}^s Solidlike contribution to the total granular stress

σ_{yx} Shear stress

σ_{yy} Normal stress

4.1 Introduction

Granular materials mimic the behavior of solid, liquid or gas when subjected to different excitation (Jaeger et al., 1996). Understanding this complex behavior poses challenging scientific questions, and is also of practical importance to many industrial processes, such as silo discharge, chute flow and dense-phase pneumatic conveying (Sundaresan, 2001). Much experimental work has been performed to probe the diverse behavior of granular materials. As classical examples, Reynolds (1885) examined the dilatancy behavior of quasi-statically deformed granular assemblies and Bagnold (1954) studied the inertial behavior and proposed a quadratic power relation between stress and shear rate. However, the transition between regimes, and the ensuing intermediate regime behavior is even more fascinating and difficult to quantify. This paper presents the transitional and intermediate behavior observed in our experiments and simulations and addresses continuum modeling of the behavior as well.

The experimental technique of choice in this study is shearing granular materials in an annular Couette cell, which has been adopted from fluid rheology to study granular rheology for some years (Savage and Sayed, 1984; Miller et al., 1996; Tardos et al., 2003; Tsai and Gollub, 2004; G.D.R. MiDi, 2004). For example, Savage and Sayed (1984) reported shear and normal stress variations with respect to shear rates obtained from an annular shear cell. Velocity profiles in annulus have also been measured (G.D.R. MiDi, 2004). In these experiments, however, either the flow behavior was in a single regime (G.D.R. MiDi, 2004) or the transition from quasi-static regime to inertial regime was not explicitly controlled (Savage and Sayed, 1984). To facilitate the control of flow regime transition, a modified Couette cell was devised in this study by connecting a hopper to the bottom of the cylindrical cell (see Fig. 4.1). A secondary vertical flow can thus be introduced in the granular material in the annulus by discharge from the hopper. It will be shown that the transition can be triggered by the onset of this secondary flow.

The stress and shear rate relation for intermediate flow will also be presented.

Discrete element method (DEM) (Cundall and Strack, 1979) has been used extensively to simulate Couette shear flow. Simulations have been performed to study a two-dimensional (2D) Couette cell for photoelastic disks, and found to be in reasonable agreement with the corresponding experimental results on velocity profiles (Schöllmann, 1999). Similar 2D simulations also produced variation of pressure versus volume fraction that was consistent with experiments (Majmudar et al., 2007). In this paper, DEM simulations in a simplified three-dimensional (3D) domain have been set up to study the essential flow characteristics probed by the modified Couette cell experiments. The results will verify the transitional and intermediate behavior observed in the experiments, and demonstrate the robustness of these trends against variations in particle and flow properties.

An objective order parameter model (Gao et al., 2005) was linearized and employed to predict the granular stress in intermediate regime. The order parameter is defined as the ratio between solidlike and fluidlike stresses as proposed by Volfson et al. (2003a). The decomposition of stress into solidlike and fluidlike parts is based on characteristics of the contributing particle contacts. This micromechanics based approach provides an alternative to the one proposed by Savage (1983, 1998), in which inertial stress calculated according to the kinetic theory for granular flows (KTGF) (Lun et al., 1984) is directly added to the quasi-static stress from soil mechanics theories (Nedderman, 1992). However, it will be shown that the OP model with fluidlike stress given by a simple KTGF constitutive relation has limitations in predicting the intermediate behavior.

4.2 Couette cell experiment and simulation details

Experiments with glass beads of 0.1 mm diameter were performed in a modified annular Couette cell as shown by the schematic diagram in Fig. 4.1. The device consists

of a cylindrical portion with a rotating inner cylinder to shear the material in the annular gap and a conical hopper at the bottom. The material above the rotating cylinder (denoted as overburden in the schematic) is stationary and provides dead weight to the sheared layer. Granular material can be fed from above using a vibrating feeder (not shown) and discharged by a screw-in-cylinder metering device (also not shown) that discharges the material and allows for precise flow rate measurement. For experiments operated in a continuous mode, material is fed and discharged at the same time to achieve a steady-state vertical flow in the sheared layer. For those in a batch mode, no mass flows in or out of the device. Shear stress can be measured indirectly from the torque on the rotating cylinder. Additional details of the experimental setup can be found in Kheiripour Langroudi et al. (2010a,b).

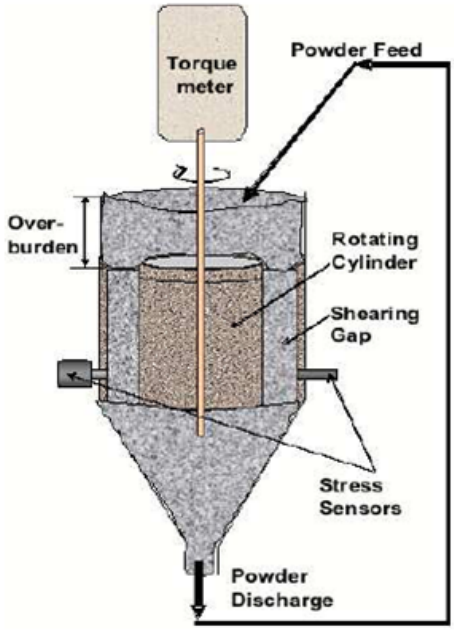

Figure 4.1 Schematic of the Couette device with adjustable axial flow.

DEM simulations were carried out to verify experimental findings and to further study parametric dependence of the granular rheology. The simulations were performed

in 3D using monodisperse, non-cohesive spheres of diameter d_0 and mass m_0, under the influence of gravity g. A soft-sphere contact model, the linear spring-dashpot model, was used, in which particles interact only on contact for finite duration. A set of non-dimensional equations is solved, where the scaling factor for distance, time, velocity, force, elastic constants and stresses are d_0, $t_0 = \sqrt{d_0/g}$, $v_0 = \sqrt{gd_0}$, $F_0 = m_0 g$, $k_0 = m_0 g/d_0$ and $\sigma_0 = m_0 g/d_0^2$, respectively. As the problem involves both gravity and shearing motion non-dimensionalization based on both gravity and shear-rate is compared in Table 4.1. The gravity scaling was selected because its characteristic time ($\sqrt{d_0/g} = 3.2 \times 10^{-3}$ s, with $d_0 = 0.1$ mm) is shorter than that with the shear scaling ($\dot{\gamma}_{max}^{-1} = 7.7 \times 10^{-3}$ s), even at the maximum shear rate used in the experiments. Details of the computational model used in the discrete element simulations are given in Sec. 3.1.

Table 4.1 Scaling for computational parameters.

Parameters	Gravity Scaling	Shear Scaling
Length, L_0	d_0	d_0
Time, t_0	$\sqrt{d_0/g}$	$1/\dot{\gamma}$
Velocity, v_0	$\sqrt{gd_0}$	$d_0\dot{\gamma}$
Force, F_0	$m_0 g$	$m_0 d_0 \dot{\gamma}^2$
Stiffness, k_0	$m_0 g/d_0$	$m_0\dot{\gamma}^2$
Stress, σ_0	$m_0 g/d_0^2$	$m_0\dot{\gamma}^2/d_0$
Damping Coefficient, γ_n	$m_0\sqrt{g/d_0}$	$m_0\dot{\gamma}$

The total number of particles in the whole experimental system, including those in the overburden and hopper, is extremely large for DEM simulation. To avoid this expensive simulation, but still capture the essential rheological behavior, a representative slice of the sheared granular layer was simulated, with the curvature of the layer ignored due to the relatively large cylinder diameter. A cubic domain with side length $L = 14d_0$ was used as shown in Fig. 4.2. The effect of system size was examined by varying the side

length from $7d_0$ to $20d_0$. Asymptotic stress was found after the side length exceeded $10d_0$, consistent with the findings by Campbell (2002). Periodic boundary conditions were

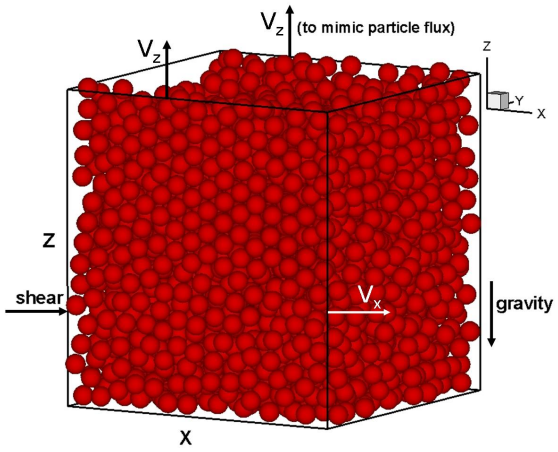

Figure 4.2 Schematic of spherical particles bounded in a cubical domain. V_z denotes the relative velocity due to the axial particle flow and V_x the relative velocity due to shearing, with the arrows pointing to the positive directions.

applied in the x direction (which corresponds to the azimuthal direction in the Couette cell) and "shrink wrap" boundary condition were applied at $z = L$ (gravity pointing to the negative z direction), respectively. The shrink-wrap boundary condition ensures that the domain encompasses the particles moving in that direction. Wall boundary condition was applied to the rest of the domain boundaries. All the walls used in the simulations were flat and frictional, with a particle-wall friction coefficient $\mu_w = 1.0$. The relative axial velocity of the walls located at $y = 0$ and at $y = L$ (corresponding to radial coordinates for the Couette cell), V_z, was varied from zero for batch mode simulation, to values determined by the axial flow rates in the continuous mode operation. The relative shearing velocity for the wall located at $y = 0$, V_x, was calculated based on the shear rates used in the experiments.

DEM simulations were performed at three different initial solid volume fractions,

0.64, 0.62 and 0.60, which would no longer remain spatially uniform due to inhomogeneities developed during simulation. However, the particle volume fraction was not measured in the experiments. As stress increases with the initial solid volume fraction, we present results of simulations with a solid volume fraction of 0.64, which gives the closest match to experimental results. For particle properties not measured experimentally, reasonable values were assigned to reflect the bulk material behavior in the experiments. For instance, the normal spring stiffness was assigned to be $2 \times 10^5\ k_0$, which captures the general behavior of medium to high stiffness systems (Silbert et al., 2001), such as the glass bead assembly used in the experiments. Similarly, the restitution coefficient and particle-particle friction were set to 0.9 and 0.19, respectively. The integration time step $\triangle t$ was set to one fiftieth of the binary collision time t_c to achieve a temporally converged numerical solution without excessive computational time (Silbert et al., 2001). Simulations were run for a non-dimensional time of $\dot{\gamma}t = 500$ to attain a statistically stationary solution (Campbell, 2002). The basic computational parameters are summarized in Table 4.2.

4.3 Experimental and simulation results

4.3.1 Transitional and intermediate behavior

Rheology of sheared granular material probed by the Couette cell experiments and simulations is presented in this section. The average stress is calculated by dividing the force acting on the inner wall by the area of the granular bed contacting the wall, considering its expansion or compaction. In Fig. 4.3 the average shear stress on the inner wall is plotted against time for the batch mode. Figure 4.3 shows that changing the shear rate more than fivefold in the DEM simulation does not result in any significant change in the shear stress, which is a feature of the quasi-static regime. DEM results show initial fluctuations in the stress level, but attain a statistically stationary state

Table 4.2 Parameters used in the DEM simulations.

Parameters	Values
Number of particles	3348
Particle diameter	d_0
Particle density	$1.91(m_0/d_0^3)$
Particle normal stiffness coefficient, k_n	$2 \times 10^5(k_0)$
Particle tangential stiffness coefficient, k_t	$2/7k_n$
Particle normal damping coefficient, γ_n	$40(1/t_0)$
Particle tangential damping coefficient, γ_t	$0(1/t_0)$
Particle friction coefficient, μ_p	0.19
Particle restitution coefficient, e	0.9
Wall normal stiffness coefficient	$2 \times 10^5(k_0)$
Wall tangential stiffness coefficient	$2/7k_n$
Wall normal damping coefficient	$40(1/t_0)$
Wall tangential damping coefficient	$20(1/t_0)$
Wall friction coefficient, μ_w	1.0
Time step, $\triangle t$	$1 \times 10^{-4}(t_0)$

after approximately 30 t_0. Quasi-static stress was also observed in the experiments, as the experiments were also performed with different values of shear rates, although only one of those (corresponding to $\hat{\gamma} = \dot{\gamma}/(g/d_0)^{1/2} = 1.40 \times 10^{-1}$) is presented in Fig. 4.3 due to their close proximity. However, the magnitude of the measured shear stress is about 2.5 times higher than that predicted in the simulations.

The variation of shear stress with shear rate in the continuous mode with a vertical speed, $V_z = 3.2 \times 10^{-3}\sqrt{gd_0}$ corresponding to the flow rate in experiments is shown in Fig. 4.4(a) (the left vertical axis corresponds to the DEM simulation results and the right vertical axis corresponds to the experimental data). The experimental and DEM results in Fig. 4.4(a) show that the flow exhibits two distinct regimes: a quasi-static regime, where the shear stress is independent of the shear rate (at very low shear rates), and an intermediate regime, where the dependence takes the form of a power-law. The transition starts at a non-dimensional shear rate $\hat{\gamma}$, of about 0.1, whereas the flow in the

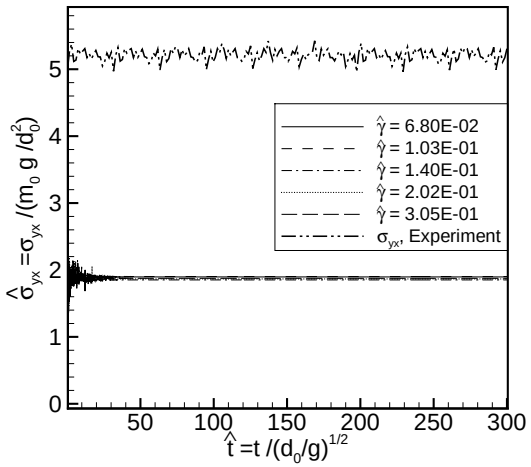

Figure 4.3 Temporal evolution of the average non-dimensional shear stress on the Couette cell wall during the batch mode operation.

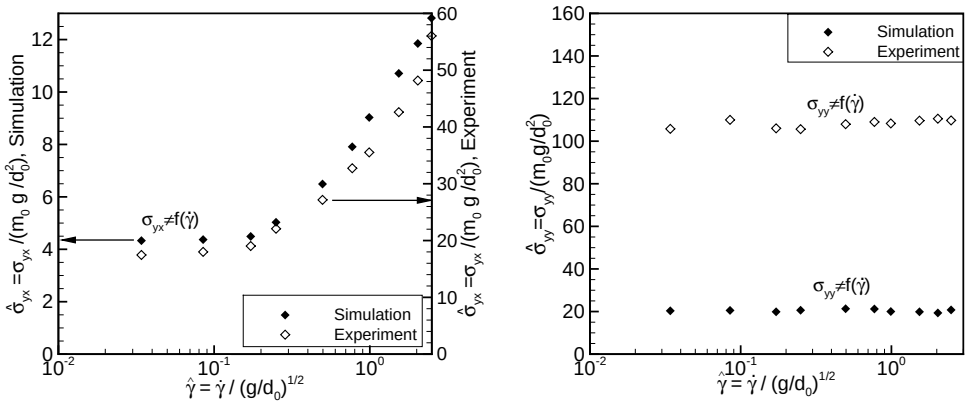

(a) (b)

Figure 4.4 Variation of (a) the average shear stress and (b) the average normal stress with the non-dimensional shear rate for the continuous-mode operation. The filled symbols denote the DEM simulation results, while the open symbols are for data obtained from experiments. Different scales are used on the left and right axes for the DEM and experimental data, respectively, to emphasize the similarity in their trends.

batch mode at the same $\hat{\gamma}$ does not undergo transition (see the quasi-static behavior at even higher shear rates in Fig. 4.3). This transitional behavior indicates that the axial flow in continuous mode facilitates regime transition.

The DEM shear stress, however, is about 4.5 times lower in magnitude than its experimental counterpart, consistent with a factor-of-two difference found in a similar study performed by Ji et al. (2009). This difference could be due to differences in particle properties, domain geometry, system setup and solid volume fraction. The normal stress, on the other hand, remained almost constant in experiments and simulations as shown in Fig. 4.4(b). The experimental results for normal stress are also about five times of the DEM counterparts, which shows the effect of the overburden present in the experiments but ignored in the simulations.

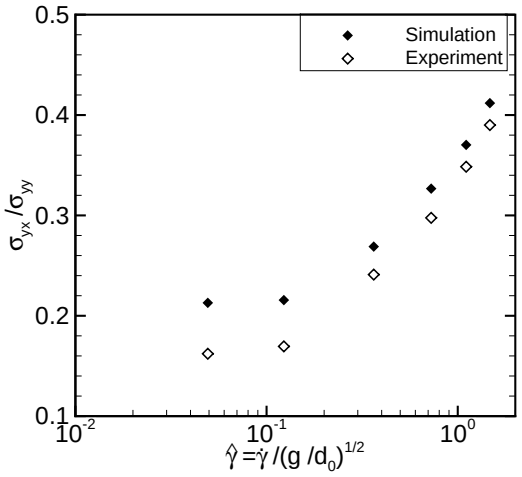

Figure 4.5 Ratio of shear to normal stress as a function of shear rate for the continuous mode of operation. Filled symbols correspond to DEM simulation data whereas the open symbols are for experimental data.

The ratio of shear to normal stress (σ_{yx}/σ_{yy}) is plotted in Fig. 4.5 as a function of the non-dimensional shear rate for the continuous mode of operation. The variation

of this ratio also manifests the same transition and intermediate behavior: it remains almost a constant approximately equal to the particle friction coefficient for lower shear rates; it has a power-law dependence as the shear rate increases beyond a certain critical value. The experimental ratios are close to, albeit slightly lower than, the DEM results. The better agreement again confirms that the large difference in stress magnitude is mostly due to the different confinements (with/without overburden, etc.) and that the simulations reveal essentially the same rheology as in the experiments.

In section 4.4, another non-dimensional shear rate $\gamma^* = \dot{\gamma}/(\rho d_0^3/k_n)^{1/2}$ is used according to the physical characteristics in a different system. It should be noted that the shear rates in the experiments corresponds to γ^* values ranging from 10^{-5} to 10^{-3}.

4.3.2 Simulation parametric study

As reported earlier, reasonable values were assigned to some computational parameters that were not measured in the experiments. In order to quantify the effect of these parameters on the stress level, we performed a parametric study of initial solid volume fraction, particle stiffness, wall friction coefficient and axial velocity. These simulations were performed using the same computational setup as discussed in section 3.3.1, but with inter-particle friction coefficient equal to 0.2. The results are summarized in the following.

Figure 4.6(a) shows the variation of average shear stress against initial solid volume fraction with wall friction coefficient fixed at 0.5. As expected, the stress level increases with increasing solid volume fraction, most pronouncedly above 0.60. As Fig. 4.6(b) shows, shear stress has nearly no change with respect to particle stiffness ranging from 10^5 k_0 to 10^6 k_0 with initial solid volume fraction kept at 0.62, because the granular bed is allowed to expand freely. The shear stress increases fivefold as the wall friction coefficient increases from 0.3 to 1.0 as shown in Fig. 4.6(c) where initial solid volume fraction is kept at 0.62. The variation of stress with the axial velocity in the shear

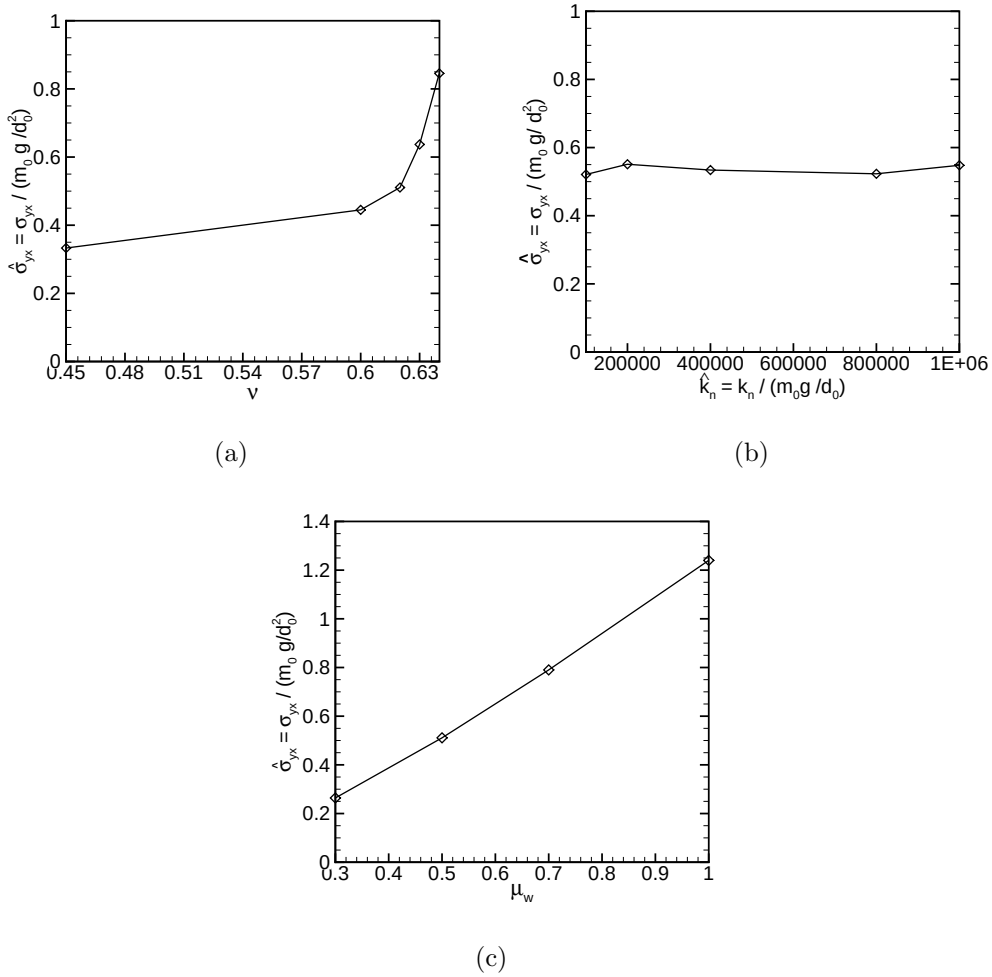

Figure 4.6 Variation of average shear stress versus (a) solid volume fraction, (b) particle stiffness, and (c) wall friction coefficient.

gap was investigated over a limited range of values and the stress exhibits a sudden (factor-of-two) increase in the magnitude when the axial velocity is increased from 0 to $1.6 \times 10^{-3}\sqrt{gd_0}$, which is half the value used in the experiment (result not presented here). However, any further increase in the axial velocity up to $6.4 \times 10^{-3}\sqrt{gd_0}$ does not result in any appreciable change in the stress.

4.4 Order parameter modeling and analysis

The OP is defined as the ratio of space-time averaged number of "enduring" (solidlike) contacts $\overline{\langle Z_s \rangle}$ to all contacts $\overline{\langle Z \rangle}$ within a sampling volume (Volfson et al., 2003a). A contact is considered solidlike only if it is in a stuck state ($F_t < \mu_t F_n$) and its duration is longer than a typical time t^*, which is generally taken as 1.1 times the binary collision time t_c (Volfson et al., 2003a). The first requirement eliminates long lasting sliding contacts, and the second excludes short term collisions. When either of the requirements is not fulfilled, the contact is defined as "fluidlike". The OP equals unity if a granular assembly is in a solid state, whereas OP is zero at a completely fluidlike state.

Based on the OP concept, granular stress can be decomposed into solidlike and fluidlike contributions (Volfson et al., 2003b) that arises from solidlike contacts and a fluidlike contribution that arises from fluidlike contacts plus the streaming stress (defined later in this section), respectively. Either of these individual contributions may be described by known constitutive relations, such as KTGF or Newtonian fluid relations for the fluidlike contribution. The total stress can thus be calculated as a function of the individual contribution and the OP. A linear objective OP model (Gao et al., 2005) is employed in this study to predict the rheology in intermediate regime. In this model the stresses are expressed as

$$\sigma_{ij} = \frac{\sigma_0}{\beta}\{\frac{\sigma_{ij}^f}{\sigma_0} + \delta_{ij}(\beta - \alpha)\}, \tag{4.1}$$

$$\sigma_{ij}^s = \sigma_0\{(1-\alpha)\delta_{ij} + (1-\beta)b_{ij}\}, \tag{4.2}$$

where σ_{ij} is the total granular stress, σ^f_{ij} is the fluidlike stress, σ^s_{ij} is the solidlike stress and $\sigma_0 = \sigma^f_{ii}/3\alpha$ is the scale of stress (summation is implied over repeated indices). The normalized deviatoric stress tensor b_{ij} is defined as

$$b_{ij} = \frac{\sigma_{ij}}{\sigma_0} - \delta_{ij}. \tag{4.3}$$

The scalar model coefficients α and β [2] are functions of the OP, which have been extracted from 3D DEM simulations of homogeneously sheared granular flow (Subramaniam and Vidyapati, 2009). The model with so-determined coefficients is denoted as the refined order parameter (ROP) model. In this study, a KTGF constitutive relation (Lun et al., 1984) was used for fluidlike stress, which together with the ROP model is denoted as the ROP-KT model. Details of the ROP model can be found in Subramaniam and Vidyapati (2009).

The OP was first demonstrated to have correct response to variation in flow conditions and particle properties in homogeneous shear flow. Figure 4.7(a) shows that the OP increases as the volume fraction increases and is indeed strongly dependent on the coefficient of friction. An increase of 300% in the values of the OP is seen when the coefficient of friction increases from 0.1 to 1.0 at the same volume fraction. This is because the larger inter-particle friction prevents more particles from sliding, resulting in more solidlike contacts and higher OP values.

In Fig. 4.7(b) the OP values are plotted as a function of the non-dimensional shear rate, $\gamma^* = \dot{\gamma}/(\rho d_0^3/k_n)^{1/2}$, which shows that the OP value decreases with increasing shear rate, indicating a decrease in solidlike contacts. The OP asymptotically approaches 1 at the solid limit for significantly high values of inter-particle friction coefficient and solid volume fraction at low shear rates. Both Figs. 4.7(a) and 4.7(b) lead to the conclusion that the OP is able to capture the changes in particle and flow properties.

[2] It should be noted that $\alpha = \beta = 0$ if and only if $\sigma^f_{ij} = 0$, which ensures that σ_{ij} has finite value in Eq. 4.1 all the time.

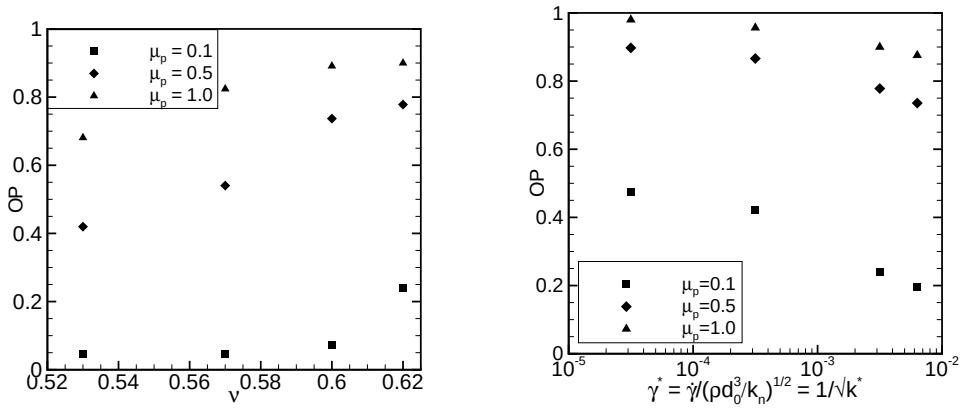

(a) (b)

Figure 4.7 Order parameter as a function of (a) volume fraction and (b) shear rate ($\gamma^* = \dot{\gamma}/(\rho d_0^3/k_n)^{1/2} = 1/\sqrt{k^*}$) for homogeneous shear flow. $\gamma^* = 3 \times 10^{-3}$ and $\nu = 0.62$ in (a) and (b), respectively.

The ROP-KT model is now examined to determine if it is capable of predicting the correct power-law dependence in the intermediate regime. The solid volume fraction used for the homogeneous flow simulations ($\nu = 0.58$) was chosen to match that of the vertically central part of the granular assembly from the Couette cell simulations reported earlier in this study (as noted earlier, the volume fraction field is not uniform). The particle friction coefficient μ_p and coefficient of restitution e used are the same as used in the Couette cell simulations.

Figure 4.8 shows a logarithmic plot of the elastically scaled shear stress as a function of the non-dimensional shear rate. In this plot, stress variation for quasi-static flow will follow a horizontal line, and that in the inertial regime appears as a line with slope 2. Lines with slope between 0 and 2 indicate the intermediate flow. It can be seen that the ROP-KT model does not predict the correct stress dependence when compared with the DEM data. The predicted slope is 1.92, whereas the DEM data points follow a slope of 0.82. This difference in the stress magnitude and strain-rate dependence is attributed to the fact that the *fluidlike* stress is modeled by the KTGF constitutive relation, which may

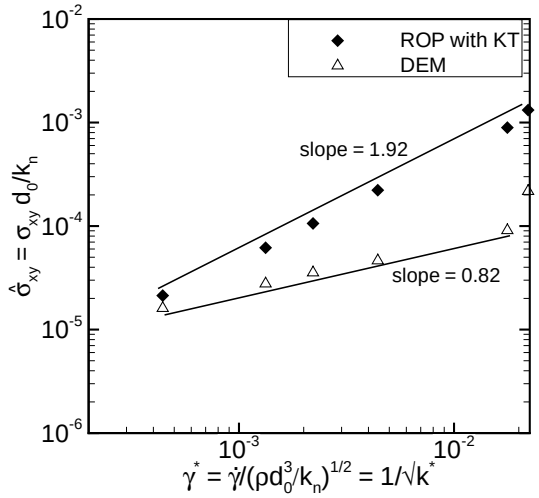

Figure 4.8 Comparison of ROP-KT model prediction with DEM results of shear stress against shear rate for homogenous shear flow.

not be valid for this intermediate flow, where both collisional and frictional interactions between particles are important. The performance of the ROP-KT model has been tested over a range of solid volume fractions for homogeneous shear flow (Subramaniam and Vidyapati, 2009). It is found that the ROP-KT model predicts the total granular stress within error range of 15% for assemblies with a solid volume fraction up to 0.57. However, the model performance deteriorates in the deep intermediate regime where solid volume fraction is higher than 0.57.

To further investigate the scaling of the stress-shear rate relation in the intermediate regime, we also decomposed the total granular stress obtained from DEM simulations into contact and streaming contributions. The contact contribution due to particle contacts in a domain of volume V is given by

$$\boldsymbol{\sigma}^{\text{contact}} = \frac{1}{V} \sum_{i}^{N} \sum_{j,j \neq i} \frac{1}{2} \mathbf{r}^{(i)(j)} \otimes \mathbf{f}^{(i)(j)}, \tag{4.4}$$

where $\mathbf{r}^{(i)(j)}$ is the vector pointing from the center of particle j to the center of particle i, $\mathbf{f}^{(i)(j)}$ is the contact force acting on particle i by particle j, and $\otimes$ denotes a dyadic

product. The streaming contribution arises from momentum flux and is given as

$$\boldsymbol{\sigma}^{\text{streaming}} = \frac{1}{V}\sum_{i}^{N} m_0^{(i)} \mathbf{v}'^{(i)} \otimes \mathbf{v}'^{(i)}, \tag{4.5}$$

where m_0 is the mass of a particle, $\mathbf{v}'$ is the fluctuating velocity and i is a particle index.

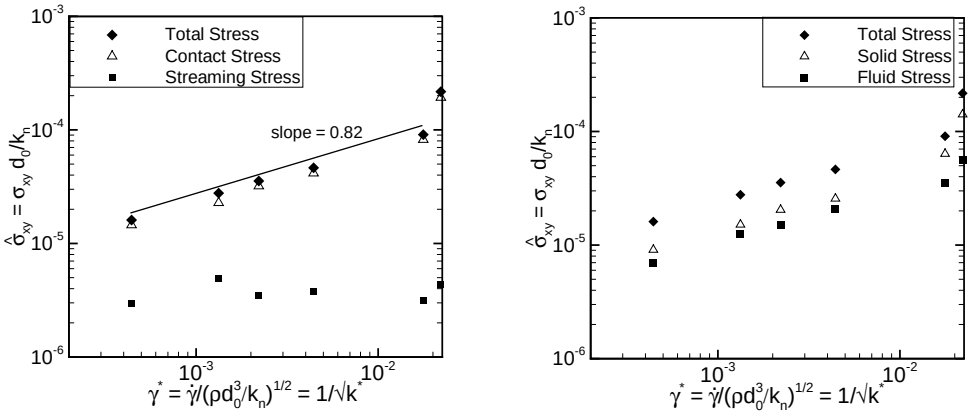

(a) (b)

Figure 4.9 Decomposition of the total shear stress into (a) contact and streaming, and (b) solidlike and fluidlike contributions.

The contact and streaming stresses from the same simulation as shown in Fig. 4.8 are plotted in Fig. 4.9(a) with non-dimensional shear rate. The contact part contributes more than 95% to the total granular stress and follows the same scaling, whereas the streaming part does not exhibit this scaling. We then decomposed the total granular stress obtained from DEM simulations into fluidlike and solidlike contributions, which are plotted in Fig. 4.9(b) with shear rate. The solidlike contribution is about 60–70% of the total stress. Both contributions approximately follow the same scaling ($\sigma \propto \dot{\gamma}^n, n = 0.82$) as the total stress because both carry portions of streaming and contact stress, the difference being whether the contacts are enduring or not.

4.5 Conclusions

Experiments and DEM simulations have been performed to study transitional rheology of dense granular materials in a modified annular Couette shear cell operated in batch or continuous mode. Shear stress and shear-to-normal-stress ratio were found to have quasi-static behavior ($\sigma \neq f(\dot{\gamma})$) in the batch mode and to have an axial flow-induced transition to the intermediate behavior characterized by a power-law relation with shear rate ($\sigma \propto \dot{\gamma}^n, 0 < n < 2$) in the continuous mode. It has also been shown by the simulations that this transition and the power-law relation are robust rheological features, insensitive to particle properties and operational details.

The OP concept has been shown to be useful in reflecting the transitional behavior. The ROP-KT mode has been assessed to be applicable to assemblies with volume fractions less than 0.57 for prediction of intermediate behavior, as the power-law exponent cannot be correctly predicted for denser assemblies. This study illuminates that suitable constitutive relations should be sought for the fluidlike (or solidlike) stress in order for models based on OP to correctly predict certain intermediate behavior.

CHAPTER 5. GRANULAR RHEOLOGY AND PHASE TRANSITION: DEM SIMULATIONS AND ORDER–PARAMETER BASED CONSTITUTIVE MODEL

A paper published in *Chemical Engineering Science* [1]

Vidyapati and S. Subramaniam

Abstract

DEM (discrete element method) simulations are used to characterize granular rheology and granular phase transition by studying order parameter (OP) dynamics. These DEM simulations reveal the existence of a third stable granular phase that is neither completely fluid–like nor completely solid–like. Hence, a modified form of the free energy density function is proposed to account for this third stable granular phase observed in DEM simulations. Further, a constitutive model for granular flows is developed based on an objective version [Gao et al., Phys. Rev. E, 71(021302), 2005] of the original OP concept proposed by Volfson et al. [Phys. Rev. E, 68(021301), 2003], with the intention of capturing the transitional behavior in a continuum description of granular flows. This OP–based model is refined by extracting new model coefficients from 3D DEM simulations of homogeneous shear flow. The proposed linear version of the objective OP model has the advantage that the total granular stress is a linear combination of the solid–like and fluid–like stresses, and it is denoted as the refined order parameter (ROP) model.

[1] *Chemical Engineering Science*, vol. 72, pp. 20–34, 2012.

The performance of this ROP model along with other existing constitutive models is assessed in homogeneous shear flow, and the results are explained by analyzing granular stress data from DEM simulations.

Notation for section 5.1 to section 5.9

$\triangle t$ Time step for simulation

D_c Diffusion coefficient in Ginzburg–Landau equation

d_0 Particle diameter

e Particle restitution coefficient

F Free energy density function

F^* Modified form of the free energy density function

F_n Normal force

F_t Tangential force

g Acceleration due to gravity

$g(\mathbf{r})$ Pair correlation function function

I Inertia number

J_{coll} Dissipation term

k^* Nondimensional shear rate

k_n Particle normal stiffness coefficient

L Side length of the domain

m Slope

m_0 Particle mass

N_c Number of contacts

N_{CN} Coordination number

P Isotropic pressure

p_c Critical state pressure

$\mathbf{R}$ Fabric tensor

$\mathbf{S}$ Rate of strain tensor

T Granular temperature

t Time

t^* Typical time of collisional for solidlike contacts

t_c Binary collision time

$\mathbf{u}$ Mean velocity vector

V Volume

$\mathbf{v}'$ Fluctuating velocity

Z Total number of contacts

Z_s Number of solidlike (enduring) contacts

Greek symbols

α,β,γ Model coefficients for the OP model

α_k Constant in kinetic theory

δ, δ^* Parameters in the free energy density function

δ_{ij} Kronecker delta

$\dot{\gamma}$ Shear rate

η_k Constant in kinetic theory

$\hat{\epsilon}$ Relative error in least–squares solution

μ, μ_b Constants in kinetic theory

μ_p Particle friction coefficient

μ_t Tangential coefficient of friction

μ_w Wall friction coefficient

ν Solid volume fraction

ν_{max} Packed bed void fraction

ρ Order parameter

ρ_3 Steady state value of OP

ρ_s Particle density

σ_0 Scale of the stress

σ_{ij} Total granular stress

σ_{ij}^{f} Fluidlike contribution to the total granular stress

σ_{ij}^{fric} Frictional contribution of the stress

σ_{ij}^{kin} Kinetic contribution of the stress

σ_{ij}^{s} Solidlike contribution to the total granular stress

η Viscosity

ϕ Angle of internal friction

5.1 Introduction

A quantitative description of the large–scale behavior of granular flow in industrial devices—such as hopper discharge, chute flow, and dense–phase pneumatic conveying—rely on a continuum description of granular flows (Sundaresan, 2001). The difficulty in modeling granular rheology is that granular matter can exhibit constitutive behavior like a solid (in a sand pile), like a liquid (when poured from a hopper or silo), or like a gas (when it is strongly agitated) (Jaeger et al., 1996). These different constitutive behaviors depend on both the microscale properties (e.g., particle friction and coefficient of restitution) as well as on macroscale properties (e.g., solid volume fraction and shear rate). Further, these different behaviors pose significant challenges in formulating a comprehensive constitutive theory that can describe all the regimes of granular rheology. For the two extreme regimes— rapid and quasi–static—constitutive equations have been proposed based on the kinetic theory for rapid flows (Goldhirsch, 2003), and soil mechanics for quasi–static flow (Nedderman, 1992; Schaeffer, 1987). However, the transitional (intermediate) regime, where both collisional and frictional interactions between the particles are important, still lacks a predictive constitutive model and has motivated many studies over the past decade (Jop et al., 2006; G.D.R. MiDi, 2004; Vidyapati et al., 2012). Nevertheless, these theories were unable to capture the transition between solid–like and fluid–like behavior of the granular material.

Most constitutive models (Savage, 1998; Johnson and Jackson, 1987; Srivastava and Sundaresan, 2003) that are used to predict the behavior of granular flows are based on an additive decomposition of the total granular stress as a weighted sum of kinetic and frictional contributions ($\sigma_{ij} = \sigma_{ij}^{kin} + \sigma_{ij}^{fric}$), with the weight factor specified solely as a function of the solid volume fraction. A continuum theory for slow dense granular flows based on so–called associated flow rule is proposed by Savage (1998). This theory relates the shear stress and the strain rate in a plastic frictional system. Averaging strain–rate

fluctuations yields a Bingham–like constitutive relation in which the shear stress has two contributions: a viscous part, and a strain–rate independent part. According to this theory the stress and strain rate tensors are always coaxial. Furthermore, the theory also postulates that the viscosity diverges as the density approaches the close packing limit. A similar hydrodynamic model based on a Newtonian stress–strain constitutive relation with density–dependent viscosity is proposed by Losert et al. (2000). In this model also the viscosity diverges when the density approaches the random close packing density of grains. Jop et al. (2006) proposed a constitutive relation for dense granular flows inspired by the analogy between granular flows and visco–plastic fluids such as Bingham fluids. In their work (Jop et al., 2006), granular flow is described as an incompressible fluid with the stress tensor given as a function of the inertia number, $I = \dot{\gamma} d_0/(P/\rho_s)^{0.5}$.

Experiments in a 2D granular shear cell (GSC) (McCarthy et al., 2010; Jasti and Higgs, 2008) as well as DEM simulations (Volfson et al., 2003a) reveal that grain contacts in the transitional regime are characterized by a mix of enduring solid–like and fluid–like contacts that is indicative of a granular phase transition. In particular, these grain interactions are not determined by the solid volume fraction alone, but are dependent on particle properties (such as particle friction coefficient and inelasticity) as well as flow properties (such as the shear rate). Consequently, simple additive models are not able to capture the complex constitutive behavior in the transitional regime. Since most constitutive models in use are phenomenological, this observation motivates the development of a constitutive model for the transitional regime that reflects the phase transition based on microscale physical interaction between the grains.

Volfson et al. (2003a) proposed a different approach based on the order parameter (OP) description of granular matter. The OP is defined as the ratio of number of solid–like (enduring) contacts to all contacts in a given sampling volume. The OP attains its maximum value of 1 when the granular matter is in a 'solid' state and takes its minimum value of 0 in the completely 'fluid' limit. They decomposed the total granular

stress σ_{ij} into the sum of a "solidlike" stress σ_{ij}^{s} and a "fluidlike" stress σ_{ij}^{f}. The relative magnitude of the solidlike and fluidlike contributions is a function of the OP. Models are then proposed for the "solidlike" and "fluidlike" contributions, in terms of the total granular stress tensor σ_{ij}. The postulated form of the free energy density function $F(\rho, \delta)$ in Volfson's (Volfson et al., 2003a) work has only two stable states for the OP: either zero, or unity. In this functional form of the free energy density function, ρ corresponds to the order parameter and δ is the ratio of shear to normal stress. The OP values obtained from this procedure need to be validated against DEM data in order to verify this postulated form of the free energy density function. The validity of this free energy density function is examined in this work using DEM simulations. Also the original OP model (Volfson et al., 2003a; Aranson and Tsimring, 2002) does not satisfy the objectivity requirement (Gao et al., 2005).

The original OP model by Volfson et al. (2003a) was generalized to an objective form by Gao et al. (2005), which makes it independent of the coordinate system. The model coefficients of the objective OP model specified by Gao et al. (2005) were obtained by fitting DEM data (obtained from Volfson et al. (2003a)) for 2D inhomogeneous Couette flow with wall boundary conditions. In the present work, new model coefficients for the objective OP model are extracted from data of 3D DEM simulations of homogeneous shear flows. The objective OP model (Gao et al., 2005) is linearized to allow easy inversion of the total granular stress from fluidlike or solidlike stress relations, and it is found that the simple linear model incurs only 11% more error than the full nonlinear model. This linearized OP model with new coefficients is denoted as the refined order parameter (ROP) model. Following Aranson and Tsimring (2002), it is assumed that the fluidlike contribution of the total granular stress can be computed using a constitutive relation from the kinetic theory of granular flows (KTGF) (Lun et al., 1984). The performance of this ROP–KT model is assessed by comparing predicted granular stress with DEM data in different regimes of granular flow.

5.2 Order parameter description of granular 'phase' transition

In a homogeneous granular flow, the OP is defined (Volfson et al., 2003a) as the ratio of the number of space–time averaged "enduring" (solidlike) contacts $\overline{\langle Z_s \rangle}$ to all contacts $\overline{\langle Z \rangle}$ within a sampling volume,

$$\rho \equiv \frac{\overline{\langle Z_s \rangle}}{\overline{\langle Z \rangle}}, \tag{5.1}$$

where $\langle \zeta \rangle$ and $\overline{\zeta}$ stand for averaging of ζ in space and time, respectively. The OP is useful in characterizing two limiting cases: (i) a solidlike state when the granulate is in a state of "enduring" contacts, and (ii) a fluidlike state when it is strongly agitated, i.e., completely fluidlike. In the solidlike state all contacts are enduring and hence $\rho = 1$. In the fluid limit $\overline{\langle Z_s \rangle}$ is zero and $\overline{\langle Z \rangle}$ is small but finite, and therefore $\rho = 0$. Since the OP distinguishes between "solidlike" contacts and "fluidlike" contacts in the granular material, its computation requires a precise definition of these two types of contacts. A contact is considered enduring (solidlike), if it is in stuck state ($F_t < \mu_t F_n$) and its duration is longer than a typical time of collision t^*, which is generally taken as 1.1 times the binary collision time t_c (Volfson et al., 2003a). The first requirement eliminates long–lasting sliding contacts and the second requirement excludes short–term collisions. When either of the requirements is not fulfilled, the contact is defined as "fluidlike".

In order to understand the granular phase transition through the OP, we extract this quantity from 3D DEM simulations of sheared granular flow over a range of solid volume fractions, particle friction coefficients and shear rates. In the following section we describe these 3D DEM simulations of sheared granular flow.

5.3 DEM simulations of sheared granular flow

The OP is extracted by performing three–dimensional (3D) discrete element method (DEM) simulations of monodisperse, non–cohesive spheres of diameter d_0 and mass

m_0 subjected to homogeneous shear over a range of solid volume fractions, particle friction coefficients and shear rates. A soft–sphere model is used in which particles interact via contact laws and friction only on contact. Since the realistic modeling of particle deformation is complicated, a simplified contact force model based on a linear spring–dashpot combination is used in this work (Silbert et al., 2001). Details of the computational model used in the discrete element simulations are given in Sec. 3.1.

These constant–volume DEM simulations of sheared granular flow are performed in a cubical domain of side length $L = 14d_0$, for solid volume fraction ranging from 0.20 to 0.62. The effect of system size is examined by varying the box length from $7d_0$ to $20d_0$. It was found that the stress asymptotes once the box length exceeds $10d_0$, consistent with the estimates reported by Campbell (2002). For all the simulations reported, the mass and diameter of the particles are set to 1, so the density of the particles is $6/\pi$. The value of normal spring stiffness k_n is set to 2×10^5 (in $m_0 g/d_0$ units), which captures the general behavior of intermediate to high k_n systems (Silbert et al., 2001). The value of the coefficient of restitution e is chosen to be 0.7. All these simulations are performed with zero gravity. The integration time step Δt for all the simulations is selected to be $t_c/50$, where t_c is the binary collision time. This time step is shown to be sufficiently small to ensure temporal convergence (Silbert et al., 2001). Simulations are run to a nondimensional time of $\dot{\gamma}t = 500$, which is long enough to attain a statistically stationary solution (Campbell, 2002). After reaching steady state the quantities are time–averaged over a time window corresponding to $200\dot{\gamma}^{-1}$. As a first step we verified our OP calculations with previously published results of Volfson et al. (2003b) for inhomogeneous wall–bounded shear simulation and confirmed that the OP is capable of capturing granular phase transition from solidlike to fluidlike behavior. Results from this study are summarized in Appendix *A*.

5.3.1 Granular rheology through regime map

In order to characterize the physics of granular phase transition and to generate benchmark data for model assessment in different regimes, we performed *homogeneous* shear simulations (where the stress is independent of position) over a wide range of solid volume fractions, shear rates and particle friction coefficients (see Table 5.1). These homogeneous shear simulations are performed with periodic boundary conditions in all directions (x, y, z) and uniform shear is generated in the domain using the "SLLOD" algorithm (Evans and Morriss, 1990). The SLLOD algorithm (Evans and Morriss, 1990) is an improved form of the Lees-Edwards boundary condition (Lees and Edwards, 1972) to generate simple shear flows. The shearing motion induced by the Lees-Edwards boundary condition takes time to develop. Therefore, the flow would not be homogeneous immediately after a shear rate change, which raises questions about the suitability of this algorithm to study homogeneous time–dependent flows. This difficulty can be greatly alleviated through the use of the SLLOD algorithm. The SLLOD algorithm originates from ideas in nonequilibrium statistical mechanics (Evans and Morriss, 1990) where nonequilibrium flows such as shear flow are simulated by applying a force to the entire system (as opposed to simply moving the boundaries of the system faster or slower, as done in Lees-Edwards). Although we do not study time–dependent shear in this article, the SLLOD algorithm was applied to all the simulations performed in this study to be consistent with other work.

Using data obtained from these homogeneous shear simulations we established a comprehensive regime map by assigning each of these simulations different regimes (inertial, intermediate and quasi–static) based on the scaling of shear stress with strain rate. In the inertial regime the stress scales as square of the strain rate ($\sigma \propto \dot{\gamma}^2$) (Bagnold, 1954), whereas in the quasi–static regime stress remains independent of the strain rate ($\sigma \neq f(\dot{\gamma})$) (Campbell, 2002). In between these two extreme regimes there exists

an intermediate regime where stress is related with the strain rate in the form of a power law ($\sigma \propto \dot{\gamma}^n$), where n takes values between 0 to 2 based on particle and flow properties (Tardos et al., 2003).

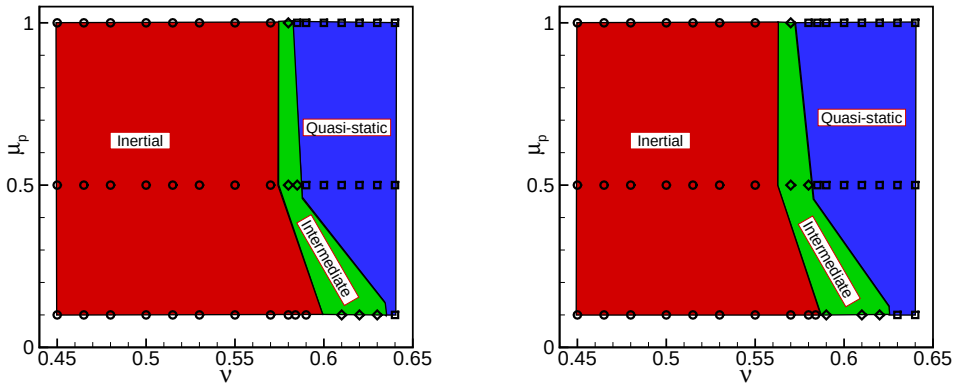

Figure 5.1 Regime map for granular flows, constructed from data of 3D DEM simulations of homogenously sheared granular flow (a) $k^* = k_n/\left(\rho_s d_0^3 \dot{\gamma}^2\right) = 2.5 \times 10^4$ and (b) $k^* = k_n/\left(\rho_s d_0^3 \dot{\gamma}^2\right) = 10^9$. (For interpretation of the references to color in this figure legend, the reader is referred to the web version of this article.)

Figures 5.1(a) and 5.1(b) show the regime maps obtained from these DEM simulations of homogeneously sheared granular flow in the space of solid volume fraction ν and particle friction coefficient μ_p, for non–dimensional shear rates $k^*(k_n/\rho_s d_0^3 \dot{\gamma}^2)$ of 2.5×10^4 and 10^9, respectively. In Figs. 5.1(a) and 5.1(b) the inertial regime ($\sigma \propto \dot{\gamma}^2$) is represented in red, whereas blue indicates the quasi–static regime ($\sigma \neq f(\dot{\gamma})$). In between these regimes, there exists an intermediate regime ($\sigma \propto \dot{\gamma}^n, 0 < n < 2$) which is the green region in Figs. 5.1(a) and 5.1(b). The principal observations concerning granular rheology from these regime maps are:

1. As particle friction coefficient decreases the intermediate regime expands for both k^* values shown. This is important because the friction coefficient for many granular materials (such as glass beads) varies between 0.15 to 0.5, and hence the

expansion of the intermediate regime will affect granular flow in practical devices. Studies performed by Campbell (2002) (for monodisperse system) and Ji and Shen (2008) (for polydisperse system) also confirm this dependence of regime transition on particle friction coefficient in granular media.

2. Figure 5.1(b) shows that at higher k^* the intermediate regime starts at lower values of solid volume fraction, although its extent in solid volume fraction remains the same.

3. For sufficiently low values of k^* (high shear rates) and particle friction coefficient μ_p, the quasi–static regime can completely disappear as seen in Fig. 5.1(a).

There have been other attempts to represent granular rheology of monodisperse systems using similar regime maps. Tardos et al. (2003) presented a schematic of different regimes in powder flow based on the results obtained from their Couette cell experiments. However, the effect of particle friction coefficient was not incorporated in that map. Campbell (Campbell, 2002) proposed a regime map for different values of friction coefficients, however the intermediate regime was not discussed in that work.

5.3.2 OP dynamics from homogeneous shear simulations

As noted earlier, the OP gives one characterization of the phase or state of the granular material. Aranson and Tsimring (2002) in their original work related the OP to the free energy density function $F(\rho, \delta)$, that they specified as:

$$F(\rho, \delta) = \int^{\rho} \rho(\rho - 1)(\rho - \delta) d\rho, \tag{5.2}$$

through the Ginzburg–Landau equation:

$$\frac{D\rho}{Dt} = D_c \nabla^2 \rho - \frac{\partial F(\rho, \delta)}{\partial \rho}. \tag{5.3}$$

Further they postulated that this free energy density function $F(\rho, \delta)$ (Eq. 5.2) has two local minima at $\rho = 1$ (completely solidlike) and $\rho = 0$ (completely fluidlike) to account for bistability near the solid–fluid transition. The relative stability of the two phases is controlled by the parameter δ, which is the ratio of shear to normal stress. For small δ the solidlike state is more favorable, and vice versa. A typical profile of the free energy density function postulated by Aranson and Tsimring (2002), is shown in Fig. 5.2, for different values of δ. While the OP cannot take any values lower than zero and higher than one, a scale which goes below zero and beyond one has been used for the OP in Fig. 5.2 to clearly show that $\rho = 0$ and $\rho = 1$ are the two stable states of the OP for this free energy density function. With the formulation of the free energy density function $F(\rho, \delta)$ in Eq. 5.2, the solution of the Ginzburg–Landau equation (Eq. 5.3) always results in a steady state value of the OP which is either zero (completely fluidlike) or one (completely solidlike), depending on the value of the parameter δ.

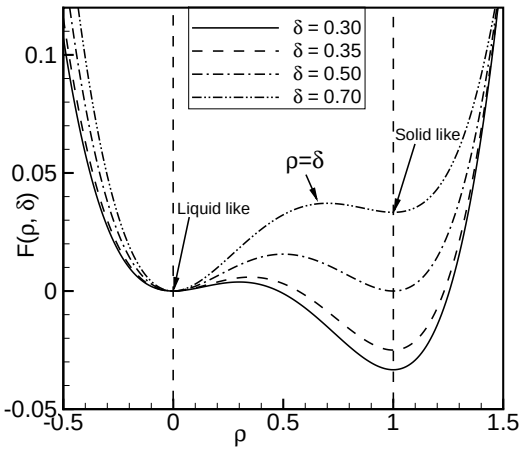

Figure 5.2 Typical profile of the free energy density function $F(\rho, \delta)$ postulated by Aranson and Tsimring (2002).

In order to understand the OP dynamics from DEM simulations, we plot the time

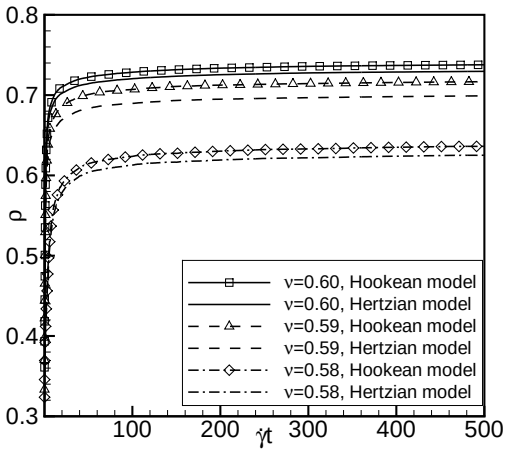

Figure 5.3 Time evolution of the OP obtained from DEM simulations for $\mu_p = 0.5$, $k^* = k_n/\rho_s d_0^3 \dot{\gamma}^2 = 10^5$ and $e = 0.7$.

evolution of the OP in Fig. 5.3 for three different values of the solid volume fraction and with two different contact force models, i.e. Hookean and Hertzian (Silbert et al., 2001). Figure 5.3 shows that the OP evolves with time and attains a steady state value that is neither zero (completely fluidlike) nor one (completely solidlike), irrespective of the two contact force models used. This result reveals that there should be one more intermediate local minimum in the free energy density function postulated by Aranson and Tsimring (2002) (see Eq. 5.2 and Fig. 5.2) at $\rho = \rho_3$, which results in the OP attaining a steady value that is neither zero (completely fluidlike) nor one (completely solidlike). To account for this third granular phase at $\rho = \rho_3$, the following modification to the form of the free energy density function is proposed:

$$F^*(\rho, \delta) = \int^{\rho} \rho(\rho - 1)(\rho - \rho_3)(\rho - \delta)(\rho - \delta^*) d\rho \tag{5.4}$$

Figure 5.4 shows typical profiles of the proposed free energy density function $F^*(\rho, \delta)$ for $\delta = 0.28$, $\rho_3 = 0.60$, $\delta^* = 0.85$, where ρ_3 and δ^* are obtained from DEM simulations. The triangles in Fig. 5.4 corresponds to unsteady evolution of the OP obtained from

DEM simulation for $\nu = 0.59$, $\mu_p = 0.5$, and $e = 0.7$, whereas the circles corresponds to unsteady evolution of the OP obtained from DEM simulations for $\nu = 0.64$, $\mu_p = 1.0$, and $e = 0.7$. These data points also reveal that the OP evolves with time and attains a steady state value that is not necessarily zero or one.

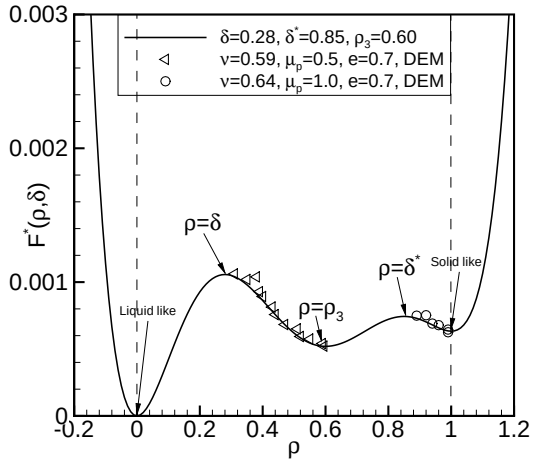

Figure 5.4 Typical profile of proposed free energy density function $F^*(\rho, \delta)$ with third intermediate local minima at $\rho = \rho_3$.

We further study the behavior of the steady value of the OP for different solid volume fractions, particle friction coefficients and shear rates. We note that for all these DEM simulation conditions the steady value of the OP is neither zero not unity, but corresponds to the third stable phase ρ_3 that is dependent on solid volume fraction, particle friction coefficient and shear rate. In Fig. 5.5(a) these steady values of the OP are plotted with solid volume fraction for three different values of the particle friction coefficient. Figure 5.5(a) shows that the OP is indeed a strong function of the particle friction coefficient. An increase of about 300% in the value of the OP is seen when the particle–particle coefficient of friction increases from 0.1 to 1.0 at the same solid volume fraction. This result is expected because at higher interparticle friction the particles

are prevented from sliding over each other, resulting in a greater fraction of solidlike contacts. A sudden jump in the OP is seen near the maximum packing limit. This sudden increase in the OP is ascribed to the presence of strong force chains near the packing limit. Figures 5.5(b)– 5.5(d) shows similar plots of the OP with solid volume fraction as described in Fig. 5.5(a), but for different values of shear rates. These plots (Figs. 5.5(a)– 5.5(d)) show that the OP is most sensitive to the particle–particle friction coefficient, whereas shear rate has the least impact on OP values.

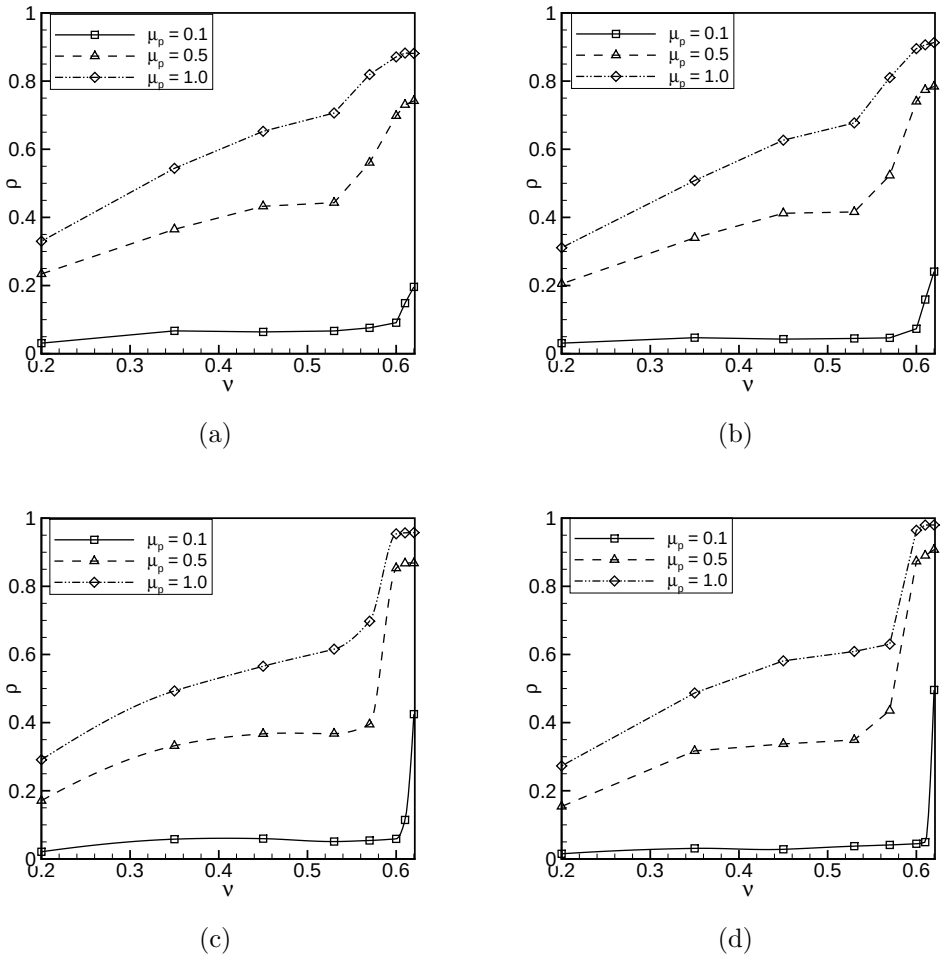

Figure 5.5 The OP (at steady state) plotted with solid volume fraction (a) for $k^* = 2.5 \times 10^4$ and $e = 0.7$, (b) for $k^* = 10^5$ and $e = 0.7$, (c) for $k^* = 10^7$ and $e = 0.7$ and (d) for $k^* = 10^9$ and $e = 0.7$.

Figures 5.5(a)– 5.5(d) reveal that the sudden jump in the OP value (near the maximum packing limit) becomes increasingly sharp as the non–dimensional shear rate $k^*(k_n/\rho_s d_0^3\dot{\gamma}^2)$ increases (going from Fig. 5.5(a) to Fig. 5.5(d)). Also as the particle friction coefficient increases this sudden jump in the OP occurs at progressively lower values of solid volume fraction. This finding is consistent with the results of Song et al. (2008), who studied the jamming of packed spheres through a phase diagram and showed that the minimum solid volume fraction required for jamming decreases with increase in the particle friction coefficient. It is also noteworthy that at the highest value of k^* (which corresponds to lowest shear rate, see Fig. 5.5(d)), the OP attains its limiting value of unity near the maximum packing limit, whereas the OP approaches its other limiting value of zero, when both solid volume fraction and friction coefficient tend towards zero.

Neglecting the small variation of ρ_3 with shear rate k^*, we propose the following fit for ρ_3, the third stable value of the OP, as a function of solid volume fraction ν and friction coefficient μ_p using data shown in Fig. 5.5(b):

$$\rho_3 = \begin{cases} a\sin(b\pi\nu\mu_p) & 0 < \nu \leq \nu^* \\ A\log(B\nu^2\mu_p) + C\exp(\nu^2 - \mu_p) & \nu^* < \nu < \nu_{max}, \end{cases} \tag{5.5}$$

with $a = 0.804$, $b = 0.678$, $A = 0.555$, $B = 6.769$ and $C = 0.685$. In Eq. 5.5, $\nu^* = 0.53$ and ν_{max} is the solid volume fraction corresponding to the close–packed limit. In order to verify the new specification of the free energy density function in Eq. 5.4, we solve the Ginzburg–Landau equation :

$$\frac{D\rho}{Dt} = D_c\nabla^2\rho - \frac{\partial F^*(\rho,\delta)}{\partial\rho}, \tag{5.6}$$

for a homogeneously sheared granular assembly with the specification of ρ_3 in Eq. 5.4 given by the fit in Eq. 5.5. Figure 5.6 shows that the steady solution of the Ginzburg–Landau equation (Eq. 5.6) with the new formulation of free energy density function $F^*(\rho,\delta)$ matches the steady OP values obtained from DEM within 5%, whereas the

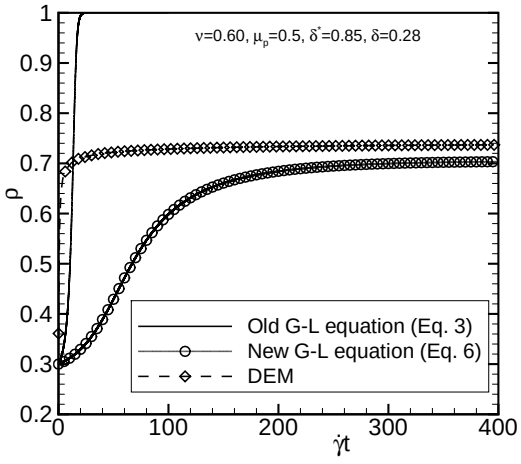

Figure 5.6 Solution of Ginzburg–Landau equation (Eq. 5.6) with new formulation of free energy density function F^* (Eq. 5.4).

original form of the free energy density results in a stable value of unity. This result validates the form of the new free energy density function F^*.

Further we attempt to quantify this third stable phase of the granular material by investigating structural quantities such as the average coordination number N_{CN}, the fabric tensor $\mathbf{R}$ and pair correlation function $g(r)$. These structural quantities are chosen because they are relevant to constitutive modeling of granular rheology (Sun and Sundaresan, 2010). The average coordination number N_{CN} that is defined as the average number of contacts per particle is a measure that is sensitive to the local particle configuration. It has been used to characterize the equilibrium state in static packings (Silbert et al., 2002). The fabric tensor $\mathbf{R}$ describes the anisotropy of the contact distribution in granular media (Bathurst and Rothenburg, 1990; Cowin, 2004). Components of this tensor can be calculated on the basis of particle contact information using:

$$R_{ij} = \frac{1}{N_c} \sum_{c \in V} n_i n_j, \tag{5.7}$$

where R_{ij} is a symmetric second–order fabric tensor, N_c is the number of contacts, n_i

and n_j are the unit vectors corresponding to the contact vector from particle center to point of contact. Figure 5.7 shows the variation of average coordination number N_{CN} and fabric tensor $\mathbf{R}$ (the xz component) with the order parameter ρ. While the average coordination number is sensitive to change in the OP, there is no appreciable change in the fabric tensor for the same change in the OP values. This result indicates that the average coordination number is more sensitive to this phase change as indicated by stable OP values, than the fabric tensor.

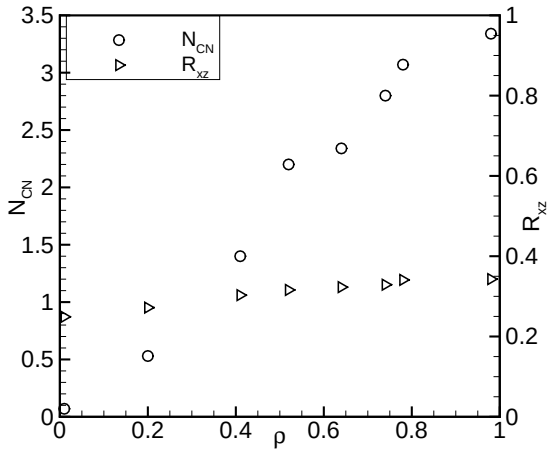

Figure 5.7 Variation of the average coordination number and fabric tensor with the order parameter for a homogeneously sheared granular flow.

Another quantity that gives insight into the microstructure of granular media is the pair correlation function or the radial distribution function $g(r)$ (Silbert et al., 2002; Donev et al., 2005). Figure 5.8(a) shows the pair correlation function corresponding to the third stable granular phase ($\rho_3 = 0.64$). The first peak (at $r = d_0$) corresponds to the high probability of having a neighbor in contact. We also observed a secondary peak at $r = 2d_0$, and this secondary peak in $g(r)$ diminishes with increase in the particle friction coefficient μ_p (result not shown here). This behavior of $g(r)$ with particle friction

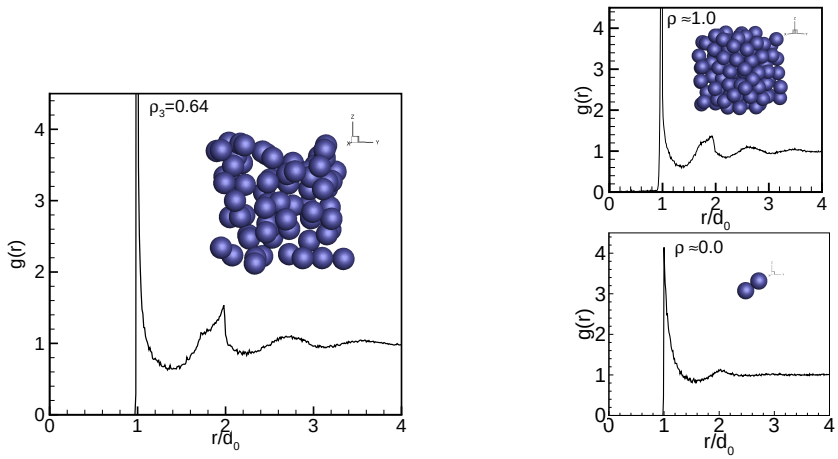

(a) (b)

Figure 5.8 (a) The pair correlation function corresponding to the third stable phase ($\rho_3 = 0.64$), inset shows the corresponding snapshot of internal structure for the solidlike contacts at this third stable phase and (b) The pair correlation function corresponding to $\rho \approx 1.0$ (completely solidlike phase) and $\rho \approx 0.0$ (completely fluidlike phase), respectively. Inset shows the corresponding snapshots of internal structure for the solidlike contacts for these two limiting phases.

coefficient has been previously observed by Silbert et al. (2002) in their numerical simulations. Inset of Fig. 5.8(a) shows an instantaneous realization of the internal structure (shown in a cube of $4d_0$, note that the pair correlation function has reached its uniform value of one by $r = 4d_0$) for the solidlike contacts corresponding to this third stable granular phase. Figure 5.8(b) shows the pair correlation function corresponding to the OP value of 1.0 (completely solidlike phase) and 0.0 (completely fluidlike phase), respectively. Inset shows an instantaneous realization of the corresponding internal structure of the solidlike contacts for these two limiting phases. The lower panel of Fig. 5.8(b) shows that in the completely fluidlike state ($\rho \approx 0$), the third peak in the pair correlation function disappears, whereas it is seen in the other two states. The instantaneous structures confirm the behavior of the average coordination number with the OP: namely, the average coordination number is clearly a strong function of the steady OP value as evidenced by the difference in number of contacting particles in the realization.

In a previous study by Jaeger et al. (1996) described different regimes of granular flow (i.e. solid, liquid and gas) where they point out the lack of scale separation in granular liquids, the tight coupling between scales in granular solids, and the importance of inelasticity and energy loss in granular gases. They relate the different regimes to the interaction between grains and force networks. The characterization of granular flow in the current work using the OP and other structural quantities follows the same ideas by exploring the coupling between mesoscale structure and macroscale rheology. We have shown that the connection between structure and grain interaction is provided by the OP dependence on the particle properties such as interparticle friction. Forterre and Pouliquen (2008) characterized regimes of granular flow using the contact time between grains. This idea is closely related to the current work, where the contact time between grains forms an integral part of the definition of the OP.

It should also be noted that, the third steady state observed in the current study, is combination of 'fluidlike' and 'solidlike' states. It is a stable state between completely

fluidlike and completely solidlike states. Any value of the OP between zero and one represent a state where some of the contacts are 'solidlike' and the remaining are 'fluidlike'. However, in the original definition of the OP by Volfson et al. (2003a), only $\rho = 0$ qualifies as completely fluidlike and $\rho = 1$ qualifies as completely solidlike. The pair correlation function corresponding to third stable phase (shown in Fig. 5.8(a)) suggests that the new granular phase is indeed 'liquidlike'. With this better understanding of the OP dynamics in hand, the next step is to explore and improve the objective OP model (Gao et al., 2005) in order to make it tractable.

5.4 Order parameter model description and refinement

5.4.1 OP model description

The original order parameter model was developed by Aranson, Tsimring and Volfson in a series of papers (Aranson and Tsimring, 2002; Volfson et al., 2003b,a). The fundamental premise of this model is that one can define an OP in granular flows similar to that used in the Landau theory of phase transitions (Landau and Lifshitz, 1980). This original OP model (Volfson et al., 2003b) decomposes the total granular stress tensor into "solidlike" and "fluidlike" contributions based on the OP. The OP model gives expressions for the "solidlike" and "fluidlike" stress tensors that are functions of the order parameter ρ and the total granular stress tensor σ_{ij}. In the original Aranson and Tsimring (2002) OP theory, the fluidlike stress was modeled using a constitutive relation from the KTGF (kinetic theory of granular flows), and the total granular stress and solidlike contribution were obtained through relations that are coordinate– system dependent.

This original OP model by Volfson et al. (2003b) is generalized to an objective form by Gao et al. (2005). The objective expressions for σ_{ij}^{f}, the "fluidlike" contribution, and σ_{ij}^{s}, the "solidlike" contribution to the total granular stress, which are coordinate system

independent, are (Gao et al., 2005):

$$\sigma_{ij}^{f} = \sigma_0\{\alpha\delta_{ij} + \beta b_{ij} + \gamma[(b^2)_{ij} - \frac{1}{3}(b^2)_{ll}\delta_{ij}]\}, \tag{5.8}$$

$$\sigma_{ij}^{s} = \sigma_0\{(1-\alpha)\delta_{ij} + (1-\beta) b_{ij} - \gamma[(b^2)_{ij} - \frac{1}{3}(b^2)_{ll}\delta_{ij}]\}, \tag{5.9}$$

where $\sigma_0 = \sigma_{ii}/3$ is the scale of stress (summation is implied over repeated indices). In Eqs. 5.8 and 5.9, b_{ij} is the normalized, symmetric, anisotropy tensor defined as,

$$b_{ij} = \frac{\sigma_{ij}}{\sigma_0} - \delta_{ij}. \tag{5.10}$$

The components of the second–order tensor b^2 are defined as:

$$(b^2)_{ij} = b_{ik} b_{kj}, \tag{5.11}$$

and $(b^2)_{ll}$ is a scalar that is defined as,

$$(b^2)_{ll} = b_{lk} b_{kl}. \tag{5.12}$$

The significance of the model coefficients, α, β and γ is as follows. The coefficient γ represents the degree of nonlinearity in the model, so $\gamma = 0$ results in a linear model. If we consider a linear model, then α and β represent the respective weight factors that multiply the isotropic and deviatoric parts of the total granular stress, to obtain the fluidlike stress. If $\alpha = \beta$ in the linear model, then the fluidlike stress is coaxial with the total granular stress (and then so is the solidlike part). These model coefficients α and β are functions of the order parameter ρ, which are specified in Gao et al. (2005) as:

$$\alpha = (1-\rho)^{1.8}, \tag{5.13}$$

$$\beta = (1-\rho)^{2.5}. \tag{5.14}$$

These model coefficients were obtained using DEM data from 2D inhomogeneous Couette flow with wall boundary conditions. It should be noted that in 2D the term in γ is redundant, and there are only two coefficients α and β, because the characteristic

equation for the stress tensor is a quadratic (instead of a cubic for the 3D case), and there are only two invariants: the sum and product of the two principal values of the stress tensor. A complete specification of the objective OP model requires data from 3D DEM simulations in order to calculate all three coefficients (α, β , and γ), and in this case the nonlinear term may not be zero. We obtained model coefficients from 3D DEM data of homogeneously sheared granular flow to specify a complete set of coefficients for the objective OP model.

5.4.2 Refinement of the OP model

The model coefficients α, β and γ for the objective OP model (Gao et al., 2005) that best fit the fluidlike stress tensor σ_{ij}^{f} relation given by Eq. 5.8 are computed using 3D DEM data for the total granular stress σ_{ij} (for which σ_0 and b_{ij} are computed) and fluidlike stress σ_{ij}^{f} from homogeneous shear flow simulations. In a 3D granular flow there are six independent non–zero components for the fluidlike stress tensor (assuming the stress tensor is symmetric). As there are three unknowns model coefficients, α, β and γ and six equations for the fluidlike stress, one can only solve the system of equations using a least–squares method. We solve this set of equations over a range of flow conditions (simulation parameters for these cases are summarized in Table 5.1) for which we performed DEM simulations, and the corresponding OP values for each of these flow conditions corresponds to the abscissas of the data points in Fig. 5.9(a). The ordinate of the data points in Fig. 5.9(a) corresponds to the least–squares solutions for the model coefficients obtained using this method. Figure 5.9(a) shows the variation of model coefficients α, β and γ with the OP, and the lines are a polynomial fit to the data. The coefficients α and β are very nearly equal, indicating that the fluidlike stress is nearly coaxial with the total granular stress, although not exactly so. Note that the magnitude of the third model coefficient γ remains close to zero for the complete range of OP values. Since the model coefficient γ determines the magnitude of the nonlinear

Table 5.1 Parameters for homogeneous shear simulations.

Solid volume fraction	Particle friction coefficient	Shear rate (k^*)
0.45	$0.1, 0.5, 1.0$	$2.5 \times 10^4, 10^5, 10^7, 10^9$
0.53	$0.1, 0.5, 1.0$	$2.5 \times 10^4, 10^5, 10^7, 10^9$
0.57	$0.1, 0.5, 1.0$	$2.5 \times 10^4, 10^5, 10^7, 10^9$
0.58	$0.1, 0.5, 1.0$	$2.5 \times 10^4, 10^5, 10^7, 10^9$
0.59	$0.1, 0.5, 1.0$	$2.5 \times 10^4, 10^5, 10^7, 10^9$
0.60	$0.1, 0.5, 1.0$	$2.5 \times 10^4, 10^5, 10^7, 10^9$
0.62	$0.1, 0.5, 1.0$	$2.5 \times 10^4, 10^5, 10^7, 10^9$

terms in Eq. 5.8, this indicates the possibility of forming a linear model.

The model coefficients α and β corresponding to a linear objective model are computed by dropping the term containing γ in Eq. 5.8, and performing the least–squares solution of Eq. 5.15:

$$\sigma_{ij}^f = \sigma_0\{\alpha\delta_{ij} + \beta b_{ij}\}. \tag{5.15}$$

Figure 5.9(b) shows model coefficients α and β with the OP for the proposed linear

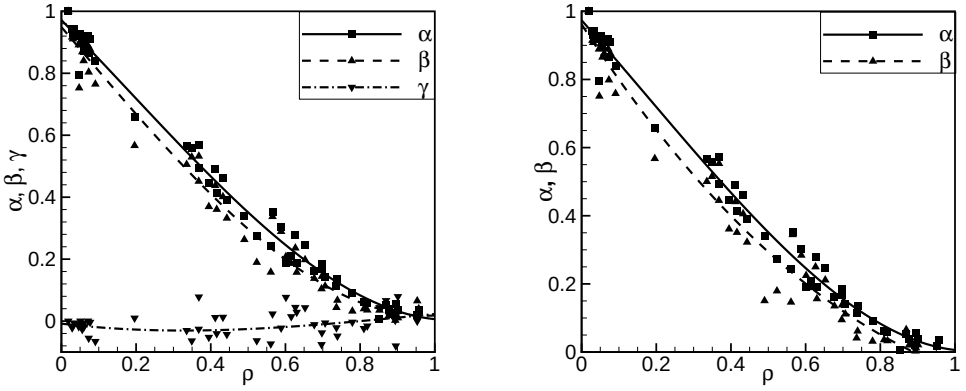

(a) (b)

Figure 5.9 The objective OP model coefficients as a function of the order parameter (a) for a nonlinear objective model and (b) for a linear objective model.

objective model. At $\rho = 0$, the model coefficients α and β are equal to unity, which

indicates that the total granular stress is solely due to fluidlike contribution. At $\rho = 1$, the model coefficients α and β are zero, which indicates that the total granular stress is due to only the solidlike contribution. The error incurred in both (nonlinear and linear) objective models is quantified by the vector norm of the relative error in the least–squares solution:

$$\hat{\epsilon} = \frac{||\mathbf{Kx} - \mathbf{y}||_2}{||\mathbf{y}||_2}, \tag{5.16}$$

where $\mathbf{x}$ is the solution vector for the model coefficients, $\mathbf{Kx}$ is the total granular stress components given by the OP model and $\mathbf{y}$ is the total granular stress from DEM.

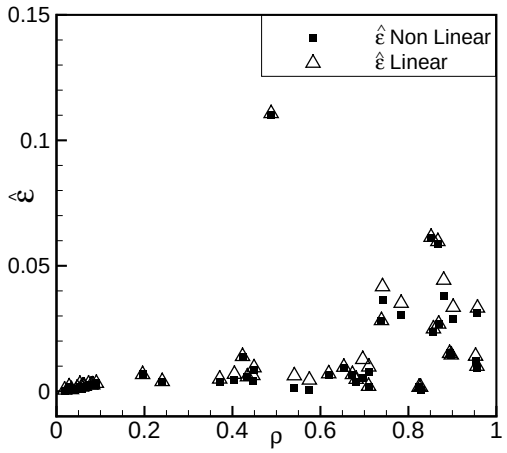

Figure 5.10 Error in the total granular stress objective models as a function of the OP for both linear and nonlinear models.

The error incurred in terms of this vector norm is shown in Fig. 5.10 for the complete range of OP, for both nonlinear and linear objective models. As Fig. 5.10 shows, the error incurred in both the objective models is less than 11%. The percentage error incurred in the linear model is approximately same as the error incurred in the nonlinear model. Therefore, a linear version of the objective OP model with new model coefficients extracted from 3D DEM data of homogeneous shear flow is now proposed. This linear

version of the objective OP model is referred to as the refined order parameter (ROP) model. In the following section we present the complete specification of the proposed ROP model.

5.5 Specification of the ROP model

The model equations for the proposed linear ROP model are:

$$\sigma_{ij}^{f} = \sigma_0\{\alpha\delta_{ij} + \beta b_{ij}\}, \tag{5.17}$$

$$\sigma_{ij}^{s} = \sigma_0\{(1-\alpha)\delta_{ij} + (1-\beta)b_{ij}\}. \tag{5.18}$$

The model coefficients (α and β) of the linear ROP model are specified as polynomial fits to the data in Fig. 5.9(b) with

$$\alpha = a + b\rho + c\rho^2 + d\rho^3, \tag{5.19}$$

where $a = 1.0$, $b = -1.23$, $c = -0.31$ and $d = 0.54$, and

$$\beta = A + B\rho + C\rho^2 + D\rho^3, \tag{5.20}$$

with $A = 1.0$, $B = -1.69$, $C = 0.76$ and $D = -0.07$. Specification for the order parameter ρ is taken from its steady values obtained from DEM simulations (as shown in Figs. 5.5(a)– 5.5(d)). The advantage of the linear ROP model is that now the total granular stress can be inverted from the solidlike and fluidlike stress relations, as follows:

$$\sigma_{ij} = \frac{\sigma_0}{\beta}\left[\frac{\sigma_{ij}^{f}}{\sigma_0} + \delta_{ij}(\beta - \alpha)\right], \tag{5.21}$$

where $\sigma_0 = \sigma_{ii}^{f}/(3\alpha)$. One should note that Eq. 5.21 diverges as the order parameter goes to unity (its solidlike limit), reflecting the fact that the ROP–KT model for the total stress does not contain any information about the solidlike stress.

Previously Aranson and Tsimring (2002) showed that a constitutive relation from the kinetic theory for the fluidlike stress gave a good match for the kinematic variables

in dense chute flow. Therefore, we follow Aranson and Tsimring (2002) and model the "fluidlike" stress using a constitutive relation from the kinetic theory of granular flows (KTGF) even in the dense regime. Once the fluidlike contribution of the total granular stress is known, the total granular stress tensor σ_{ij} can be expressed in terms of the "fluidlike" stress and the ROP model coefficients (α and β) using Eq. 5.21. The kinetic theory closures are taken from Lun et al. (1984) to compute the fluidlike contribution of the total granular stress tensor, which are:

$$\sigma_{ij}^{f} = \left[\rho_s \nu \left(1 + 4\eta_k \nu g_0\right) T - \eta_k \mu_b \nabla \cdot \mathbf{u}\right] \delta_{ij} - \left(\frac{2+\alpha_k}{3}\right) \times \left\{\frac{2\mu}{g_0 \eta_k \left(2-\eta_k\right)} \left(1 + \frac{8}{5}\nu\eta_k g_0\right) \left[1 + \frac{8}{5}\eta_k \left(3\eta_k - 2\right) g_0\right] + \frac{6}{5}\eta_k \mu_b\right\} S_{ij}, \tag{5.22}$$

$$S_{ij} = \frac{1}{2}\left(\frac{\partial u_i}{\partial x_j} + \frac{\partial u_j}{\partial x_i}\right) - \frac{1}{3}\frac{\partial u_i}{\partial x_i}, \tag{5.23}$$

$$\mu = \frac{5\rho_s d_0 (\pi T)^{1/2}}{96}, \tag{5.24}$$

$$\mu_b = \frac{256\mu\nu^2 g_0}{5\pi}, \tag{5.25}$$

$$\eta_k = \frac{(1+e)}{2}, \tag{5.26}$$

$$g_0\left(\nu\right) = \frac{1}{1 - \left(\nu/\nu_{max}\right)^{1/3}}, \tag{5.27}$$

$$\alpha_k = 1.3, \tag{5.28}$$

where σ_{ij}^{f} is the fluidlike part of the stress tensor, ρ_s is the density of the solid particle, ν is the solid volume fraction, T is the granular temperature, $\mathbf{u}$ is the mean velocity vector, and S_{ij} is the strain rate tensor. For inhomogeneous granular flows the granular temperature T is obtained as the solution to a transport equation (Lun et al., 1984). However, for homogeneous shear flows the granular temperature can be obtained through a simple algebraic relation.

5.5.1 Homogeneous shear case

For a steady homogeneously sheared granular flow the granular temperature results from a balance of production and dissipation terms. This balance results in a algebraic equation for the granular temperature T (MFIX, 1993):

$$T = \left\{ \frac{-K_1 \nu S_{ii} + \sqrt{{K_1}^2 (S_{ii})^2 \nu^2 + 4K_4 \nu \left[K_2 (S_{ii})^2 + 2K_3 \left(S_{ij} S_{ij}\right)\right]}}{2\nu K_4} \right\}^2, \tag{5.29}$$

where constants K_1, K_2, K_3 and K_4 are:

$$K_1 = 2\left(1+e\right)\rho_s g_0 \tag{5.30}$$

$$K_2 = 4 d_0 \rho_s \left(1+e\right)\nu g_0 / \left(3\sqrt{\pi}\right) - \frac{2}{3} K_3 \tag{5.31}$$

$$\begin{aligned} K_3 = & \frac{d_0 \rho_s}{2}\left[\frac{\sqrt{\pi}}{3\left(3-e\right)}\left[0.5\left(3e+1\right)\right.\right. \\ & \left.\left. +0.4\left(1+e\right)\left(3e-1\right)\nu g_0\right] + \frac{8\nu g_0 \left(1+e\right)}{5\sqrt{\pi}}\right] \end{aligned} \tag{5.32}$$

$$K_4 = \frac{12\left(1-e^2\right)\rho_s g_0}{d_0\sqrt{\pi}}. \tag{5.33}$$

We extract the granular temperature using Eq. 5.29, and compare those values to the

Table 5.2 Comparison of granular temperature $\hat{T} = T/(d_0\dot{\gamma})^2$ obtained from Eq. 5.29 and DEM. The last column shows the corresponding OP values from DEM data. Simulation parameters: $\mu_p = 0.5$, $e = 0.7$ and $k^* = k_n/\left(\rho_s d_0^3 \dot{\gamma}^2\right) = 10^5$.

Solid volume fraction	Algebraic Equation	DEM	OP
0.45	0.529	0.603	0.412
0.53	0.514	0.570	0.416
0.58	0.508	0.553	0.542
0.60	0.505	0.550	0.740
0.62	0.503	0.528	0.784

granular temperature obtained from DEM simulations in Table 5.2. The interparticle

friction coefficient used for these simulations is 0.5, with a coefficient of restitution of 0.7. The non-dimensional shear rate $k^*(k_n/\rho_s d_0^3\dot{\gamma}^2)$ is set to be 10^5 for this comparison. Table 5.2 shows that the maximum difference in the steady state granular temperature obtained from the algebraic equation (Eq. 5.29) and DEM simulation is less than 14% over the range of solid volume fractions considered.

With the specification of the fluidlike contribution to the total granular stress σ_{ij}^f and the model coefficients (α and β), one can solve the ROP model to obtain the total granular stress σ_{ij} using Eq. 5.21. The next step is to assess the performance of the proposed ROP model, which is presented in the following section.

5.6 Assessment of the ROP model for homogeneous shear flows

The ROP model with the constitutive relation for the fluidlike stress contribution obtained from the kinetic theory of granular flows is denoted the ROP–KT model. The ROP–KT model's predictions for the total granular stress are compared with those from DEM simulations of homogeneously sheared granular flow in different regimes that are characterized by a regime map in Fig. 5.1(a). The validity of the kinetic theory closure for the fluidlike stress is also assessed in different regimes by comparing σ_{ij}^f with the corresponding fluidlike stress tensor obtained from DEM data.

5.6.1 Inertial regime (solid volume fraction of 0.45)

Figure 5.11(a) shows a logarithmic plot of the elastic scaling of the shear component of the total granular stress as a function of shear rate for a solid volume fraction of 0.45. In this scaling, stress values in the inertial regime where $\sigma \propto \dot{\gamma}^2$ correspond to a line with slope -1 (in Fig. 5.11(a) the slope of the line is denoted by m). The shear component of the total granular stress obtained from the ROP–KT model is shown by

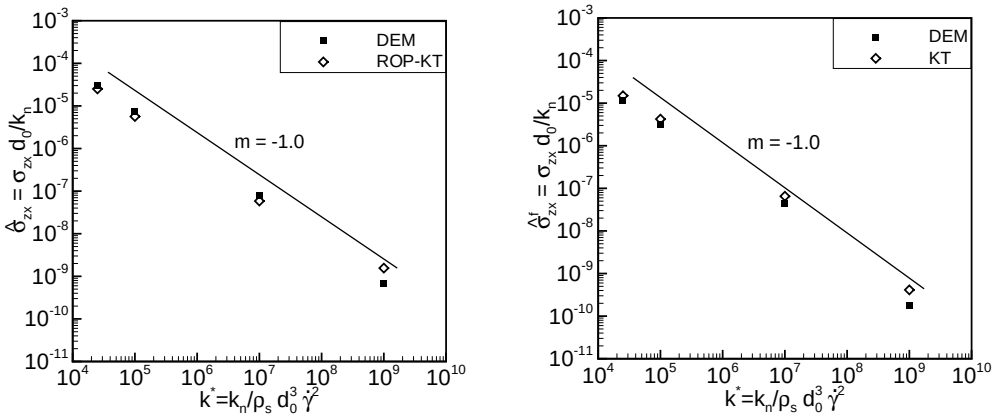

(a) (b)

Figure 5.11 (a) The total granular stress as a function of shear rate k^* and (b) The fluidlike stress contribution to the total granular stress as a function of shear rate k^*. Simulation parameters: $\nu = 0.45$, $\mu_p = 0.5$, $e = 0.7$.

blank diamonds, whereas the filled squares show the data from DEM simulations. The total granular stress predicted using ROP–KT model closely follows the data obtained from the DEM simulations. The ROP–KT model is able to predict the total granular stress in the inertial regime within 5%. The total granular stress obtained from both, the model and DEM follows the inertial scaling ($\sigma \propto \dot{\gamma}^2$) of stress with applied shear rate. Figure 5.11(b) shows that the fluidlike contribution to the total granular stress obtained using kinetic theory closely follows the fluidlike stress contribution obtained from DEM simulations. Both the DEM data and predictions obtained from kinetic theory follow inertial scaling ($\sigma \propto \dot{\gamma}^2$) with the shear rate. This type of scaling of the shear stress with the applied shear rate has been previously reported by Campbell (2002) in the inertial regime.

5.6.2 Near transitional regime (solid volume fraction of 0.53)

In order to quantify the performance of the ROP–KT model near the transition from inertial to intermediate regime, we considered a higher solid volume fraction of 0.53. Figure 5.12(a) compares the total granular stress predicted by ROP–KT model with data from the DEM simulations. In the near transitional regime ($\nu = 0.53$) the ROP–KT model predicts the total granular stress well (see Fig. 5.12(a)), with an maximum error of 5% when compared with the DEM data. At this volume fraction there are multiparticle contacts as indicated by the mean coordination number value of 1.6 obtained from DEM simulations (result not shown here).

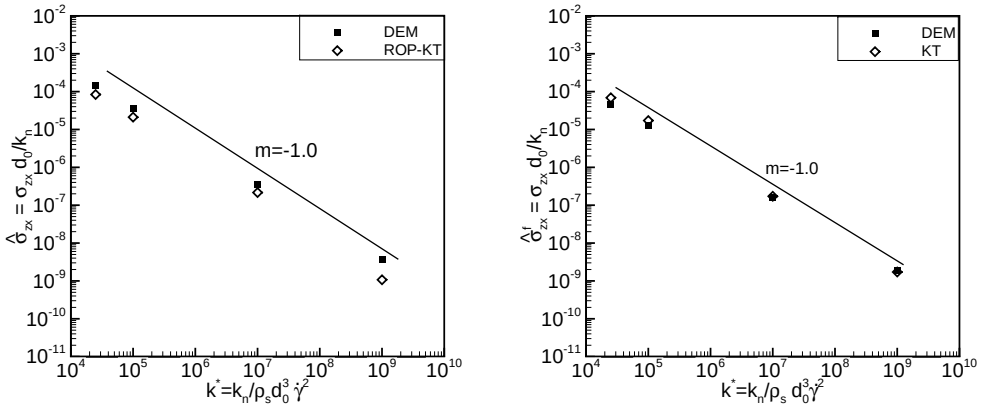

(a) (b)

Figure 5.12 (a) The total granular stress as a function of shear rate k^* and (b)The fluidlike stress contribution to the total granular stress as a function of shear rate k^*. Simulation parameters: $\nu = 0.53$, $\mu_p = 0.5$, $e = 0.7$.

In Fig. 5.12(b) the variation of the fluidlike contribution of the stress obtained from kinetic theory as well as from the DEM data is shown. This plot shows that the kinetic theory closure performs surprisingly well in predicting the fluidlike stress contribution when compared with the DEM data.

5.6.3 Deep intermediate regime (solid volume fraction of 0.62)

To assess the performance of the ROP–KT model in the deep intermediate regime, we selected a case with solid volume fraction of 0.62 and interparticle friction coefficient of 0.1. At this solid volume fraction the ROP–KT model does not predict either the magnitude or the scaling of the total granular stress (Fig.5.13(a)) or the fluidlike stress (Fig.5.13(b)) correctly. The fluidlike contribution obtained from DEM data clearly shows the intermediate scaling of the stress ($\sigma \propto \dot{\gamma}^n, n = -2m = 0.66$) with shear rate, whereas the kinetic theory closure necessarily follows the inertial scaling of the stress ($\sigma \propto \dot{\gamma}^2$) with applied shear rate.

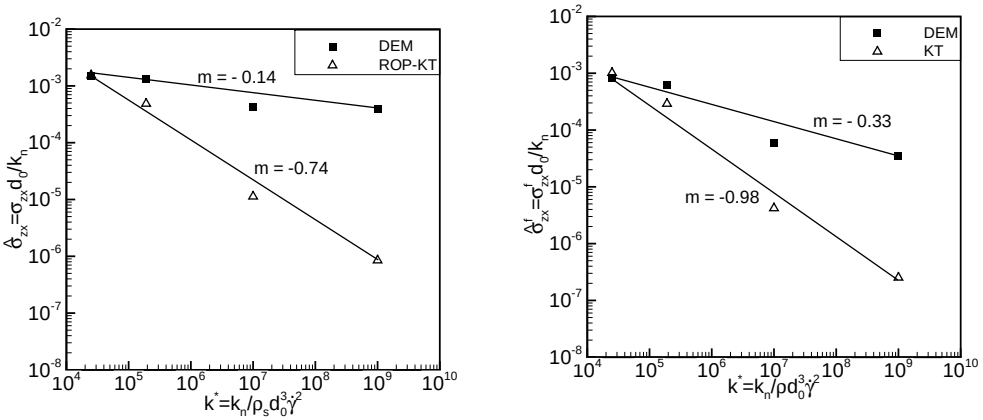

(a) (b)

Figure 5.13 (a) The total granular stress as a function of shear rate and (b) Fluidlike stress contribution to the total granular stress as a function of shear rate. Simulation parameters: $\nu = 0.62$, $\mu_p = 0.1$, $e = 0.7$.

Although the ROP–KT model decomposes the total granular stress into solidlike and fluidlike parts, unlike other models (Savage, 1998; Johnson and Jackson, 1987; Srivastava and Sundaresan, 2003) the weighting factors for these contributions depends on the shear rate and particle friction coefficient through the OP (see Eqs. 5.19 and 5.20). Note that as a consequence the total granular stress predicted by the ROP–KT model actually

shows an intermediate scaling ($\sigma \propto \dot{\gamma}^2, n = -2m = 1.48$) with shear rate, even though the fluidlike stress follows a inertial scaling.

5.6.4 Summary of ROP model performance

Based on this assessment study, we conclude that the ROP–KT model has the capability to accurately predict the total granular stress up to a solid volume fraction of 0.53. As the solid volume fraction exceeds 0.53 the flow transitions to the intermediate regime and the ROP–KT model fails to capture the correct trend of shear stress with shear rate. The differences in the magnitude of the stress prediction in the intermediate regime is attributed to the fact that the ROP–KT model assumes that the fluidlike stress contribution follows the kinetic theory closure even in the dense regime. However, this assumption does not hold in the deep intermediate regime where both collision and frictional interactions between the particles are important. Although the ROP model coefficients α and β include a dependence on shear rate and particle friction coefficient through the OP, this dependence is not able to accurately predict the stress–strain scaling in the deep intermediate regime of flow.

5.7 Performance evaluation of different constitutive models in the intermediate regime

The performance of different constitutive models is assessed in the intermediate regime of granular flow. In Fig. 5.14, the shear component of the total granular stress is plotted with shear rate for a solid volume fraction of 0.62 with interparticle friction coefficient of 0.1 (this combination of solid volume fraction and particle friction coefficient corresponds to the intermediate regime).

The different constitutive models assessed are listed below:

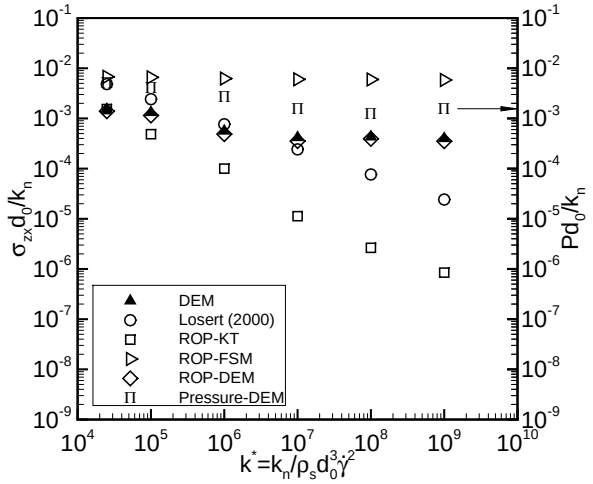

Figure 5.14 Shear component of the total granular stress (different symbols represent result obtained with different constitutive models) plotted with shear rate. Simulation parameters: $\nu = 0.62$, $\mu_p = 0.1$, $e = 0.7$.

1. Losert (2000): Losert et al. (2000) proposed a constitutive model with density–dependent viscosity. The shear stress in this model is given as,

$$\sigma_{xy} = \eta\dot{\gamma} \tag{5.34}$$

where viscosity is a function of the density as follows,

$$\eta = (\nu_{max} - \nu)^{-1.75}. \tag{5.35}$$

Figure 5.14 shows that the shear stress predicted using this model fails to capture the correct scaling of shear stress with shear rate in the intermediate regime. It should be noted that this model (Losert et al., 2000) was proposed based on the experimental data obtained from shear flow of granular material in a Couette geometry.

2. ROP–KT: This is the constitutive model proposed in present work, where the ROP model is coupled with the kinetic theory of granular flows (KTGF) (Lun et al.,

1984) for the fluidlike stress contribution of the total granular stress. As discussed earlier, this model fails to capture the correct trends of shear stress with shear rate in the deep intermediate regime.

3. ROP–FSM: A frictional stress model (FSM) is proposed by Srivastava and Sundaresan (2003) for the frictional part of the total granular stress. The FSM model is used to compute the solidlike stress contribution σ_{ij}^s and then the ROP model is solved to obtain the total granular stress as follows:

$$\sigma_{ij} = \frac{\sigma_0}{(1-\beta)}\left[\frac{\sigma_{ij}^s}{\sigma_0} + \delta_{ij}(\beta+\alpha)\right], \tag{5.36}$$

where $\sigma_0 = \sigma_{ii}^s/3(1-\alpha)$. One should note that Eq. 7.53 diverges as the order parameter goes to zero (its fluidlike limit), which reflects that the ROP–FSM model for the total stress does not contain any information about the fluidlike stress. This frictional stress model is based on the critical state theory of soil mechanics. At the critical state the granular assembly deforms without any volume change and the frictional contribution of the stress is given by:

$$\frac{\boldsymbol{\sigma}^{fric}}{p_c(\nu)} = \mathbf{I} - \sqrt{2}\sin\phi\frac{\mathbf{S}}{\sqrt{\mathbf{S}:\mathbf{S}}}, \tag{5.37}$$

where the form for $p_c(\nu)$ (critical state pressure) is taken from Johnson and Jackson (1987)

$$p_c(\nu) = \begin{cases} F\frac{(\nu-\nu_{min})^r}{(\nu_{max}-\nu)^s} & \text{if } \nu > \nu_{min} \\ 0 & \text{if } \nu \leq \nu_{min} \end{cases} \tag{5.38}$$

where F, r and s are constants, taken from Srivastava and Sundaresan (2003). As shown in Fig. 5.14, this model when coupled with the ROP model for the solidlike stress contribution predicts stresses that are independent of the shear rate (a behavior characteristic of the quasi–static regime). However, the data obtained from the DEM simulations show a dependency of shear stress on shear

rate in this regime. The ROP–FSM results show that it is not simply a matter of modeling the fluidlike or solidlike parts of the total granular stress. Rather, what is lacking is a fundamental description of the dependence of stress on strain rate in the intermediate regime.

4. ROP–DEM: In this constitutive model, the fluidlike contribution to the total granular stress is supplied from the DEM data and then the ROP model (see Eq. 5.21) is solved to compute the total granular stress. Figure 5.14 shows that, the ROP–DEM model is capable of predicting the total granular stress accurately (within 5%) even in the intermediate regime, provided the fluidlike (or the solidlike) stress contribution is taken from the DEM data. This result shows that the limitation is not in the objective ROP model concept, but in the constitutive model for the fluidlike (or solidlike) stress contributions in the intermediate regime.

Figure 5.14 also shows the variation of the isotropic pressure (right vertical axis) obtained from the DEM simulations with shear rate for a homogeneously sheared granular assembly. This plot shows that the pressure follows the same scaling with shear rate as the shear stress in the intermediate regime. Hence, it is important for a constitutive model to capture the correct behavior of the pressure with strain rate in the intermediate regime.

5.8 Decomposition of the total granular stress from DEM

In order to better understand the scaling of the granular stress in the intermediate regime, the total granular stress obtained from DEM simulations is first decomposed into contact (virial) and streaming (dynamic) contributions. The contact contribution due to particle contacts in a domain of volume V is given by

$$\boldsymbol{\sigma}^{\text{contact}} = \frac{1}{V}\sum_{i}^{N}\sum_{j,j\neq i}\frac{1}{2}\mathbf{r}^{(i)(j)} \otimes \mathbf{f}^{(i)(j)}, \tag{5.39}$$

where $\mathbf{r}^{(i)(j)}$ is the vector pointing from the center of particle j to the center of particle i, $\mathbf{f}^{(i)(j)}$ is the contact force acting on particle i by particle j, and $\otimes$ denotes a dyadic product. The streaming contribution arises from momentum flux and is given as

$$\boldsymbol{\sigma}^{\text{streaming}} = \frac{1}{V}\sum_{i}^{N} m_0^{(i)} \mathbf{v}'^{(i)} \otimes \mathbf{v}'^{(i)}, \tag{5.40}$$

where m_0 is the mass of a particle, $\mathbf{v}'$ is the fluctuating velocity and i is a particle index. In Fig. 5.15(a) the contact contribution to the total granular stress is plotted

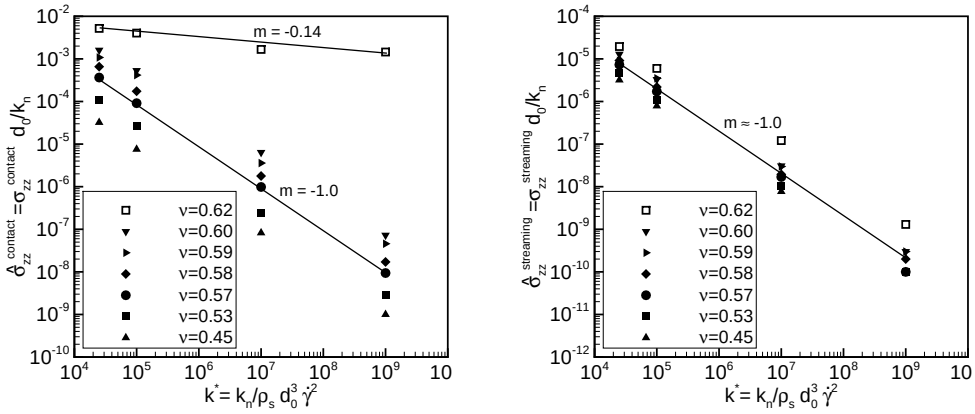

Figure 5.15 (a) Contact (virial) contribution of the total granular stress as a function of shear rate and (b) Streaming (dynamic) contribution of the total granular stress as a function of shear rate. Simulation parameters: $\mu_p = 0.1$, $e = 0.7$. The data points corresponding to the intermediate regime are shown with blank square symbols.

with shear rate for a range of solid volume fractions. Figure 5.15(a) shows that the contact contribution of the total granular stress follows the same scaling ($\sigma \propto \dot{\gamma}^n, n = -2m = 0.28$) with shear rate as the total granular stress in the intermediate regime (data points corresponding to the intermediate regime are shown with blank squares). However, the streaming contribution (shown in Fig. 5.15(b)) of the total granular stress in the intermediate regime still follows the inertial scaling of the stress ($\sigma \propto \dot{\gamma}^2$) with

the shear rate. As expected, at this high value of the solid volume fraction the contact part of the stress contributes more than 95% to the total granular stress. Hence it is critical for the performance of any constitutive model in the dense regime to accurately capture the behavior of the contact stress.

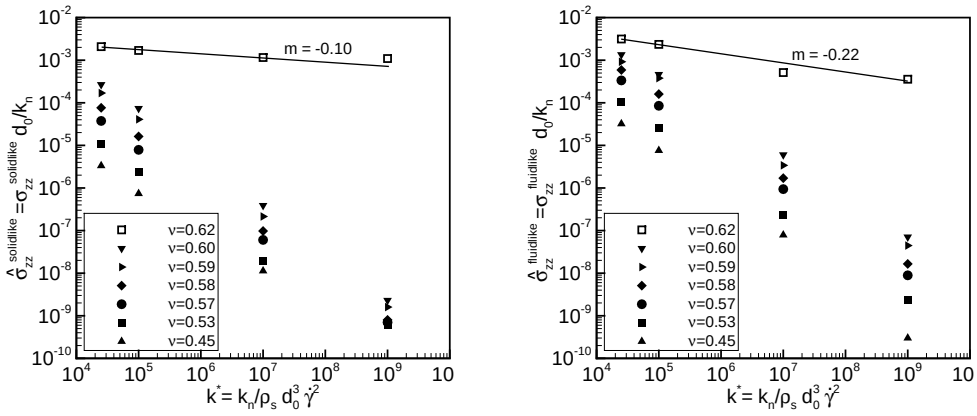

(a) (b)

Figure 5.16 (a) Solidlike contribution of the total granular stress as a function of shear rate and (b) Fluidlike contribution of the total granular stress as a function of shear rate. Simulation parameters: $\mu_p = 0.1$, $e = 0.7$. The data points corresponding to the intermediate regime are shown with blank square symbols.

In order to evaluate the ROP model directly, the total granular stress obtained from the DEM simulations is decomposed into solidlike (stress arise from solidlike contacts) and fluidlike (stress arise from fluidlike contacts plus streaming stress) contributions. These contributions to the total granular stress are plotted with shear rate k^*, in Figs. 5.16(a) and 5.16(b), respectively. It is noteworthy that both the solidlike and fluidlike stress follow intermediate scaling of the stress ($\sigma \propto \dot{\gamma}^n, n_{solidlike} = 0.20, n_{fluidlike} = 0.44$), because both of them carry portions of contact stress as well; the only difference is whether the contacts are enduring or not.

5.9 Conclusions

The characterization of granular phase transition using an order parameter (OP) is explored. DEM simulations reveal that indeed the OP is capable of capturing the granular phase transition from solidlike to fluidlike behavior through its dependence on particle properties (such as particle friction coefficient) and flow properties (such as shear rate). Through these DEM simulations we also discovered a third stable granular phase that is neither completely fluidlike nor completely solidlike. Hence, a modification to the form of the free energy density function is proposed to account for this third stable granular phase. The refined OP model (ROP model) enables a linear implementation of the objective form (coordinate system independent) of the OP model (Gao et al., 2005) through a simplification that allows inversion of total granular stress from solidlike and fluidlike stress relations.

A regime map constructed from DEM data of homogeneously sheared granular flow reveals that the intermediate regime expands as the particle friction coefficient decreases. The ROP–KT model (fluidlike contribution obtained from the kinetic theory) model accurately predicts the total granular stress (to within 5%) up to a solid volume fraction of 0.53. Beyond a solid volume fraction of 0.53 the flow transitions to the intermediate regime. Comparison of the total granular stress predicted by different constitutive models with DEM data for homogeneous shear flow in the intermediate regime reveals that none of the models captures the correct trends of shear stress with shear rate. The assumption in the ROP–KT model that the fluidlike contribution is adequately modeled by KTGF clearly breaks down in the intermediate regime, although it appears to be adequate even up to a solid volume fraction of 0.53 where multiparticle interactions are present in the flow dynamics. However, modeling the solidlike stress using the ROP-FSM (Srivastava and Sundaresan, 2003) formulation does not result in accurate rheological prediction either. The models due to Losert (Losert et al., 2000) also do not

reproduce intermediate regime behavior.

Decomposition of the DEM granular stress into contact and streaming parts reveals that the contact (virial) contribution to the stress dominates ($> 95\%$), and follows the same scaling as the total granular stress in the intermediate regime. However, the streaming contribution always follows the inertial scaling even in the intermediate regime. The decomposition of the granular stress obtained from DEM into solidlike and fluidlike contributions (based on the OP) reveals that both these follow the same scaling as the total granular stress in the intermediate regime. This indicates that an entirely new model for the contact stress is needed in the intermediate regime.

CHAPTER 6. GRANULAR FLOW IN SILO DISCHARGE: DEM SIMULATIONS AND MODEL ASSESSMENT

This chapter is a manuscript in preparation titled "Granular flow in Silo discharge: DEM simulations and model assessment" authored by Vidyapati and S. Subramaniam.

Abstract

Discharge dynamics of granular particles from a flat–bottomed silo is studied using both continuum modeling and discrete element method (DEM) simulations. DEM simulations are used as a tool to investigate and quantify the influence of different simulation parameters affecting the discharge rate from silo by probing individual particle in the system. Further, to understand the complex flow behavior in a silo discharge problem spatial extent of different regimes is quantified using a regime map established from the DEM data of homogeneously sheared granular flow. It is shown that all three different regimes of granular flows (inertial, intermediate, and quasi–static) co–exist in this silo discharge problem. A quantitative comparison between results of continuum and DEM simulations is performed by comparing discharge rates, solid velocities and solid stresses for a three–dimensional (3D) flat–bottomed silo. It is found that continuum simulations over–predict the discharge rate from silo when compared to DEM data. Further, by correlating the error in solid stress prediction with spatial extent of different regimes it is shown that the intermediate regime renders significant challenges to the performance of a given continuum model.

Notation for section 6.1 to section 6.4

$\triangle t$	Time step for DEM simulation
$\dot{m}$	Discharge rate
C	Constant in Beverloo equation
D	Size of discharge outlet
d_p	Particle diameter
e	Particle restitution coefficient
e_w	Coefficient of restitution at wall
Fr	Constant in Princeton frictional model
H	Fill height at silo centerline
H_0	Thickness of the bin
I_{2D}	Second invariant of strain–rate tensor
J_s	Granular energy dissipation due to inelastic collision
k	Beverloo constant
k^*	Nondimensional shear rate
k_n	Particle normal stiffness coefficient
m_0	Initial mass in silo
m_d	Amount of mass discharged from silo
m_p	Particle mass
n	Coefficient in the frictional model
P_c	Critical state pressure
P_f	Frictional pressure
P_s	Solid pressure
r, s	Constant in Princeton frictional model
t	Time
t_c	Binary collision time

T_d Discharge time scale

W Silo width

$\mathbf{g}$ Acceleration due to gravity

$\mathbf{I}$ Identity tensor

$\mathbf{n}$ Unit normal

$\mathbf{q}$ Flux of granular energy

$\mathbf{S_S}$ Strain rate tensor

$\mathbf{v_s}$ Solid velocity

Greek symbols

δ Angle of wall friction

$\dot{\gamma}$ Shear rate

μ_f Frictional viscosity

μ_g Gas viscosity

μ_p Particle friction coefficient

μ_w Wall friction coefficient

ν Solid volume fraction

ν^{max} Maximum solid packing

ν^{min} Minimum frictional solid volume fraction

ϕ Angle of internal friction

$\phi^{'}$ Specularity coefficient

$\hat{\epsilon}$ Relative error in least–squares solution

ρ_b Bulk density of solid

ρ_g Gas density

ρ_s Particle density

σ Granular stress

Θ_s Granular temperature

τ_f Frictional stress tensor

τ_k Kinetic stress tensor

μ_t Tangential coefficient of friction

6.1 Introduction

Granular flows in Nature and in technological applications are among the most challenging problems to be addressed (Fenistein and Hecke, 2003). For example, solids processing is a multi–billion dollar industry that remains a critical part of the pharmaceutical (e.g., capsule, tablet solids), agricultural (e.g., fruits, seed processing), and consumer product (e.g., cereal, detergent, can goods) industries. Granular flow is ubiquitous in many applications such as silos, hoppers, nuclear pebble–bed reactors (Rycroft et al., 2006), and clean coal technologies (Syamlal et al., 2009). Understanding the behavior of granular materials is an active research area that continues to yield exciting and often surprising results. This is due to fact that the granular flows are highly complex materials that typically exhibit nonlinear constitutive behavior under shear (Campbell, 2002), with different regimes that depend on microscale properties (e.g., interparticle friction and coefficient of restitution) as well as on macroscale properties (e.g., solid volume fraction and shear rate). Silos are one of the important devices widely used in the processing and handling of these granular materials in many industrial and agricultural applications (Sundaresan, 2001). Accurate prediction of the discharge rate is critical for a dependable design and optimum performance of these devices. In order to accurately predict the discharge rate from the silo, a reliable and accurate continuum description of granular flows is needed. However, for a silo discharge problem, it is very likely to encounter flow regimes that are dense and frictional, which poses a significant challenge to formulate a comprehensive continuum theory.

There have been many studies in past in order to understand the discharge dynamics of granular particles from silo and hoppers. Ketterhagen et al. (2009) performed a systematic study to quantify the modes of powder flow in a series of three–dimensional conical hoppers and quasi–three-dimensional wedge–shaped hoppers. These flow modes (mass flow or funnel flow) are quantified using a Mass Flow Index (MFI), which is de-

fined by the ratio of the mean particle velocity at the hopper wall to the mean particle velocity at the hopper centerline. Landry et al. (2004) studied the vertical stress profiles in a two–dimensional (2D) and three–dimensional (3D) silo and further examined how this stress profile changes with dimensionality. Their analysis revealed that the Janseen theory does not fully describe these packings, especially at the top of the piles. Goa and Ebert (2005) performed a detailed study on a three–dimensional silo and examined the distributions of normal wall forces and pressure developed at the end of filling process. In an another work, Engblom et al. (2011) studied the segregation mechanics of powder mixtures in a cylindrical silo due to variation in material properties. Benyahia (2008) performed validation studies of continuum granular frictional flow theories using a two–dimensional (2D) bin discharge problem by computing discharge rates of granular particles and compared them with the Beverloo correlation (Beverloo et al., 1961).

In principle there are two approaches for modeling this particulate system: continuum and discrete. The first approach (continuum) is more relevant for industrial applications that involve large amount of solids. The second approach (discrete) is a powerful numerical method, in which motion of individual particle is determined on the basis of all the forces acting upon it (Cundall and Strack, 1979). The exponential increase of computing power and advances in numerical methods have made is possible to perform these detailed and accurate simulations of particulate flows using methods such as discrete element method (DEM) simulations. In contrast to the continuum techniques, DEM simulations can be used to evaluate and develop improved continuum models for particulate flows. Assessment of these continuum models is critical for a silo discharge problem, where both dilute (near orifice outlet) and dense regimes could co–exist simultaneously. The inertial (rapid flow) regime has been successfully studied by means of corrections to the kinetic theory of gases (Lun et al., 1984; Jenkins and Savage, 1983; Jenkins and Richman, 1985), whereas the quasi–static regime is generally described by plasticity theories (Schaeffer, 1987; Nedderman, 1992; Sun and Sundaresan,

2011). However, no unified theory has been proposed for the intermediate (transitional) flow regime, in which energy is dissipated by inelastic collisions and interparticle friction (G.D.R. MiDi, 2004; Tardos et al., 2003; Vidyapati et al., 2012). The primary objective of this study is to evaluate the performance of different continuum models by comparing their predictions with the DEM simulations and well–known empirical correlation (Beverloo et al., 1961) of experimental data.

Through continuum simulations of discharge of granular particles from a flat–bottomed silo, performance of different continuum models is evaluated for dense granular flows. In dense regime the flow is dominated by long–lasting, frictional, and sliding contacts, hence assessment of existing continuum models is critical for overall performance of silos and hoppers. The first continuum model assessed in this work, is the model proposed by Schaeffer (1987), which has been traditionally used in the MFIX computer code (MFIX, 1993). The second model assessed, is the model developed by Srivastava and Sundaresan (2003). They also conducted validation study of their proposed model by comparing its results with the well–known Beverloo correlation (Beverloo et al., 1961) for a two–dimensional (2D) bin. Study performed by Benyahia (2008) also compares the discharge rate obtained using these two frictional theories for different values of orifice widths. One of the important and critical findings of these studies (Srivastava and Sundaresan, 2003; Benyahia, 2008), is that the discharge rate predicted by existing continuum theories does not match well with that obtained from Beverloo correlation (Beverloo et al., 1961) of experimental data.

We also confirm this observation by performing continuum simulations of the same two–dimensional (2D) bin discharge problem which is earlier studied by Srivastava and Sundaresan (2003) and Benyahia (2008). Figure 6.1 shows the temporal variation of the discharge rate obtained from two different continuum models (Schaeffer (Schaeffer, 1987) and Princeton (Srivastava and Sundaresan, 2003)) are compared with Beverloo correlation (Beverloo et al., 1961) of experimental data. This result shows that, both of

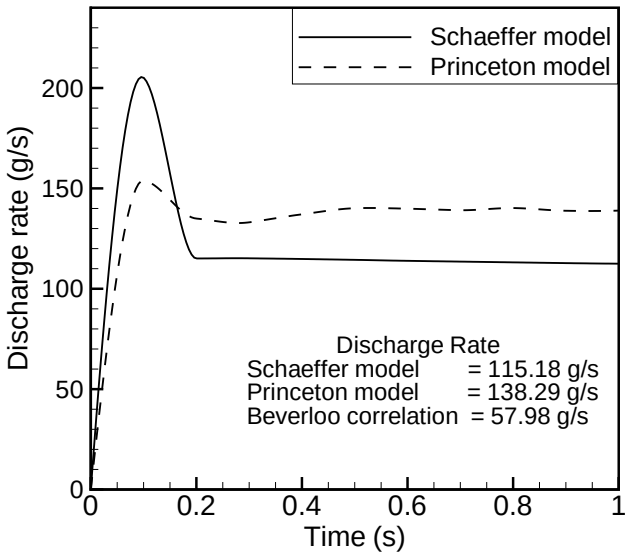

Figure 6.1 Temporal variation of discharge rate using two different continuum models. The solid line shows the discharge profile obtained from Schaeffer model, whereas the dashed line is the prediction for the discharge rate obtained using Princeton model for a two–dimensional (2D) bin.

these continuum models predict discharge rates which are much higher (more than 80%) than the discharge rate obtained using Beverloo correlation. It is also noticed that both of these continuum models are unable to capture the formation of stagnant shoulders at the corners of the bin, which has been observed in the experimental studies (Nedderman et al., 1982). One of the plausible reasons for this discrepancy in the discharge rate prediction, could be **not** all particle–particle, particle–fluid interactions are correctly represented or modeled in the continuum simulations. This observation motivates use of DEM simulations as a possible approach to isolate and improve specific sub–models in the continuum simulations.

Discrete element method (DEM) simulations have been used in the past to model the discharge of granular particles from the silos and hoppers (Ketterhagen et al., 2009; Landry et al., 2004; Goa and Ebert, 2005; Anand et al., 2008). Anand et al. (2008) studied the discharge from a rectangular hopper using DEM and quantified the effect of different simulation parameters on the discharge rate from hopper. Nevertheless, there has been no comprehensive study, which addresses the issue of direct quantitative comparison between results of DEM and continuum simulations for a silo discharge problem. In this work, a 3D flat–bottomed silo is simulated using DEM and also effect of different simulation parameters on the discharge rate is quantified by probing the individual particle in the system. These kinds of information are difficult to infer from experiments, for example there have been no comprehensive experimental studies, investigating the effect of interparticle friction coefficient or coefficient of restitution on silo discharge rate. There is an inherent assumption in most of the experimental correlation that these interaction parameters play very little or no role in predicting the discharge rate from silo (Anand et al., 2008). DEM is a useful tool which can help researchers and engineers in answering these questions and suggest possible ways to improve the overall design of silos and hoppers. DEM simulations can also be used to assess the performance of continuum models and help in improving the model performance by revealing the complex

flow dynamics involved in this silo discharge problem. In this work, the model assessment is accomplished by comparing result for discharge rates, solid velocities and solid stresses obtained using continuum models with that of DEM simulations. The discharge rates obtained using DEM simulations are also compared with the existing correlation of experimental data (Beverloo et al., 1961).

6.2 Discrete element method (DEM) simulations

In order to understand the flow dynamics inside silo and to have quantitative comparison with continuum simulations, we perform three–dimensional (3D) DEM simulations of silo discharge. For all the DEM simulations performed in this study granular material is modeled as a particle assembly consisting of monodisperse, spherical, cohesionless particles of diameter d_p and mass m_p. A soft sphere model is used, in which particles interact via contact laws and friction only on contact. Since the realistic modeling of particle deformation is complicated, a simplified contact force model based on linear spring–dashpot combination is used in this work (Silbert et al., 2001). Details of the computational model used in these discrete element simulations are given in Sec. 3.1. For all the DEM simulations reported, the mass and diameter of particles are set to 1, so the density of particles is $6/\pi$. The value of normal spring constant k_n is set to 2×10^5 ($m_p g/d_p$ units), which captures the general behavior of intermediate to high k_n system (Silbert et al., 2001). The integration time step Δt for all the DEM simulations is selected to be $t_c/50$, where t_c is the binary collision time. This time step is shown to be sufficiently small to ensure temporal convergence (Silbert et al., 2001).

6.2.1 DEM simulations of silo discharge

The movement of individual particles during the outflow caused by gravity, is studied using 3D DEM simulations. The domain size selected for the simulations is $18 \times 18 \times 36$

particle diameter units in x, y and z directions, respectively. The domain size is selected in such a manner that the discharge rate remains unchanged with any further change in the domain size. The only external force acting on the system is gravity in the negative z direction. In all these DEM simulations the discharge outlet is circular in shape with diameter $6d_p$, where d_p is the particle diameter (except for some simulations which are performed to quantify the effect of discharge outlet size on the discharge rate). The domain is bounded with flat–frictional wall in all the directions (x, y and z). The number of particles simulated in this study varies between 11136 to 13340 depending on the initial solid volume fraction of the specific simulation, for a given domain size.

To ensure a constant and domain size independent discharge rate from the silo, following design constraints are used (Anand et al., 2008):

1. $H > D$, where H is the fill height at centerline and D is the size of discharge outlet.

2. $W > 2.5D$, where W is the silo width and D is the size of discharge outlet.

3. $D \geq 6d_p$, where D is the size of discharge outlet and d_p is the particle diameter.

In order to ensure that the discharge rate from the silo remains unchanged with the domain size selected, we performed DEM simulations with different domain sizes and study the discharge rate. Figure 6.2 shows the amount of mass discharged with time for a simulation with initial solid volume fraction of 0.60, for three domain sizes of $15d_p \times 15d_p \times 30d_p$, $16d_p \times 16d_p \times 30d_p$ and $18d_p \times 18d_p \times 36d_p$, respectively. Slope of the straight portion of Fig. 6.2 gives the discharge rate. It can be inferred from Fig. 6.2 that the discharge rate is almost independent of the domain size selected, provided it meets the minimum design constraint of $W > 2.5D$, where W is silo width and D is the size of discharge outlet. This result is in good agreement with the findings of Brown and Richards (1960), who also reported that the discharge rate remains constant as long as $W > 2.5D$.

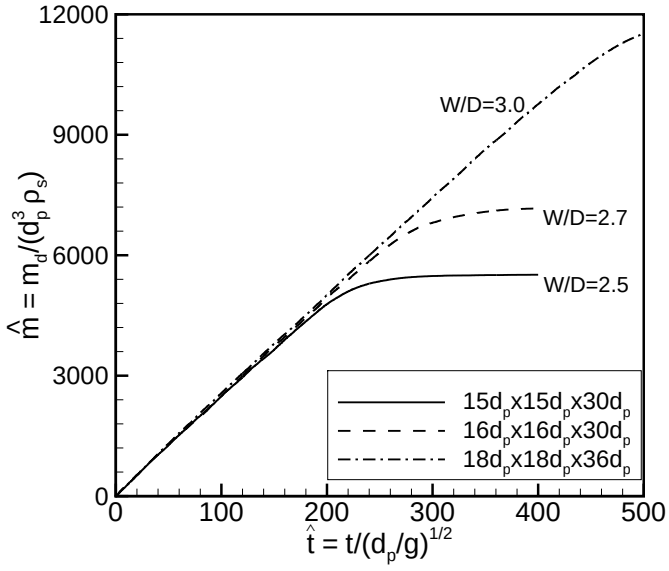

Figure 6.2 Effect of domain size on discharge rate from a flat–bottomed silo. Simulation parameters: $D = 6d_p$, $\mu_p = \mu_w = 0.1$, $e = 0.88$.

Figures 6.3(a), 6.3(b), and 6.3(c) show the snapshots of the particle discharge from flat–bottomed silo at time $t = \frac{T_d}{40}$, $t = \frac{T_d}{2}$ and $t = \frac{T_d}{4}$ respectively, where T_d is the discharge time scale (time required to discharge the complete mass from silo) extracted from DEM simulations. These figures show that, as the simulation evolves with time, the number of particles in the domain decreases due to discharge from the bottom orifice.

6.2.2 Influence of different simulation parameters on silo discharge from DEM simulations

In order to quantify the influence of different physical and numerical parameters on the discharge rate from silo, we perform series of DEM simulations with different values of these parameters and study the discharge rate. Friction is expected to play an important role in determining the discharge rate from silo. However, in most of the experimental

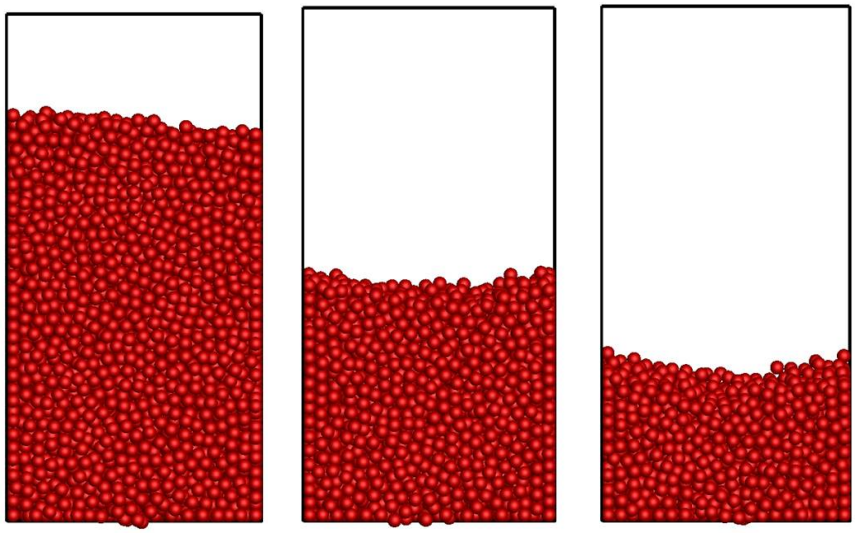

(a) (b) (c)

Figure 6.3 (a) Snapshot of the particle discharge from silo (a) At time $t = \frac{T_d}{40}$, (b) At time $t = \frac{T_d}{2}$, and (c) at time $t = \frac{T_d}{4}$.

correlation it is an implicit assumption that friction coefficient (both particle–particle and particle–wall) plays a small or no role in the determining the discharge rate from silos or hoppers (Anand et al., 2008). To further understand and quantify the effect of friction coefficient (both particle–particle and particle–wall), we performed DEM simulations with different values of particle–particle and particle–wall friction coefficient and compute the discharge rate.

In Fig. 6.4(a) the amount of mass discharged (scaled with initial mass in the silo, m_0) is plotted with time for 3 different values of particle–particle friction coefficient of 0.10, 0.25 and 0.50 for a fixed wall friction coefficient of 0.10. Figure 6.4(a) shows that, as the particle–particle coefficient of friction increases the discharge rate decreases. The discharge rate decreases by about 30% when the particle–particle friction coefficient increases from 0.1 to 0.5. Hence, it can be concluded that, the particle–particle friction coefficient is an important parameter which governs the discharge rate from the silo, and hence cannot be neglected, as generally assumed in experimental correlations. However,

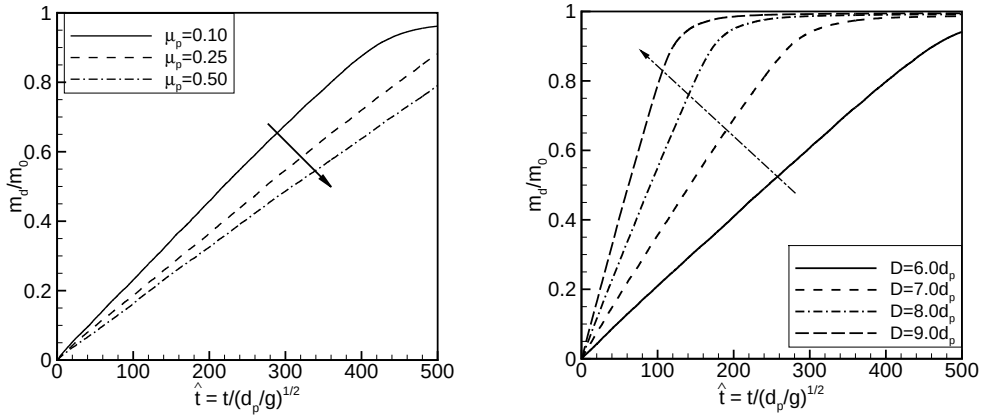

(a) (b)

Figure 6.4 (a) Amount of mass discharged (scaled with the initial mass in the silo, m_0) with time for three different values of particle—particle friction coefficient. Simulation parameters: $\mu_w = 0.1$, $e = 0.88$, and (b) The amount of mass discharged (scaled with the initial mass in the silo, m_0) plotted with time for different widths of discharge outlets. Simulation parameters: $\mu_p = \mu_w = 0.1$, $e = 0.88$.

our DEM simulations reveal (results not shown here) that, the wall friction coefficient has a negligible or no influence on the discharge rate from silo. Increasing the wall friction coefficient from 0.10 to 0.75 also does not lead to any significant change in the discharge rate from silo. This result can be attributed to the fact that, for a broad silo ($W/D \geq 3$), the wall friction coefficient does not affects the flow near the orifice outlet and hence has a small or no effect on the discharge rate.

The coefficient of restitution is one such another parameter which has not been completely explored in the experimental studies. In order to understand its influence on the discharge rate, we performed DEM simulations with different values of particle restitution coefficient (ranging from 0.70 to 0.95, this range belongs to the actual value of coefficient of restitution of particles generally used in solid processing industries). Nevertheless, we find almost no change in the discharge rate (results not shown here)

when particle restitution coefficient is increased from 0.70 to 0.95. In a study performed by Ristow (1997) reported a change in discharge rate of 1.2% when the coefficient of restitution increased from 0.5 and 0.9. This finding can be ascribed to the fact that, the silo flows are dense in nature which are dominated by long–lasting, frictional, multiparticle contacts. Hence, it is not surprising that the effect of coefficient of restitution will have a negligible influence on the silo discharge dynamics.

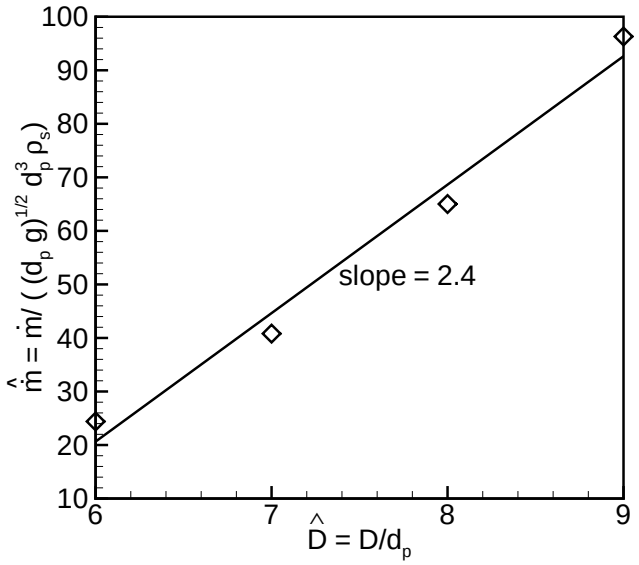

Figure 6.5 Discharge rate with orifice outlet width. Simulation parameters: $\mu_p = \mu_w = 0.1$, $e = 0.88$.

Discharge outlet size is an another parameter which affects the discharge rate from the silo. Figure 6.4(b) shows the amount of mass discharged (scaled with the initial mass in the silo, m_0) with time for 4 different outlet sizes of $6d_p$, $7d_p$, $8d_p$ and $9d_p$. It is seen from Fig. 6.4(b) that, the discharge rate increases with increase in the discharge outlet size, and it is one of the most important parameter in the silo discharge problem. Discharge rate increases almost four times by increasing the discharge outlet size from $6.0d_p$ to $9.0d_p$. In Fig. 6.5, discharge rate is plotted with discharge outlet size ($\hat{D} = D/d_p$) for a

simulation with particle–particle and particle–wall friction coefficient of 0.10. Figure 6.5 shows that the discharge rate is a function of outlet width raised to 2.4 power for circular orifices, which matches extremely well with the Beverloo correlation, that predicts the discharge rate as function of outlet width raised to 2.5 power for a three–dimensional silo (see Eq. 6.26).

6.2.3 Characterization of different regimes in silo discharge using DEM

Depending up on particle (friction coefficient, coefficient of inelasticity) and flow (shear rate) properties, granular materials exhibit different constitutive behaviors in different regimes (inertial, intermediate and quasi–static) of flow. In general these regimes are classified based on scaling of shear stress with strain–rate (Campbell, 2002). In inertial regime the stress scales as square of strain rate ($\sigma \propto \dot{\gamma}^2$) (Bagnold, 1954), whereas in the quasi–static regime stress remains independent of the strain rate ($\sigma \neq f(\dot{\gamma})$) (Campbell, 2002). In between these two extreme regime there exist an intermediate regime where stress is related with strain rate in form of power law ($\sigma \propto \dot{\gamma}^n$), where n takes values between 0 to 2 based on particle (e.g., friction coefficient) and flow (e.g., shear rate) properties (Tardos et al., 2003). In order to quantify spatial extent of different regimes in a silo discharge problem, we first establish a regime map for granular flows using DEM data obtained from homogeneously sheared assembly of granular particles (where the stress is independent of the position), for a wide range of solid volume fractions, shear rates and particle friction coefficients. Later, this regime map is used as a guideline to quantify the spatial extent of different regimes in a silo discharge problem. For complete details about the aforementioned regime map reader is directed to a recent article by Vidyapati and Subramaniam (2012a). In the current work we only use pertinent information needed to quantify the spatial extent of different regimes in this silo discharge problem based on our previous study (Vidyapati and Subramaniam, 2012a).

The idea is to extract values of local solid volume fraction, mean strain rate in

each cell, from DEM simulation of flat–bottomed silo and assign them different regimes (inertial, intermediate and quasi–static) following a regime map established in Vidyapati and Subramaniam (2012a), for a given value of particle friction coefficient μ_p. These calculations are performed in a thin slice of thickness $2d_p$ (in y direction) which is located at the center of the silo. In the x (along width of the silo) and z direction (along the height of the silo) a grid size of $2d_p$ is used to extract local quantities such as, solid volume fraction and mean strain rate. Using this criterion, different cells are assigned an integer value of 0, 2 and 1 for quasi–static, inertial (rapid flows) and intermediate regimes, respectively. Steps followed to quantify the spatial extent of different regimes in a silo geometry are explained below:

1. Solid volume fraction: At different spatial locations the local solid volume fraction is obtained from the DEM simulation data of silo discharge.

2. Mean strain rate: The strain rate tensor in 3D is given by,

$$\dot{\gamma}_{ij} = \begin{bmatrix} \dot{\gamma}_{xx} & \dot{\gamma}_{xy} & \dot{\gamma}_{xz} \\ \dot{\gamma}_{yx} & \dot{\gamma}_{yy} & \dot{\gamma}_{yz} \\ \dot{\gamma}_{zx} & \dot{\gamma}_{zy} & \dot{\gamma}_{zz} \end{bmatrix}.$$

   To compute the mean strain rate the second invariant of strain rate tensor (I_{2D}) is used,

$$I_{2D} = \frac{1}{2}\left[[tr(\dot{\gamma})]^2 - tr(\dot{\gamma}^2)\right]. \tag{6.1}$$

   Using Eq. 6.1 and the definition of the strain rate tensor $\dot{\gamma}_{ij}$, the second invariant of the strain rate tensor can be written as,

$$I_{2D} = \left[(\dot{\gamma}_{xx}\dot{\gamma}_{yy} + \dot{\gamma}_{yy}\dot{\gamma}_{zz} + \dot{\gamma}_{xx}\dot{\gamma}_{zz}) - (\dot{\gamma}_{xy}\dot{\gamma}_{yx} + \dot{\gamma}_{xz}\dot{\gamma}_{zx} + \dot{\gamma}_{yz}\dot{\gamma}_{zy})\right]. \tag{6.2}$$

3. Particle friction coefficient: Two different values (0.50 and 0.25) of particle friction coefficient is used to characterize the spatial extent of different regimes in a silo

geometry. These values of friction coefficients offer a reasonable representation of general granular material (Silbert et al., 2001).

We extract these quantities (local solid volume fraction and mean strain rate) from DEM simulation of discharge from a flat–bottomed silo and assign each cell a value 0 (for quasi–static regime), 2 (for inertial regime), or 1 (for intermediate regime). Figures 6.6(a) and 6.6(b) show the spatial extent of different regimes in flat–bottomed silo obtained using above described method for a particle friction coefficient of 0.50 and 0.25, respectively. In Figs. 6.6(a) and 6.6(b) the red represents the presence of inertial regime (which found to be exist near the discharge orifice), the blue indicates the quasi–static regime (which exists near walls and regions far away from discharge outlet), and presence of any other color represents the intermediate regime.

From this study, it is evident that all three different regimes (inertial, intermediate, and quasi–static) co-exist even for a simple problem like discharge of granular particles from a silo. It is also interesting to note that, the intermediate regime spans a considerable spatial region in the silo. A careful study of these figures reveals that the spatial extent of intermediate regime expands as the particle friction coefficient decreases from 0.50 to 0.25. The friction coefficient for most of the granular material (such as glass beads) used in the solid processing industries varies between 0.15 to 0.50, and hence expansion of the intermediate regime will affect granular flow in practical devices. This result also indicates that, it is critical to understand the rheological behavior of the intermediate regime which still poses significant challenges for a continuum model (Vidyapati and Subramaniam, 2012a). Most of the traditionally used continuum models do not perform satisfactory in this regime, where both collisional and frictional interaction between the particles are important.

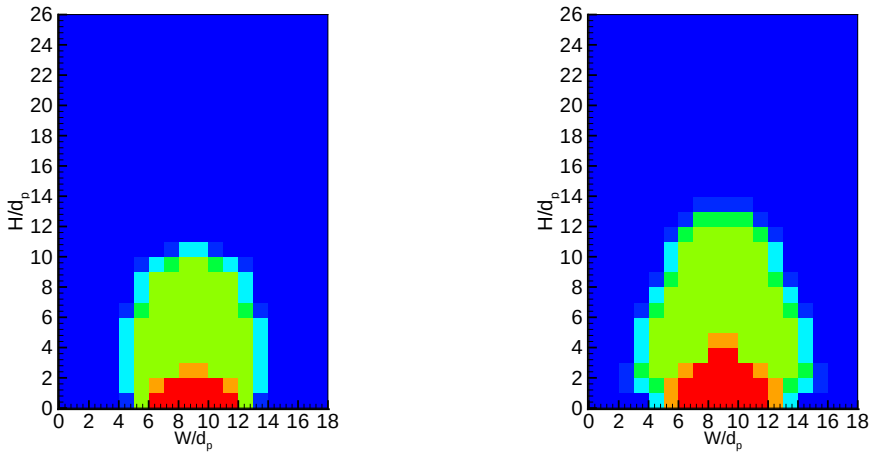

(a) (b)

Figure 6.6 Characterization of spatial extent of different regimes of granular rheology in a flat–bottomed silo based on local solid volume fraction, mean strain rate and particle friction coefficient. The Blue represents the quasi–static regime, the Red represents the inertial (rapid flow) regime, whereas presence of any other color indicates the spatial extent of the intermediate regime. (a) Simulation parameters: $D = 6d_p$, $\mu_p = 0.5$, $e = 0.91$, and (b) Simulation parameters: $D = 6d_p$, $\mu_p = 0.25$, $e = 0.91$. (for interpretation of the references to color in this figure legend, the reader is referred to the web version of this article.)

6.3 Continuum simulations

To perform a quantitative assessment of different continuum models, we directly compare the results for the discharge rate, solid velocities and solid stresses obtained from DEM and continuum simulations for a same three–dimensional (3D) silo. These continuum descriptions of granular flow plays an important role in simulating problems at larger and industrial scale. We have also performed continuum simulations of a two–dimensional (2D) bin and measured quantities like discharge rate and solid velocities. However, those results are not presented in the current article because of good agreement with the similar simulations performed by Srivastava and Sundaresan (2003) and Benyahia (2008) in past.

6.3.1 Setup for continuum simulations

Simulations of particle discharge from a three–dimensional flat–bottomed silo is performed using the averaged two–fluid (TF) continuum equations using MFIX computer code (MFIX, 1993). MFIX is an Eulerian–Eulerian computational fluid dynamics (CFD) model in which gas and granular solids are modeled as interspersed continua. However, the current study focuses only on dense granular flows, so the effect of interstitial fluid can be neglected (provided the particle diameters are relatively larger, e.g., Geldart type B). Hence no effect of fluid is introduced in the model equations. The "dry" granular kinetic theory model used in MFIX code (MFIX, 1993) is essentially the same as that derived from Lun et al. (1984). Conservation of mass for constant solid density is given as:

$$\rho_s \left[\frac{\partial \nu}{\partial t} + \nabla \cdot (\nu \mathbf{v}_s) \right] = 0, \tag{6.3}$$

where ρ_s is the solid density, ν is the solid volume fraction, and $\mathbf{v}_s$ is the velocity vector for solid phase. Conservation of linear momentum is given by:

$$\rho_s \left[\frac{\partial \nu \mathbf{v}_s}{\partial t} + \nabla \cdot (\nu \mathbf{v}_s \mathbf{v}_s) \right] = \nabla \cdot (\boldsymbol{\tau}_k + \boldsymbol{\tau}_f) + \nu \rho_s \mathbf{g}, \tag{6.4}$$

where $\boldsymbol{\tau}_k$ and $\boldsymbol{\tau}_f$ are the kinetic and frictional part of the stress tensor, respectively. The translational granular energy conservation equation is given by:

$$\frac{3}{2}\rho_s \left[\frac{\partial \nu \Theta_s}{\partial t} + \nabla \cdot (\nu \Theta_s \mathbf{v}_s) \right] = -\nabla \cdot \mathbf{q} + \boldsymbol{\tau}_k : \nabla \mathbf{v}_s - \rho_s J_s, \tag{6.5}$$

where Θ_s is the granular temperature, $\mathbf{q}$ is the flux of granular energy, and J_s is the granular energy dissipation due to inelastic collisions. Solids kinetic–collisional and frictional stress terms are given by:

$$\boldsymbol{\tau}_k = \left[-P_s + \eta \mu_b \nabla \cdot \mathbf{v}_s \right] \mathbf{I} + 2\mu_s \mathbf{S}_S, \tag{6.6}$$

$$\boldsymbol{\tau}_f = -P_f \mathbf{I} + 2\mu_f \mathbf{S}_S, \tag{6.7}$$

$$\mathbf{S}_S = \frac{1}{2}\left[\nabla \mathbf{v}_s + (\nabla \mathbf{v}_s)^T \right] - \frac{1}{3} \nabla \cdot \mathbf{v}_s \mathbf{I}, \tag{6.8}$$

where P_s is the solid pressure, η is a constant depending on particle restitution coefficient (Srivastava and Sundaresan, 2003), μ_b is the bulk viscosity of the solid phase, $\mathbf{I}$ is the identity tensor, μ_s is the granular viscosity, and $\mathbf{S}_S$ is the strain–rate tensor as given in Eq. 6.8. The closures for different terms are taken from Lun et al. (1984).

The problem studied is a 3D flat–bottomed silo with domain size $18 \times 18 \times 36$ particle diameter in x, y and z directions, respectively, with an open top and an orifice centered at the bottom. The width of the center orifice at the bottom is set to $6d_p$, where d_p is the particle diameter. A $5d_p$ high region below the silo is included in the domain so that a boundary condition is not required right at the exit of the bin. A grid resolution of 1, 1 and 2 mm is used in the x, y and z directions, respectively. According to Srivastava and Sundaresan (2003) such a fine mesh is required to effectively resolve variations in the velocities and solid volume fractions near the orifice region. The initial solid volume

fraction in the bin is set to 0.60, whereas initial granular temperature is taken to be non–zero everywhere (1 cm^2/s^2). The only difference between continuum and DEM simulations is that, the continuum simulations have a square shaped outlet, whereas the DEM simulations have a circular outlet. However, the effective diameter (hydraulic diameter) of both the discharge outlets are kept same as $6d_p$. Table 6.1 lists the values of the model parameter used in the simulations, most of which taken from Srivastava and Sundaresan (2003).

Table 6.1 Values of model parameters used in simulations.

Parameter	Values
gas density, ρ_g	1.3×10^{-3} g/cm^3
gas viscosity, μ_g	1.8×10^{-4} g/cm-s
solid density, ρ_s	2.9 g/cm^3
particle diameter, d_p	1 mm
angle of internal friction, ϕ	28.5
angle of wall friction, δ	12.3
specularity coefficient, $\phi^{'}$	0.25
particle–particle coefficient of restitution, e	0.91
coefficient of restitution at wall, e_w	0.91
maximum solid packing, ν^{max}	0.65

The boundary condition for momentum and pseudo–thermal energy (PTE) for the particulate phase at the walls of the bins are taken from Johnson and Jackson (1987). This can be written as:

$$\mathbf{n} \cdot (\boldsymbol{\tau}_k + \boldsymbol{\tau}_f) \cdot \frac{\mathbf{v}_{sl}}{|\mathbf{v}_{sl}|} + (\mathbf{n} \cdot \boldsymbol{\tau}_f \cdot \mathbf{n}) \tan\delta + \frac{\pi\sqrt{3}}{6\nu^{max}} \phi^{'} \rho_s \nu g_0 \Theta_s^{1/2} \mathbf{v}_{sl} = 0, \tag{6.9}$$

$$\mathbf{n} \cdot \mathbf{q} = \frac{\pi\sqrt{3}}{6\nu^{max}} \phi^{'} \rho_s \nu g_0 \Theta_s^{1/2} |\mathbf{v}_{sl}|^2 - \frac{\pi\sqrt{3}}{4\nu^{max}} \left(1 - e_w^2\right) \rho_s \nu g_0 \Theta_s^{3/2}, \tag{6.10}$$

where $\mathbf{n}$ is the unit normal from the boundary into the particle assembly, $\boldsymbol{\tau}_k$, $\boldsymbol{\tau}_f$ are kinetic and frictional stress tensor respectively, ν^{max} maximum solid volume fraction,

Θ_s is the granular temperature, $\mathbf{q}$ is the flux of granular energy, δ is the angle of wall friction for the material, $\phi^{'}$ is the specularity coefficient, ρ_s is the solid density, ν is the solid volume fraction, e_w is the coefficient of restitution at the wall, and $\mathbf{v}_{sl}$ is $\mathbf{v} - \mathbf{v}_{wall}$, the slip velocity of the particle assembly at the wall. The gas phase is allowed to slip freely at the wall. At the open boundaries of the domain, the gas pressure is set to be atmospheric. For all other dependent variables, the usual continuation condition (i.e. zero gradient in the direction normal to the boundary) is applied. The bin is initialized with particles at initial void fraction of 0.40 with particles at rest.

6.3.2 Description of continuum models

Three different continuum models (Schaeffer (Schaeffer, 1987), Princeton (Srivastava and Sundaresan, 2003), CSS (Chialvo et al., 2011)) have been used to simulate to simulate silo discharge problem in this work. A brief description of these models are presented below,

1. Schaeffer model (Schaeffer, 1987): This model has been traditionally used in the MFIX code (MFIX, 1993). It is used when critical state is activated, where the solid volume fraction exceeds the maximum packing limit. In this model, I_{2D} represent the second invariant of the deviator of the strain rate tensor, which is related to the norm of the square of the strain rate tensor used by Schaeffer (1987) simply by: $\sqrt{I_{2D}} = \sqrt{(\mathbf{S}_S : \mathbf{S}_S)}/2$. This model expresses the frictional stresses by the following equations (Benyahia, 2008):

$$P_f = P_c = \begin{cases} 10^{25}(\nu - \nu^{max})^{10} & \text{if } \nu > \nu^{max} \\ 0 & \text{if } \nu \leq \nu^{max} \end{cases} \tag{6.11}$$

$$\mu_f = \begin{cases} \frac{P_c \sin(\phi)}{2\sqrt{I_{2D}}} & \text{if } \nu > \nu^{max} \\ 0 & \text{if } \nu \leq \nu^{max} \end{cases} \tag{6.12}$$

where P_c is the critical state pressure, $\mathbf{S}_S$ is the strain rate tensor, ν and ν^{max} are the solid volume fraction and its value at maximum packing limit, respectively.

2. Princeton model (Srivastava and Sundaresan, 2003): This frictional model is proposed by Srivastava and Sundaresan (2003), who gave expression of the frictional stresses for a compressible granular assembly. This model is a modification of Savage model (Savage, 1998) that accounts for strain–rate fluctuations even in the dense regime of granular flow. The frictional stresses start influencing the granular flow at a minimum solid volume fraction (ν^{min}), which is below the maximum packing (ν^{max}) as proposed by Johnson and Jackson (1987). In this study, the critical state theory applies only when the granular assembly is incompressible (i.e., above maximum packing). The Princeton model (Srivastava and Sundaresan, 2003) model is expressed by the following equations:

$$P_c = \begin{cases} 10^{25}(\nu - \nu^{max})^{10} & \text{if } \nu > \nu^{max} \\ Fr\frac{\left(\nu - \nu^{min}\right)^r}{(\nu^{max} - \nu)^s} & \text{if } \nu^{max} \geq \nu > \nu^{min} \\ 0 & \text{if } \nu \leq \nu^{min} \end{cases} \tag{6.13}$$

where $Fr = 0.5$ dynes/cm^2, $r = 2$, and $s = 5$ are constants in this model (Srivastava and Sundaresan, 2003). The frictional pressure is related to critical state pressure as follows:

$$\frac{P_f}{P_c} = \left(1 - \frac{\nabla \cdot \mathbf{v}_s}{n\sqrt{2}\sin(\phi)\sqrt{\mathbf{S}_S : \mathbf{S}_S + \Theta_s/d_p^2}}\right)^{n-1} \tag{6.14}$$

$$\mu_f = \frac{\sin(\phi)}{\sqrt{2}} \frac{P_f}{\sqrt{\mathbf{S}_S : \mathbf{S}_S + \Theta_s/d_p^2}} \left(n - (n-1)\left(\frac{P_f}{P_c}\right)^{\frac{1}{n-1}}\right) \tag{6.15}$$

The coefficient n has different values depending on whether the granular assembly is experiencing a dilation or compaction:

$$n = \begin{cases} \frac{\sqrt{3}}{2}\sin(\phi) & \text{if } \nabla \cdot \mathbf{v}_s \geq 0 \\ 1.03 & \text{if } \nabla \cdot \mathbf{v}_s < 0 \end{cases} \tag{6.16}$$

In Eq. 6.16, n is a parameter which determines the shape of the yield surface.

3. CSS (Chialvo–Sun–Sundaresan) model (Chialvo et al., 2011): The general form of this recently developed CSS bridging model can be written as (Chialvo et al., 2011),

$$p = \begin{cases} p_{QS} + p_{Int} & \text{for } \nu \geq \nu_c \\ \left(p_{Inert}^{-1} + p_{Int}^{-1}\right)^{-1} & \text{for } \nu < \nu_c, \end{cases} \tag{6.17}$$

$$\tau = \begin{cases} \tau_{QS} + \tau_{Int} & \text{for } \nu \geq \nu_c \\ \left(\tau_{Inert}^{-1} + \tau_{Int}^{-1}\right)^{-1} & \text{for } \nu < \nu_c. \end{cases} \tag{6.18}$$

In Eqs. 6.17 and 6.18, subscripts QS, Int, and $Inert$ correspond to quasi–static, intermediate and inertial regime, respectively. ν and ν_c are the solid volume fraction and critical volume fraction, respectively. In Eqs. 6.17 and 6.18, individual regime contributions are defined as,

$$p_{QS} = \alpha_{QS}|\nu - \nu_c| \tag{6.19}$$

$$p_{Int} = \alpha_{Int}\hat{\dot{\gamma}}^{2/3} \tag{6.20}$$

$$p_{Inert} = \frac{\alpha_{Inert}\hat{\dot{\gamma}}^2}{|\nu - \nu_c|^2} \tag{6.21}$$

$$\tau_{QS} = \beta_{QS}|\nu - \nu_c| \tag{6.22}$$

$$\tau_{Int} = \beta_{Int}\hat{\dot{\gamma}}^{5/7} \tag{6.23}$$

$$\tau_{Inert} = \frac{\beta_{Inert}\hat{\dot{\gamma}}^2}{|\nu - \nu_c|^{9/5}}, \tag{6.24}$$

where $\hat{\dot{\gamma}}$ is defined as follows,

$$\hat{\dot{\gamma}} = \frac{\dot{\gamma} d_p}{\sqrt{k_n/(\rho_s d_p)}} = \sqrt{\frac{1}{k^*}}. \tag{6.25}$$

In Eq. 6.25, $k^* = k_n/\left(\rho_s d_p^3 \dot{\gamma}^2\right)$ is non–dimensional shear rate, $\dot{\gamma}$ is the applied shear rate, k_n is the normal spring constant, d_p is the particle diameter and ρ_s is the particle density. The constitutive parameters α_{QS}, β_{QS}, α_{Int}, β_{Int}, α_{Inert} and β_{Inert} are specified based on the work of Chialvo et al. (2011).

6.3.3 Quantitative comparison between DEM and continuum simulations of discharge from a three–dimensional (3D) silo

Discharge rate is one of the most important quantities measured in these simulations. Figure 6.7(a) shows the temporal variation of the discharge rate for a three dimensional (3D) flat–bottomed silo. The solid line shows the profile of discharge rate obtained with the Schaeffer model, the dashed line shows the discharge rate obtained with the Princeton model and the dash dot line shows the discharge rate obtained from CSS model. The discharge rate obtained from DEM simulation is shown with dash dot dot line in Fig. 6.7(a). This result shows that, at early times there is a rapid increase in the discharge rate, which is then followed by a plateau region where the discharge rate did not vary appreciably with time. Figure 6.7(a) also shows that the steady discharge obtained from Schaeffer model is 7.75 g/s, whereas the steady discharge obtained from Princeton model is 9.62 g/s. This difference in the prediction of discharge rate is attributed to the fact that, in Princeton model friction starts at a lower solid volume fraction (in the current study it is set to 0.50) than the Schaeffer model, where friction starts at maximum packing (Benyahia, 2008). However, the recently developed CSS model (Chialvo et al., 2011) predicts a discharge rate of 6.67 g/s. During the period of steady discharge, the depth of the material in the bin varied considerably. The discharge rate is, therefore, roughly independent of the height of the material in the bin. Experimentally, it has long

been known that the flow rate of Geldart type B granular material (the same type of particles simulated in this study) from bins and hoppers is independent of the surcharge level (Nedderman et al., 1982).

We also compute the discharge rate from DEM simulation and Beverloo correlation and compare them with the discharge rate obtained from different continuum models. These calculations are done for a particle with density of 2.9 g/cm^3, and the diameter of the particles are set to 1 mm. For these particle properties, DEM predicts a steady discharge rate of 4.94 g/s (shown with dash dot dot line in Fig. 6.7(a)). The Beverloo correlation (Eq. 6.26):

$$\dot{m} = 0.58\rho_b g^{0.5}(D - kd_p)^{2.5}, \tag{6.26}$$

predicts a discharge rate of 4.29 g/s. In Eq. 6.26, $\dot{m}$ is the discharge rate, $\rho_b = \rho_s \nu$ is the initial solid bulk density, g is the acceleration due to gravity, D is the outlet discharge size, k is the Beverloo constant and d_p is the particle diameter. From this result it is evident that, the two traditionally used continuum models (Schaeffer and Princeton) significantly over–predict the discharge rate compared to the discharge rate obtained from Beverloo correlation (Beverloo et al., 1961) and DEM data. The recently developed CSS model does reasonably good job by predicting the discharge rate within 35% with that of the DEM data. However, there is a good agreement between the discharge rate predicted using DEM simulations and Beverloo correlation of experimental data.

The discharge rate from silo is closely related to the discharge velocities of solids near the orifice, hence we also compare the discharge velocities obtained using different continuum models to the discharge velocities from DEM simulations, which are shown in Fig. 6.7(b). These velocity profiles are extracted during steady discharge at location $2d_p$ above the bottom orifice. As shown in Fig. 6.7(b), the velocity of solid particles increases as it approaches towards orifice for all the continuum models and DEM simulations. The solid velocity attains highest value at the center of silo. Near the walls the

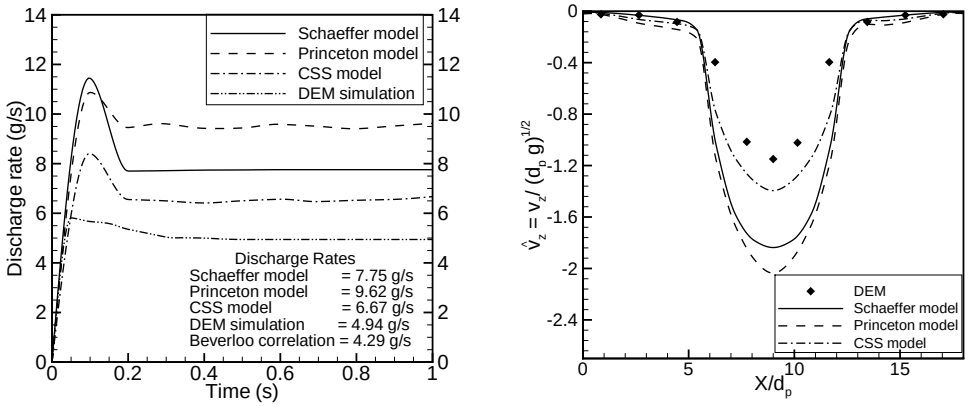

(a) (b)

Figure 6.7 (a) Temporal variation of discharge rate using three different continuum models and DEM simulations for a three–dimensional (3D) flat–bottomed silo. The solid line shows the discharge profile obtained from Schaeffer model, the dashed line is the prediction for the discharge rate obtained using Princeton model, and the dash dot line shows the discharge profile obtained from CSS model. The dash dot dot line shows the temporal variation of discharge rate obtained from DEM simulation, and (b) Transverse solid velocity profile near the orifice during steady discharge. The solid line is the predicted profile of solid velocity by Schaeffer model, the dashed line shows the prediction obtained using Princeton model, whereas the dash dot line are the solid velocity obtained from CSS model. The filled diamonds are the solid velocity data obtained from the DEM simulations. Simulation parameters: $D = 6d_p$, $\mu_p = 0.5$, $e = 0.91$.

particle flows with very low velocity as seen in Fig. 6.7(b). As expected the discharge velocities predicted by Princeton model are higher than the discharge velocity computed using Schaeffer and CSS model, which lead to higher discharge rate prediction from the Princeton model as shown in Fig. 6.7(a). The discharge velocities predicted by the DEM simulations are lowest, which also verifies the lower discharge rate prediction from the DEM simulations.

In order to understand this discrepancy in the discharge rate prediction, the error incurred in the solid stress prediction is quantified by comparing the predicted granular stress (using continuum models) with that of DEM data. We extract stresses from continuum models and DEM simulations in different cells, and quantify the error using vector norm of the relative error (see Eq. 6.27) in each cell.

$$\hat{\epsilon} = \frac{||(\sigma_{ij})_{Model} - (\sigma_{ij})_{DEM}||_2}{||(\sigma_{ij})_{DEM}||_2} \tag{6.27}$$

These stresses are extracted in a slice of thickness $2d_p$ (along y direction), which is located at the center of the silo. In x (along width of the silo) and z (along height of the silo) a grid size of $2d_p$ is used to perform this error analysis. Figures 6.8(a), 6.8(b) and 6.8(c) are the contour plots of error ($\hat{\epsilon}$) in solid stress prediction using Schaeffer, Princeton and CSS models, respectively. These figures show that the maximum error incurred in solid stress prediction (when compared with the stresses computed from DEM simulations) is around 42% and 56% for Schaeffer and Princeton model, respectively. However, the recently developed CSS model (Chialvo et al., 2011) is able to predict solid stresses within accuracy of 26% of the DEM data. The better performance of CSS model could be link to the fact that this model provides a blending function for patching each regime's asymptotic form in order to predict the stresses in different regimes. It is also interesting to note that the Princeton model predicts lowest stresses. The reason for the lower stress prediction using Princeton model can be ascribed to the fact that,

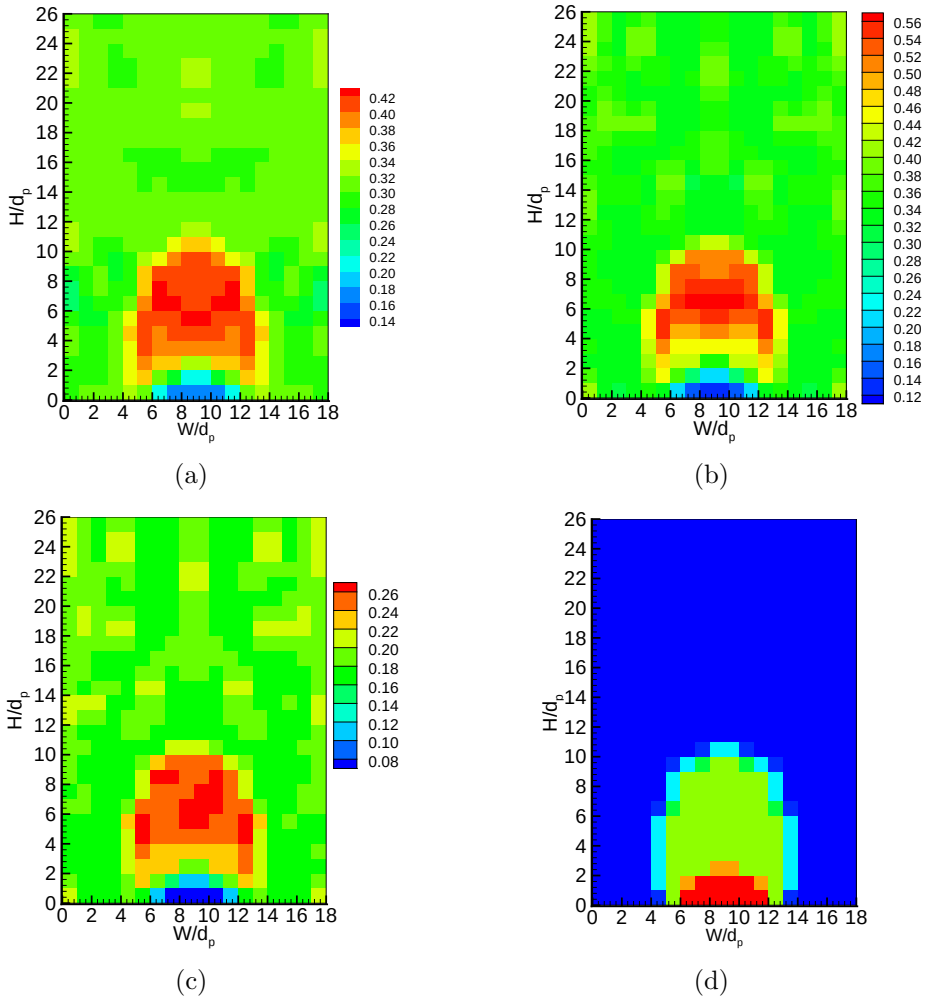

Figure 6.8 Error in stress prediction (error quantified using vector norm of relative error, see Eq. 6.27). (a) For Schaeffer model (b) For Princeton model and (c) For CSS model (d) Spatial extent of different regimes of granular rheology in a flat–bottomed silo. Simulation parameters: $D = 6d_p$, $\mu_p = 0.5$, $e = 0.91$. (for interpretation of the references to color in this figure legend, the reader is referred to the web version of this article.)

in Princeton model the friction starts at lower value of solid volume fraction than the Schaeffer model (in which friction starts at maximum packing), hence the computed stresses are lower than that of Schaeffer and CSS model. Further, it is interesting to correlate Figs. 6.8(a), 6.8(b), and 6.8(c) with Figs. 6.6(a) and 6.6(b), a close examination of these figures reveals that the maximum error incurred in the stress prediction (using continuum models) spreads around the spatial location where intermediate regime is present. Therefore, it can be concluded that this intermediate regime poses a significant challenge for performance a given continuum model, in which scaling of stress with the strain rate is itself a function of particle (such as interparticle friction coefficient, coefficient of inelasticity) and flow (such as shear rate) properties.

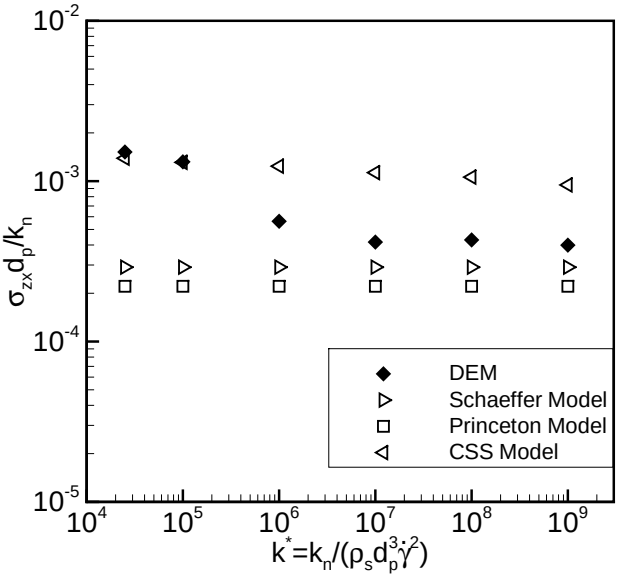

Figure 6.9 Performance of difference continuum models in a simple homogeneous shear flow. Simulation parameter: $\nu = 0.62$, $\mu_p = 0.1$ and $e = 0.7$.

To further investigate the performance of these three different continuum models in the intermediate regime of flow (where the error in error prediction is highest), we

compare their prediction for shear stress with the data obtained from DEM simulations of homogeneously sheared granular flow. These homogeneous shear simulations are performed with periodic boundary conditions in all directions (x, y, and z) and uniform shear is generated in the domain using the "SLLOD" algorithm (Evans and Morriss, 1990). The SLLOD algorithm (Evans and Morriss, 1990) is an improved form of the Lees–Edwards boundary condition (Lees and Edwards, 1972) to generate simple shear flows. For further details about these homogeneous shear simulations reader is directed to section 3.1 of our previously published article (Vidyapati and Subramaniam, 2012a). In Fig. 6.9 we compare the shear stress predicted using these three continuum model with that of DEM data in the intermediate regime for a solid volume fraction of 0.62 with interparticle friction coefficient of 0.1 (this combination of solid volume fraction and particle friction coefficient corresponds to the intermediate regime). Figure 6.9 shows that the shear stress predicted using Schaeffer (Schaeffer, 1987) and Princeton (Srivastava and Sundaresan, 2003) model are independent of applied shear rate in the intermediate regime. The CSS model (Chialvo et al., 2011) shows a dependence on applied shear rate (similar to that observed in the DEM data), but this dependence is not strong enough to accurately capture the DEM data points for all values of applied strain rate tested in the intermediate regime.

6.4 Conclusions

Discharge dynamics of granular particles from a three–dimensional (3D) flat-bottomed silo is studied using both discrete (DEM) and continuum simulations. DEM results for discharge rate in a flat–bottomed silo shown to behave robustly with variation of parameters such as interparticle friction coefficient and discharge outlet size. However, it is found that the wall friction coefficient and particle coefficient of restitution has no or negligible influence on the discharge rate from the silo. Spatial extent of different

regimes in the silo discharge problem is quantified using a regime map established from DEM simulation data of homogeneous sheared granular flow Vidyapati and Subramaniam (2012a). The results of this study reveal that, all three different regimes of granular flow (inertial, intermediate and quasi–static) co-exist in this silo discharge problem. It is also found that the spatial extent of the intermediate regime expands as the interparticle friction coefficient decreases.

The quantitative comparison study between DEM and different continuum models reveals that the two traditionally used continuum models (Schaeffer (Schaeffer, 1987) and Princeton (Srivastava and Sundaresan, 2003)) significantly over–predict the discharge rate from silo. However, the recently developed CSS model (Chialvo et al., 2011) does a reasonably good job by predicting discharge rate within 35% of the DEM data. Nevertheless, the DEM prediction of discharge rate is in very good agreement with the discharge rate computed using Beverloo correlation (Beverloo et al., 1961) of experimental data. The error incurred in the solid stress prediction is quantified using vector norm of relative error, which shows maximum error of 42%, 56% and 26% in the solid stress prediction using Schaeffer, Princeton and CSS model, respectively. It is also found that maximum error in the solid stress prediction is near the spatial locations where intermediate regime span. The results of this study reconfirm that, DEM can be used as a tool to isolate and identify one of the possible causes for poor prediction of the discharge rate in silo, such as large spatial extent of the intermediate regime and its complex rheological behavior, that currently continuum models have difficulty in capturing.

CHAPTER 7. A CONSTITUTVE MODEL BASED ON MESOSCALE DESCRIPTORS FOR DENSE GRANULAR FLOW

This chapter is a manuscript in preparation titled "A constitutive model based on mesoscale descriptors for dense granular flows" authored by Vidyapati and S. Subramaniam.

Abstract

A constitutive model is developed to capture the complex rheological behavior of dense granular flows (solid volume fraction ranging from 0.45 to 0.62) in the intermediate, quasi–static and inertial regimes. The proposed contact stress model (CSM) is based on a statistical closure for the average contact stress experienced by particles, which is shown to depend on the average relative acceleration between particle pairs. This modeling approach naturally gives rise to the dependence of average contact stress on mesoscale flow descriptors such as the coordination number and the fabric tensor. Appropriate closures for the coordination number and the fabric tensor are provided by solving their modeled evolution equation proposed by Sun and Sundaresan [J. Fluid Mech. (2011), vol. 682, pp.590-616]. The predictive capability of the proposed contact stress model (CSM) is tested in homogeneous shear flow using DEM data corresponding to the intermediate, quasi–static and inertial regimes.

Notation for section 7.1 to section 7.7

$\triangle t$ Time step for DEM simulation

d Particle diameter

$\mathbf{D}$ Modulus of strain rate tensor

e Particle restitution coefficient

$\mathbf{f}$ Contact force

F_n Normal contact force

F_t Tangential contact force

Fr Constant in Princeton frictional model

g Acceleration due to gravity

$g(\mathbf{r})$ Pair correlation function

k^* Nondimensional shear rate

k_n Particle normal stiffness coefficient

m Particle mass

N_{CN} Coordination number

N_c Number of contacts

N_1 Number of floaters

n Coefficient in the frictional model

P Pressure

P_c Critical state pressure

$\mathbf{R}$ Fabric tensor

r, s Constant in Princeton frictional model

t Time

t_c Binary collision time

T Granular temperature

$\mathbf{n}$ Unit normal

$\mathbf{r}$ Pair relative separation

$\mathbf{S}$ Strain rate tensor

$\mathbf{v}^{'}$ Fluctuating velocity of particle

V Sampling volume

$\mathbf{w}$ Pair relative velocity

$\mathbf{W}$ Spin tensor

Greek symbols

$\dot{\gamma}$ Shear rate

μ Particle friction coefficient

ν Solid volume fraction

ν_{crit} Critical solis volume fraction

ν^{max} Maximum solid packing

ν^{min} Minimum frictional solid volume fraction

ϕ Angle of internal friction

ρ_s Particle density

σ Stress

σ^{stream} Streaming contribution of the stress

σ^{cont} Contact contribution of the stress

σ^{tot} total granular stress

σ_{fric} Frictional stress tensor

σ_{kin} Kinetic stress tensor

7.1 Introduction

Continuum models for granular flow need to accurately predict global flow characteristics in practical devices, such as in hopper/silo discharge, chute flow and dense–phase pneumatic conveying (Sundaresan, 2001). However, prediction of discharge rate obtained using existing continuum models for even a simple flow such as silo, differs considerably from correlation to experimental data (Beverloo et al., 1961) and 3D DEM (discrete element method) simulations (Vidyapati and Subramaniam, 2012b). In order for continuum models to predict global flow characteristics accurately, they need accurate constitutive models that can perform well in all the regimes (inertial, intermediate and quasi–static) of granular flow. Figure 7.1 shows a schematic of granular regime map with their corresponding constitutive behavior in each regime, where σ is the shear stress, $\dot{\gamma}$ is the shear rate and n is an exponent that relates the shear stress with the shear rate.

As seen in Fig. 7.1, the kinetic theory for rapid granular flow (inertial regime) (Lun et al., 1984; Jenkins and Savage, 1983; Goldhirsch, 2003) predicts a constitutive behavior in which the characteristic scale of stress increases as the square of the strain rate ($\sigma \propto \dot{\gamma}^2$). In the other extreme regime, plasticity models applied to soil mechanics for slow quasi–static flow (Nedderman, 1992; Schaeffer, 1987) result in a stress that is independent of the applied shear rate ($\sigma \neq f(\dot{\gamma})$), and this is confirmed by DEM simulations (Campbell, 2002). Experiments performed by Tardos et al. (2003) reveal existence of a third intermediate (transitional) regime that is characterized by $\sigma \propto \dot{\gamma}^n$, where $0 < n < 2$. These experiments also indicate that the intermediate regime is broad enough in the parameter space of solid volume fraction, particle friction coefficient and shear rate to require a continuum model to capture its constitutive behavior. However, unlike the inertial (rapid flow) and quasi–static regimes, the intermediate (transitional) regime still lacks a predictive constitutive model and has motivated many studies over

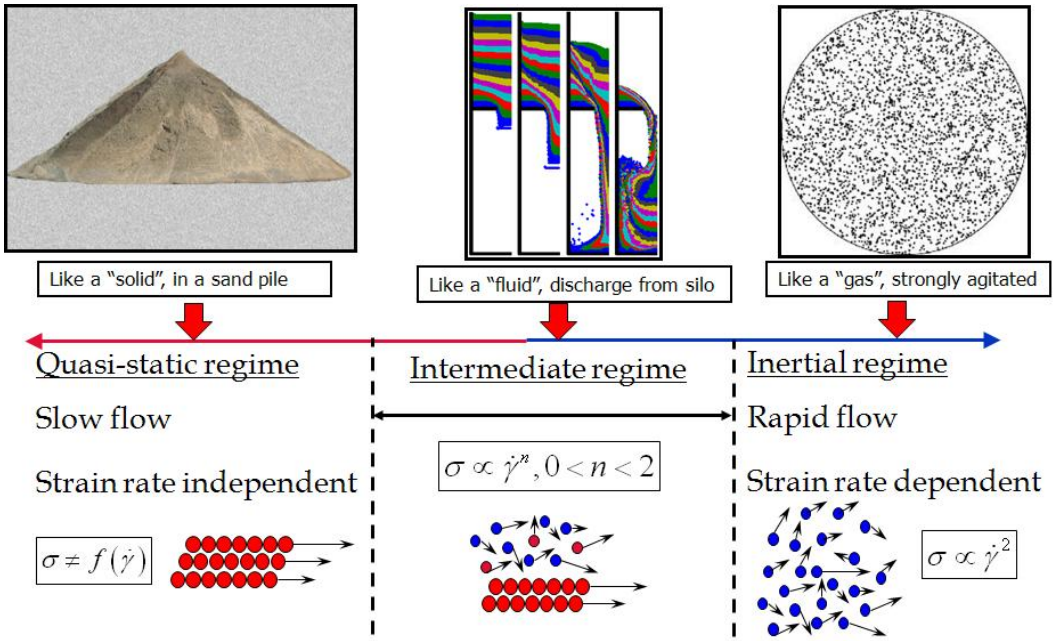

Figure 7.1 Schematic of granular regime map and their corresponding constitutive behavior in each regime.

the past decade (Jop et al., 2006; G.D.R. MiDi, 2004; Vidyapati et al., 2012; Vidyapati and Subramaniam, 2012a). These three different regimes often found to co–exist in aforementioned practical granular devices. Hence, a constitutive model that captures the correct rheology of granular flow in all the regimes is necessary.

However, development of accurate constitutive models for dense granular flows remains an open problem. Because they can exhibit different constitutive behaviors that depend on both the microscale properties (e.g., particle friction coefficient, coefficient of inelasticity) as well as on macroscale properties (e.g., solid volume fraction and shear rate) in different flow regimes. Of these three different regimes the intermediate regime where both collisional and enduring contacts between particles are important, poses significant challenge for a constitutive model. The stress tensor in the granular material is a function of both particle and flow level properties which corresponds to different scales of the problem, e.g., macroscale, mesoscale and microscale. Hence, the granular stress tensor σ_{ij} can be represented as,

$$\sigma_{ij} = f(\text{macroscale parameters}, \text{mesoscale parameters}, \text{microscale parameters}).$$

Most continuum models (Savage, 1998; Johnson and Jackson, 1987; Srivastava and Sundaresan, 2003) take in to the account the two extreme scale of the problem (e.g., macroscale and microscale) but do not incorporate the mesoscale parameters in the modeling framework. These models are based on additive decomposition of the total granular stress as a weighted sum of kinetic and frictional contribution ($\sigma_{ij} = \sigma_{ij}^{kin} + \sigma_{ij}^{fric}$), with the weight factor specified solely as a function of the solid volume fraction. A continuum theory for slow dense granular flows based on so–called associated flow rule is proposed by Savage (1998). This theory relates the shear stress and the strain rate in a plastic frictional system. Averaging strain–rate fluctuations yields a Bingham–like constitutive relation in which the shear stress has two contributions: a viscous part, and a strain–rate independent part. According to this theory the stress and strain rate

tensors are always coaxial. Furthermore, the theory also postulates that the viscosity diverges as the density approaches the close packing limit. A similar hydrodynamic model based on a Newtonian stress–strain constitutive relation with density–dependent viscosity is proposed by Losert et al. (2000). In this model also the viscosity diverges when the density approaches the random close packing density of grains. Jop et al. (2006) proposed a constitutive relation inspired by the analogy between granular flows and visco–plastic fluids such as Bingham fluids for open surface flows (such as chute flow). In their work (Jop et al., 2006), granular flow is described as an incompressible fluid with the stress tensor given as a function of the inertia number, $I = \dot{\gamma}d/(P/\rho_s)^{0.5}$, where d is the particle diameter, P is the pressure and ρ_s is the particle density. However, extension of the Jop's model (Jop et al., 2006) to the constant volume problem is non–trivial because this model does not provide constitutive equation for pressure, which is shown to be an important parameter in capturing granular rheology in the intermediate regime (Vidyapati and Subramaniam, 2012a).

Experiments have shown that solid volume fraction is insufficient as a microstructure variable in describing the correct rheology of granular flows and mesoscale parameters such as the coordination number and the fabric tensor have been measured using photo elastic particles (Oda et al., 1980; Subhash et al., 1991). Also, experiments in a 2D granular shear cell (GSC) (McCarthy et al., 2010; Jasti and Higgs, 2008) as well as DEM simulations (Volfson et al., 2003a) reveal that grain contacts in the intermediate regime are characterized by a mix of enduring solid–like and fluid–like contacts. In particular, these grain interactions are not determined by the solid volume fraction alone, but are dependent on particle properties (such as particle friction coefficient and inelasticity) as well as on flow properties (such as shear rate). Consequently, simple additive models are not able to capture the complex constitutive behavior in the intermediate (transitional) regime. Since most constitutive models in use are phenomenological, this observation motivates the development of a constitutive model for the intermediate regime that

reflects the phase transition based on microscale physical interaction between the grains.

By decomposing the total granular stress into contact and streaming contributions Vidyapati and Subramaniam (2012a) showed that contact (virial) contribution to the stress dominates ($> 95\%$), and follows the same scaling as the total granular stress in the intermediate regime. However, the streaming contribution of the total stress always follows the inertial scaling even in the intermediate regime. This result also indicates that the viscosity based models (such as proposed by Losert et al. (2000)) will not be able to capture the correct granular rheology in the intermediate regime, because viscosity is connected to streaming part of the stress tensor in the kinetic theory and it contributes less than 5% to the total granular stress in the intermediate and dense regimes of granular flow. These findings motivated need for an accurate contact stress model in the intermediate regime of granular flow.

In this work, we develop a contact stress model (CSM) which is based on statistical closure for the average contact stress experience by particle. Further, this average contact stress is shown to depend on the average relative acceleration between contacting pairs. Using a unique modeling approach the contact stress is related to mesoscale flow descriptors such as the coordination number N_{CN}, the fabric tensor $\mathbf{R}$ and the pair correlation function $g(\mathbf{r})$. Appropriate closures for the coordination number and the fabric tensor is obtained by solving their modeled evolution equations (Sun and Sundaresan, 2011) in a homogeneous shear flow. The pair correlation is further linked to the average normal contact force and its closure is proposed by specifying the probability distribution function (PDF) of the normal force (Mueth et al., 1998). In order to predict the total granular in the inertial regime, we couple the contact stress model to the ROP (refined order parameter) model (Vidyapati and Subramaniam, 2012a) using the order parameter (OP) concept (Volfson et al., 2003b). Finally predictive capability of the proposed contact stress model is demonstrated using DEM data of homogenous shear flow in different regimes of granular flow.

7.2 Contact stress model for dense granular flows

7.2.1 Model development

In this section we layout the development of contact stress model for dense granular flows. Each of the subheadings in this section will guide the reader through different steps of the model development.

Stress tensor:

The stress tensor in granular media can be decomposed in two parts (Luding et al., 2004). One part arising from momentum flux and called the streaming contribution

$$\boldsymbol{\sigma}^{stream} = \frac{1}{V}\sum_{i}^{N} m^{(i)}\mathbf{v}^{'(i)} \otimes \mathbf{v}^{'(i)}, \tag{7.1}$$

where m is the mass of a particle, $\mathbf{v}^{'}$ is the fluctuating velocity, i is a particle index and $\otimes$ denotes a dyadic product. The second part (contact contribution) due to particle contact in domain of volume V is given by

$$\boldsymbol{\sigma}^{cont} = \frac{1}{V}\sum_{i}^{N}\sum_{j,j\neq i}\frac{1}{2}\mathbf{r}^{(i)(j)} \otimes \mathbf{f}^{(i)(j)}, \tag{7.2}$$

where $\mathbf{r}^{(i)(j)}$ is the vector pointing from the center of particle j to the center of particle i, and $\mathbf{f}^{(i)(j)}$ is the contact force acting on particle i by particle j (see Fig. 7.2). Combining the streaming and contact contributions to the stress tensors, one has for smooth, soft spheres (Luding et al., 2004; Silbert et al., 2001):

$$\sigma_{\alpha\beta}^{tot} = \frac{1}{V}\left[\sum_{i} m^{(i)}v_{\alpha}^{'(i)}v_{\beta}^{'(i)} + \sum_{i}\sum_{j,j\neq i}\frac{1}{2}r_{\alpha}^{(i)(j)}f_{\beta}^{(i)(j)}\right], \tag{7.3}$$

where the first summation runs over all the particles and second summation runs over all the contacts in the averaging volume V.

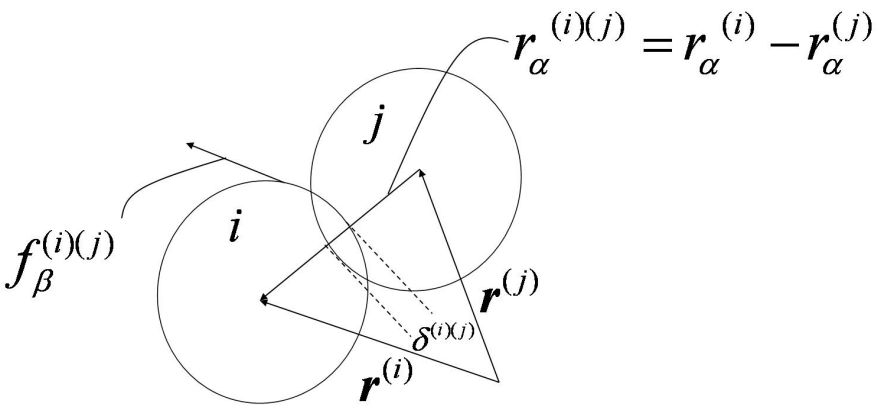

Figure 7.2 Schematic of two particles i and j contact with normal overlap $\delta^{(i)(j)}$ and position vectors $\mathbf{r}^{(i)}$, $\mathbf{r}^{(j)}$.

Expression for average contact stress:

A recent work by Vidyapati and Subramaniam (2012a) reveals that the contact contribution to the total granular stress dominates (contributes more than 95% to the total granular stress) and it has the same scaling as the total granular stress in the intermediate regime. However, the streaming contribution always follows the inertial scaling even in the intermediate regime. These results indicate that accurate modeling of the contact (virial) contribution of the granular stress is critical to capture the correct scaling of stress with the strain rate in the intermediate regime. This contact contribution of the granular stress can be written as (dropping streaming contribution of stress from Eq. 7.3)

$$\sigma_{\alpha\beta}^{cont} = \frac{1}{V}\left[\sum_i \sum_{j,j\neq i} \frac{1}{2} r_\alpha^{(i)(j)} f_\beta^{(i)(j)}\right]. \tag{7.4}$$

Note that Eq. 7.4, that is used to calculate stress in DEM (Luding et al., 2004; Silbert et al., 2001) is essentially a stress estimator.

We propose a statistical model for the average contact stress as

$$\sigma_{\alpha\beta}^{cont} = \langle \sum_i \sum_{j,j\neq i} r_\alpha^{(i)(j)} f_\beta^{(i)(j)} \rangle \approx m \langle N_c \rangle (V) \langle r_\alpha^{(i)(j)} \Delta A_\beta^{(i)(j)} \rangle, \tag{7.5}$$

where $\langle N_c \rangle(V)$ is the mean number of contacts in the sampling volume V, $\Delta\mathbf{A}^{(i)(j)}$ is the relative acceleration between particle i and j, i.e., $\Delta\mathbf{A}^{(i)(j)} = \mathbf{A}^{(j)} - \mathbf{A}^{(i)}$ and $\langle\rangle$ denotes the averaging over all multiparticle contacts. In order to completely specify the model on the right hand side of Eq. 7.5, specification of following quantities are needed:

1. The mean number of contacts ($\langle N_c \rangle(V)$): This can be written in terms of average (bulk) coordination number as follows (Zhang and Makse, 2005):

$$\langle N_c \rangle(V) = \frac{N_{CN}}{2} \langle N(V) \rangle, \tag{7.6}$$

   where N_{CN} is the average or bulk coordination number and $\langle N(V) \rangle$ is the average or expected number of particles in volume V. The average coordination number N_{CN} is the average number of contacts par particle, and in DEM simulations it is computed as:

$$N_{CN} = \frac{\sum_i N_c^{(i)}}{N - N_1}, \tag{7.7}$$

   where N_c is number of contacts for i^{th} particle, N is the total number of particles in volume V, whereas N_1 is the number of floaters (particles with less than one contact in non–gravity environment).

2. The second required quantity is $\langle r_\alpha^{(i)(j)} \Delta A_\beta^{(i)(j)} \rangle$ for a contact. To compute $\langle r_\alpha^{(i)(j)} \Delta A_\beta^{(i)(j)} \rangle$ concept of relative acceleration is used, which is discussed in the following.

Relative acceleration concept for average contact stress between particle pairs:

Relative acceleration is the key to capturing structure dependent rheology. The relative acceleration based coarse graining approach (Markutsya, 2010; Markutsya et al., 2012) based on transport equation for two–particle density has been successfully used to model the solute interactions in the presence of solvent, leading to accurate prediction of nanoparticle aggregation using Brownian dynamics simulations. The crucial unclosed

term that needs to be modeled in the two–particle transport equation is the relative acceleration between two particles conditional on their relative separation and relative velocity. This concept is used to develop a microscale physics–based model for the contact part of the granular stress in the intermediate and dense regime. The unconditional average relative acceleration between the particles can be written in terms of conditional average relative acceleration as follows

$$\langle \Delta \mathbf{A} \rangle = \frac{V}{\alpha^{(2)}} \int \langle \Delta \mathbf{A} | \mathbf{r}, \mathbf{w} \rangle \rho^{(2)}(\mathbf{r}, \mathbf{w}) d\mathbf{r} d\mathbf{w}. \tag{7.8}$$

In Eq. 7.8, $\langle \Delta \mathbf{A} | \mathbf{r}, \mathbf{w} \rangle$ is the average relative acceleration between a pair of particles each located at $\mathbf{x}_1$ and $\mathbf{x}_2$ with velocities $\mathbf{v}_1$ and $\mathbf{v}_2$ respectively, where $\mathbf{r} = \mathbf{x}_2 - \mathbf{x}_1$ is the pair relative separation and $\mathbf{w} = \mathbf{v}_2 - \mathbf{v}_1$ is the pair relative velocity. $\rho^{(2)}(\mathbf{r}, \mathbf{w})$ is the two particle density and $\alpha^{(2)} = N \times (N-1)$, where N is the number of particles. Equation 7.8, represents a closure at the two–particle level, which is consistent with DEM that assumes additive pairwise interaction. The position velocity pair correlation function $g(\mathbf{r}, \mathbf{w})$ is related to two particle density $\rho^{(2)}(\mathbf{r}, \mathbf{w})$ by

$$\rho^{(2)}(\mathbf{r}, \mathbf{w}) = n^2 g(\mathbf{r}, \mathbf{w}) \tag{7.9}$$

where n is the number density of particles. With the assumption of homogeneous point field, Eq. 7.8 can be written as (provided N is sufficiently high)

$$\langle \Delta \mathbf{A} \rangle = \frac{1}{V} \int \langle \Delta \mathbf{A} | \mathbf{r}, \mathbf{w} \rangle g(\mathbf{r}, \mathbf{w}) d\mathbf{r} d\mathbf{w}, \tag{7.10}$$

Decomposition of average relative acceleration:

Assuming a separable form at steady state the conditional average relative acceleration $\langle \Delta \mathbf{A} | \mathbf{r}, \mathbf{w} \rangle$, can be decomposed as follows:

$$\langle \Delta \mathbf{A} | \mathbf{r}, \mathbf{w} \rangle = \langle \Delta \mathbf{A} | \mathbf{r} \rangle + \langle \Delta \mathbf{A} | \mathbf{w} \rangle, \tag{7.11}$$

where $\langle \Delta \mathbf{A} | \mathbf{r} \rangle$ is the average relative acceleration conditional on pair relative separation $\mathbf{r}$, and $\langle \Delta \mathbf{A} | \mathbf{w} \rangle$ is the average relative acceleration conditional on pair relative velocity $\mathbf{w}$.

In LD (Langevin dynamics), the term $\langle \Delta \mathbf{A} | \mathbf{w} \rangle$ can be modeled in terms of inelasticity and damping. In dense regime the contribution from this term ($\langle \Delta \mathbf{A} | \mathbf{w} \rangle$) is expected to be very small and it is neglected in the current work. We focus on other term $\langle \Delta \mathbf{A} | \mathbf{r} \rangle$, the average relative acceleration conditioned on pair separation $\mathbf{r}$, which can be written as

$$\langle \Delta \mathbf{A} | \mathbf{r} \rangle = \frac{\mathbf{f}^{(i)(j)}}{m^{(i)}} - \frac{\mathbf{f}^{(j)(i)}}{m^{(j)}} = 2\frac{\mathbf{f}^{(i)(j)}}{m}, \tag{7.12}$$

where m is the mass of the particle, assuming $m^{(i)} = m^{(j)} = m$ (for monodisperse system). Now using Eqs. 7.10 and 7.12, we can write unconditional average relative acceleration as follows

$$\langle \Delta \mathbf{A} \rangle = \frac{1}{V} \int \mathbf{f}^{(i)(j)} \frac{2}{m} g(\mathbf{r}) d\mathbf{r}, \tag{7.13}$$

where $\mathbf{f}^{(i)(j)}$ is the force on particle i due to particle j.

Incorporation of normal and tangential force:

The force $\mathbf{f}^{(i)(j)}$ is written as sum of normal and tangential component:

$$\mathbf{f}^{(i)(j)} = \mathbf{f}_n^{(i)(j)} + \mathbf{f}_t^{(i)(j)}. \tag{7.14}$$

The normal component of the force $\mathbf{f}_n^{(i)(j)}$ is given as (Silbert et al., 2001):

$$\mathbf{f}_n^{(i)(j)} = f\left(\delta^{(i)(j)}/d\right) k_n \delta^{(i)(j)} \mathbf{n}^{(i)(j)}, \tag{7.15}$$

where $\delta^{(i)(j)}$ is the normal overlap between the contacting particle i and j, k_n is the normal spring stiffness, d is the particle diameter and $\mathbf{n}^{(i)(j)}$ is the unit vector along the ling joining centers of contacting particles. For a linear spring model (Hookean model) $f(\delta^{(i)(j)}/d) = 1$, hence one can write the normal component of the force as:

$$\mathbf{f}_n^{(i)(j)} = k_n \delta^{(i)(j)} \mathbf{n}^{(i)(j)}. \tag{7.16}$$

Now the tangential component of the force is added in to the model equation by invoking Coulomb criterion at slippage ($|\mathbf{f}_t^{(i)(j)}| = \mu|\mathbf{f}_n^{(i)(j)}|$). The tangential force can be written as

$$\mathbf{f}_t^{(i)(j)} = f_t^{(i)(j)}\mathbf{t}^{(i)(j)}, \tag{7.17}$$

where $\mathbf{t}^{(i)(j)}$ is orthogonal to $\mathbf{n}^{(i)(j)}$. Hence the total force (at slippage) can be written as:

$$\mathbf{f}^{(i)(j)} = k_n\delta^{(i)(j)}\mathbf{n}^{(i)(j)} + \mu f_n^{(i)(j)}\mathbf{t}^{(i)(j)}, \tag{7.18}$$

which can be further written as

$$\mathbf{f}^{(i)(j)} = k_n\delta^{(i)(j)}\left(\mathbf{n}^{(i)(j)} + \mu\mathbf{t}^{(i)(j)}\right). \tag{7.19}$$

Further, by using Eqs. 7.13 and 7.19, one can write the average unconditional relative acceleration as follows

$$\langle\Delta\mathbf{A}\rangle = \frac{2}{mV}\int k_n\delta^{(i)(j)}\left(\mathbf{n}^{(i)(j)} + \mu\mathbf{t}^{(i)(j)}\right)g(\mathbf{r})d\mathbf{r}. \tag{7.20}$$

However, to have a model for contact stress, one need to compute $\langle r_\alpha^{(i)(j)}\Delta A_\beta^{(i)(j)}\rangle$, which is obtained from Eq. 7.20 as follows

$$\langle r_\alpha^{(i)(j)}\Delta A_\beta^{(i)(j)}\rangle = \frac{2k_n}{mV}\int r_\alpha^{(i)(j)}\delta^{(i)(j)}\left(n_\beta^{(i)(j)} + \mu t_\beta^{(i)(j)}\right)g(\mathbf{r})d\mathbf{r}. \tag{7.21}$$

The unit normal vector $n_\alpha^{(i)(j)}$, in the direction of line joining the centers of contacting particles is

$$n_\alpha^{(i)(j)} = \frac{r_\alpha^{(i)(j)}}{r^{(i)(j)}}. \tag{7.22}$$

Now using Eqs. 7.21 and 7.22, we can derive following:

$$\langle r_\alpha^{(i)(j)}\Delta A_\beta^{(i)(j)}\rangle = \frac{2k_n}{mV}\int r^{(i)(j)}\delta^{(i)(j)}\left(n_\alpha^{(i)(j)}n_\beta^{(i)(j)} + \mu n_\alpha^{(i)(j)}t_\beta^{(i)(j)}\right)g(\mathbf{r})d\mathbf{r} \tag{7.23}$$

Contact stress:

Now using Eqs. 7.4, 7.5, 7.6, and 7.23, the contact stress contribution is written as:

$$\sigma_{\alpha\beta}^{cont} = \frac{1}{2V^2} N_{CN} \langle N(V) \rangle k_n \int r^{(i)(j)} \delta^{(i)(j)} \left(n_\alpha^{(i)(j)} n_\beta^{(i)(j)} + \mu n_\alpha^{(i)(j)} t_\beta^{(i)(j)} \right) g(\mathbf{r}) d\mathbf{r} \quad (7.24)$$

where $r^{(i)(j)}$ is defined as (see Fig. 7.2)

$$r^{(i)(j)} = d - \delta^{(i)(j)}. \quad (7.25)$$

Hence the contact stress can be further written as:

$$\sigma_{\alpha\beta}^{cont} = \frac{1}{2V^2} N_{CN} \langle N(V) \rangle k_n \int \left(d - \delta^{(i)(j)} \right) \delta^{(i)(j)} \left(n_\alpha^{(i)(j)} n_\beta^{(i)(j)} + \mu n_\alpha^{(i)(j)} t_\beta^{(i)(j)} \right) g(\mathbf{r}) d\mathbf{r} \quad (7.26)$$

which is simplified as

$$\sigma_{\alpha\beta}^{cont} = \frac{1}{2V^2} N_{CN} \langle N(V) \rangle k_n \int \left(d\delta^{(i)(j)} - \delta^{2(i)(j)} \right) \left(n_\alpha^{(i)(j)} n_\beta^{(i)(j)} + \mu n_\alpha^{(i)(j)} t_\beta^{(i)(j)} \right) g(\mathbf{r}) d\mathbf{r}. \quad (7.27)$$

For very small overlaps (for real particles such as glass beads), one can rewrite Eq. 7.27 as follows

$$\sigma_{\alpha\beta}^{cont} = \frac{1}{2V^2} N_{CN} \langle N(V) \rangle k_n d \int \delta^{(i)(j)} \left(n_\alpha^{(i)(j)} n_\beta^{(i)(j)} + \mu n_\alpha^{(i)(j)} t_\beta^{(i)(j)} \right) g(\mathbf{r}) d\mathbf{r}. \quad (7.28)$$

Equation 7.28 can be further written as

$$\sigma_{\alpha\beta}^{cont} = \frac{1}{2V^2} N_{CN} \langle N(V) \rangle d \left[\int k_n \delta^{(i)(j)} n_\alpha^{(i)(j)} n_\beta^{(i)(j)} g(\mathbf{r}) d\mathbf{r} + \mu \int k_n \delta^{(i)(j)} n_\alpha^{(i)(j)} t_\beta^{(i)(j)} g(\mathbf{r}) d\mathbf{r} \right] \quad (7.29)$$

which is further simplified as

$$\sigma_{\alpha\beta}^{cont} = \frac{1}{2V^2} N_{CN} \langle N(V) \rangle d \left[\int f_n^{(i)(j)}(\mathbf{r}) \, n_\alpha^{(i)(j)} n_\beta^{(i)(j)} g(\mathbf{r}) d\mathbf{r} + \mu \int f_n^{(i)(j)}(\mathbf{r}) \, n_\alpha^{(i)(j)} t_\beta^{(i)(j)} g(\mathbf{r}) d\mathbf{r} \right]. \quad (7.30)$$

The normalized distribution of contacts in granular media is generally described by three–dimensional second order fabric tensor (Bathurst and Rothenburg, 1990; Cowin, 2004)

$$R_{\alpha\beta} = \langle n_\alpha^{(i)(j)} n_\beta^{(i)(j)} \rangle. \quad (7.31)$$

We define an another tesnor $T_{\alpha\beta}$, which is denoted as orthogonal fabric tensor as follows,

$$T_{\alpha\beta} = \langle n_{\alpha}^{(i)(j)} t_{\beta}^{(i)(j)} \rangle. \tag{7.32}$$

Using Eqs. 7.31 and 7.32 one can write expression for contact as follows

$$\sigma_{\alpha\beta}^{cont} = \frac{1}{2V} N_{CN} \langle N(V) \rangle d \left[R_{\alpha\beta} \frac{1}{V} \int f_n^{(i)(j)}(\mathbf{r})\, g(\mathbf{r}) d\mathbf{r} + \mu T_{\alpha\beta} \frac{1}{V} \int f_n^{(i)(j)}(\mathbf{r})\, g(\mathbf{r}) d\mathbf{r} \right]. \tag{7.33}$$

Dependence of the stress on the PDF of normal force:

Towards this end, one can write average normal force between particle i and j as follows

$$\langle f_n^{(i)(j)} \rangle = \frac{1}{V} \int f_n^{(i)(j)}(\mathbf{r})\, g(\mathbf{r}) d\mathbf{r} \tag{7.34}$$

Hence, Eq. 7.33 simplifies to,

$$\sigma_{\alpha\beta}^{cont} = \frac{1}{2V} N_{CN} \langle N(V) \rangle d \left(R_{\alpha\beta} \langle f_n^{(i)(j)} \rangle + \mu T_{\alpha\beta} \langle f_n^{(i)(j)} \rangle \right), \tag{7.35}$$

which can be further simplified as

$$\sigma_{\alpha\beta}^{cont} = \frac{1}{2V} N_{CN} \langle N(V) \rangle d \langle f_n^{(i)(j)} \rangle \left(R_{\alpha\beta} + \mu T_{\alpha\beta} \right), \tag{7.36}$$

where $\langle f_n^{(i)(j)} \rangle$ is the mean normal force between contacting particles i and j, which can be related to PDF (probability density function) of normal force e.g., $\langle f_n^{(i)(j)} \rangle = \int f P(f) df$. The orthogonal fabric tensor $T_{\alpha\beta}$ is computed in DEM by defining a unit vector $\mathbf{t}$ as follows

$$\mathbf{t} = \frac{\mathbf{f}_t}{|f_t|}. \tag{7.37}$$

We compute this orthogonal fabric tensor $T_{\alpha\beta}$ using data from our DEM simulations of homogeneously sheared granular flow. It is found that for all the solid volume fraction beyond 0.57, the normal and shear components of the fabric tensor $R_{\alpha\beta}$ are approximately

equal (within 8% of accuracy) to the normal and shear components of the orthogonal fabric tensor $T_{\alpha\beta}$. Hence expression for the contact stress can be written as follows,

$$\sigma_{\alpha\beta}^{cont} = \frac{1}{2V} N_{CN} \langle N(V) \rangle d \langle f_n^{(i)(j)} \rangle R_{\alpha\beta} \left(1 + \mu\right). \tag{7.38}$$

Equation 7.38 is used to compute contact stress for a homogeneously sheared granular assembly. Figure 7.3 illustrate the concept of the proposed contact stress model for granular flows in the intermediate and dense regime. Figure 7.3 illustrate the concept of the proposed contact stress model for granular flows in the intermediate and dense regime.

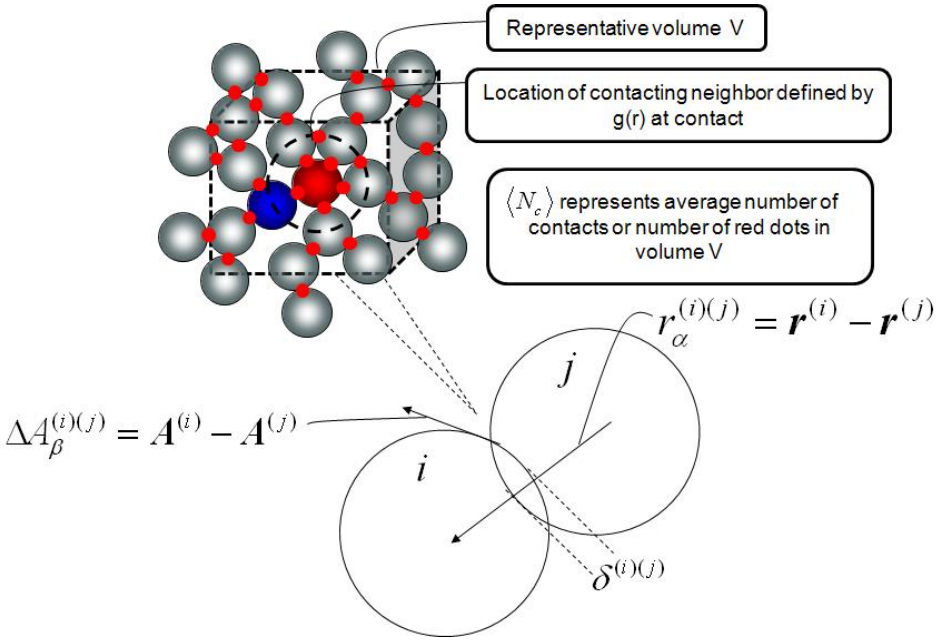

Figure 7.3 Illustration of proposed contact stress model based on mesoscale flow descriptors.

7.2.2 Inputs to the contact stress model

Three inputs are required to complete the specification of proposed contact stress model (see Eq. 7.35), which are summarized below:

1. N_{CN} (Average coordination number): It is defined as the mean number of contacts per particle in the contact network. The average (bulk) coordination number can be obtained by solving its modeled evolution equation proposed by Sun and Sundaresan (2011).

2. $R_{\alpha\beta}$ (Fabric tensor): Fabric tensor represents the anisotropy present in the granular media. In order to give a model for fabric tensor we solve its evolution equation proposed by Sun and Sundaresan (2011).

3. $\langle f_n^{(i)(j)} \rangle$ (Mean normal force): This can be computed using probability density function (PDF) of normal force. We use the normal force data obtained from our 3D DEM simulations of homogeneously sheared granular flow to construct its PDF and compare this distribution with the published results of Mueth et al. (1998). In dense granular flows the universal nature of force PDF allows simplification because the force distribution remains independent of interparticle friction μ, shear rate $\dot{\gamma}$ and solid volume fraction ν.

The validity of required closures for above model inputs are verified against DEM data of homogeneous shear flows. The following section describes these DEM simulations of homogeneously sheared granular flow.

7.3 DEM simulations of homogeneously sheared granular flow

In order to provide closures for different parameters (model inputs) and to generate benchmark data for model assessment, we performed DEM simulations of monodisperse, non–cohesive spheres of diameter d and mass m subjected to homogeneous shear (where the stress is independent of position) over a range of solid volume fractions ν, particle friction coefficient μ and shear rate $\dot{\gamma}$. A soft–sphere model is used in which particles interact via contact laws and friction only on contact. Since the realistic modeling of

particle deformation is complicated, a simplified contact force model based on a linear spring–dashpot combination is used in this work (Silbert et al., 2001). Details of the computational model used in the discrete element simulations are given in Sec. 3.1.

These constant–volume DEM simulations of sheared granular flow are performed in a cubical domain of side length $L = 14d$. The effect of system size is examined by varying the box length from $7d$ to $20d$. It was found that the stress asymptotes once the box length exceeds $10d$, consistent with the estimates reported by Campbell (2002). For all the simulations reported, the mass and diameter of the particles are set to 1, so the density of the particles is $6/\pi$. The value of normal spring stiffness k_n is set to 2×10^5 (mg/d units), which captures the general behavior of intermediate to high k_n systems (Silbert et al., 2001). The value of the coefficient of restitution e is chosen to be 0.7. All these simulations are performed with zero gravity. The integration time step Δt for all the simulations is selected to be $t_c/50$, where t_c is the binary collision time. This time step is shown to be sufficiently small to ensure temporal convergence (Silbert et al., 2001). Simulations are run to a nondimensional time of $\dot{\gamma}t = 500$, which is long enough to attain a statistically stationary solution (Campbell, 2002). After reaching steady state the quantities are time–averaged over a time window corresponding to $200\dot{\gamma}^{-1}$.

These homogeneous shear simulations are performed with periodic boundary conditions in all directions (x, y, z) and uniform shear is generated in the domain using the "SLLOD" algorithm (Evans and Morriss, 1990). The SLLOD algorithm (Evans and Morriss, 1990) is an improved form of the Lees-Edwards boundary condition (Lees and Edwards, 1972) to generate simple shear flows. The shearing motion induced by the Lees-Edwards boundary condition takes time to develop. Therefore, the flow would not be homogeneous immediately after a shear rate change, which raises questions about the suitability of this algorithm to study homogeneous time–dependent flows. This difficulty can be greatly alleviated through the use of the SLLOD algorithm. The SLLOD algorithm originates from ideas in nonequilibrium statistical mechanics (Evans and Morriss,

1990) where nonequilibrium flows such as shear flow are simulated by applying a force to the entire system (as opposed to simply moving the boundaries of the system faster or slower, as done in Lees-Edwards). Although we do not study time–dependent shear in this article, the SLLOD algorithm was applied to all the simulations performed in this study to be consistent with other work.

The next section describes the appropriate closures for the model inputs discussed in Sec. 7.2.2.

7.4 Closures for contact stress model

As mentioned in the in Sec. 7.2.2, the constitutive model for contact stress (see Eq. 7.35) requires closures for following parameters:

1. Average coordination number
2. Fabric tensor
3. Mean normal force

In this section we detail the required closures for aforementioned parameters.

7.4.1 Closure for the coordination number

The average coordination number is the average number of contacts per particle in the contact network. Coordination number characterizes the connectivity of a granular assembly and it is shown to be an important parameter that captures the phase transition in granular rheology (Vidyapati and Subramaniam, 2012a). While computing the coordination number from DEM data, we neglect particles with zero (floaters) or one contact (rattlers) as they do not participate in the contact network, consistent with the practice of other researchers (Shundyak et al., 2007). Sun and Sundaresan (2011)

proposed a postulated form of evolution equation for the coordination number N_{CN}:

$$\frac{dN_{CN}}{dt} = d_1 \left(\mathbf{R} : \mathbf{S} - \chi|\mathbf{S}|\right) + d_2|\mathbf{D}| \left(f(\nu) - N_{CN}\right) + d_3 tr(\mathbf{D}), \tag{7.39}$$

where d_1, d_2 and d_3 are the material parameters in this microstructure evolution equation. In Eq. 7.39, $\mathbf{R}$ is fabric tensor, $\mathbf{D}$ is the strain rate tensor, $\mathbf{S}$ is the deviatoric strain rate tensor $\left(\mathbf{S} = \mathbf{D} - \frac{1}{3}tr(\mathbf{D})\mathbf{I}\right)$ and ν is the solid volume fraction. For a steady simple shear flow Eq. 7.39 reduces to following form

$$\frac{dN_{CN}}{dt} = d_2|\mathbf{D}| \left(f(\nu) - N_{CN}\right). \tag{7.40}$$

The function $f(\nu)$ dictates how the coordination number varies with the solid volume fraction in steady simple shear. This function has the following form (Sun and Sundaresan, 2011):

$$f(\nu) = N_{CN,crit} + \beta_1(\nu - \nu_{crit})^{\beta_2}, \tag{7.41}$$

where model constants $\beta_1 = 7.5$ and $\beta_2 = 0.5$. In Eq. 7.41, $N_{CN,crit}$ and ν_{crit} are the critical coordination number and critical solid volume fraction, respectively. $N_{CN,crit}$ varies from 4 to 6 as particle friction coefficient changes from infinity to zero in three dimensions (Song et al., 2008). Using Eqs. 7.40 and 7.41, one can write the evolution equation of coordination for steady simple shear flow as

$$\frac{dN_{CN}}{dt} = d_2|\mathbf{D}| \left[(N_{CN,crit} - N_{CN}) + 7.5(\nu - \nu_{crit})^{0.5}\right], \tag{7.42}$$

where $d_2 = 5.6$ is a material parameter (Sun and Sundaresan, 2011) and $|\mathbf{D}| = \sqrt{\frac{1}{2}\left(D_{ij}D_{ji}\right)}$ is the modulus of strain rate tensor.

The parameters $N_{CN,crit}$ and ν_{crit} are the function of interparticle friction coefficient μ (Sun and Sundaresan, 2011). We use first order explicit scheme to march in time and obtain a steady value of the coordination number using Eq. 7.42. Figures 7.4(a) and 7.4(b) show the evolution of the coordination number for a simple homogeneous shear flow for a solid volume of 0.61 and 0.62, respectively. The solid line is the solution

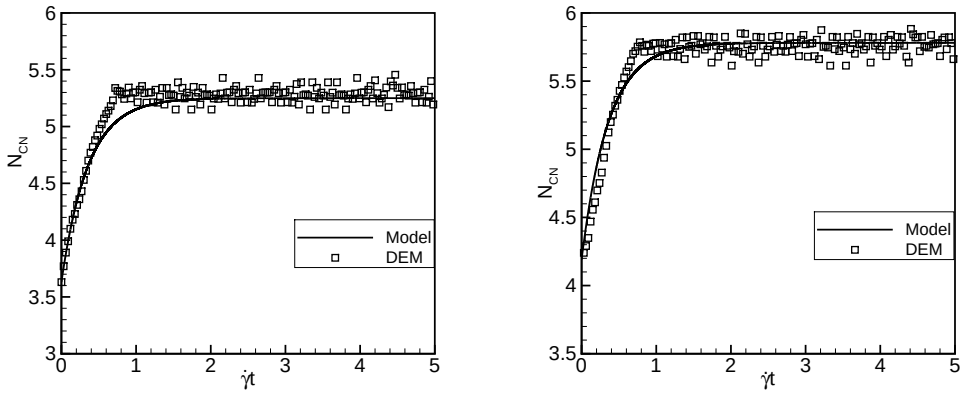

Figure 7.4 Evolution of the coordination number N_{CN} (a) For $\nu = 0.61$, $\mu = 0.1$, $k^* = k_n/\left(\rho_s d^3 \dot{\gamma}^2\right) = 1.0 \times 10^5$, $e = 0.7$ and (b) For $\nu = 0.62$, $\mu = 0.1$, $k^* = k_n/\left(\rho_s d^3 \dot{\gamma}^2\right) = 1.0 \times 10^5$, $e = 0.7$. The solid line is the solution of Eq. 7.42 whereas the symbols are the data obtained from DEM simulations.

of Eq. 7.42 and the symbols are the data obtained from DEM simulation. These figures show that the coordination number evolves with time and attains a steady value at time $\dot{\gamma}t \approx 2$. As seen in Figs. 7.4(a) and 7.4(b) the steady value of the coordination number obtained by solving Eq. 7.42 matches very closely with the DEM data. These results verify that the postulated form of the coordination number evolution equation (Eq. 7.42) captures the correct steady value of the coordination number observed in the DEM simulations for simple homogeneous shear flow.

7.4.2 Closure for fabric tensor

In order to complete the specification of the contact stress model, closure for the fabric tensor $\mathbf{R}$ is required. The fabric tensor $\mathbf{R}$ is a microstructure quantity which describes the anisotropy of the contact distribution in granular media (Bathurst and Rothenburg, 1990; Cowin, 2004; Radjai et al., 1998). Component of this tensor can be

calculated on the basis of particle contact information:

$$R_{ij} = \frac{1}{N_c} \sum_{c \in V} n_i n_j, \tag{7.43}$$

where R_{ij} is a symmetric second rank tensor, N_c is the number of contacts, n_i and n_j are the unit vectors corresponding to the contact vector from particle center to point of contact. The structural anisotropy can be easily related to the shear (xz component) of the fabric tensor $\mathbf{R}$ for simple shear flows (mean flow in x direction and shear gradient in z direction). Sun and Sundaresan (2011) postulated the following evolution equation for the fabric:

$$\acute{\mathbf{R}} = c_1 \mathbf{S} + c_2 |\mathbf{D}| \mathbf{R} + c_3 \left(\mathbf{R} : \mathbf{S} \right) \mathbf{R}. \tag{7.44}$$

In Eq. 7.44, $\acute{\mathbf{R}} = \dot{\mathbf{R}} + \mathbf{R} \cdot \mathbf{W} - \mathbf{W} \cdot \mathbf{R}$, where $\mathbf{W}$ is the spin tensor, $\mathbf{W} = \frac{1}{2} \left(\nabla \mathbf{u} - (\nabla \mathbf{u})^T \right)$, and $\dot{\mathbf{R}}$ denotes its material time derivative. In Eq. 7.44 $|\mathbf{D}| = \sqrt{\frac{1}{2} \left(D_{ij} D_{ji} \right)}$ denotes the modulus of the strain rate tensor. We solve Eq. 7.44 and compare the steady value of fabric (xz) component with that obtained from DEM data of homogeneously sheared granular flow.

Figure 7.5 shows the evolution of xz component of the fabric tensor for a simple homogeneous shear flow for a solid volume fraction of 0.61. The solid is the solution of Eq. 7.44 and the symbols are the data obtained from DEM simulations. This result reveals that the postulated form of the fabric evolution equation (Eq. 7.44) is capable of capturing the steady value of fabric within 10% when compared with the DEM data. However, the slight under–prediction of fabric in Fig. 7.5, is attributed to fact that the fabric evolution (Eq. 7.44) does not account for variation in the solid volume fraction and particle friction coefficient. Nevertheless, Vidyapati and Subramaniam (2012a) have shown that the fabric is not very sensitive to the change in the order parameter (and hence on the solid volume fraction and particle friction coefficient) when compared to other mesoscale parameters such as the coordination number for a simple homogeneous shear flow.

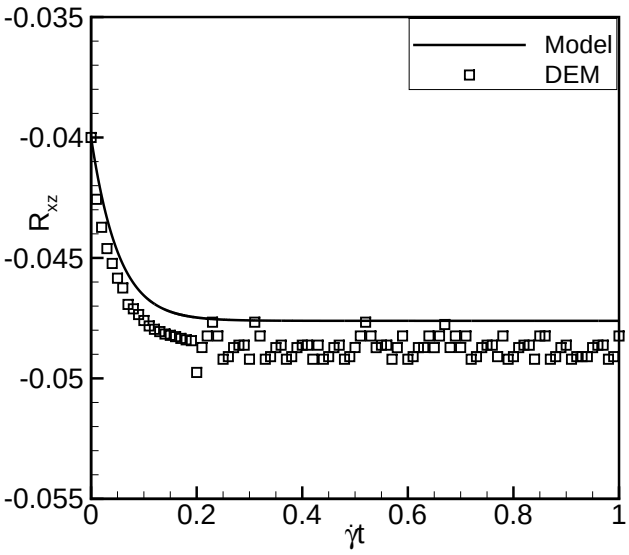

Figure 7.5 Evolution of xz component of fabric tensor $\mathbf{R}$ for $\nu = 0.61$, $\mu = 0.1$, $k^* = k_n/\left(\rho_s d^3 \dot{\gamma}^2\right) = 1.0 \times 10^5$ and $e = 0.7$ for simple homogeneous shear flow. The solid line is the solution of Eq. 7.44 and symbols are the data obtained from DEM simulations.

7.4.3 Distribution of normal contact force

In order to predict stress using proposed contact stress model (Eq. 7.35), the information of mean normal force $\langle f_n^{(i)(j)} \rangle$ between the contacting particles is required. This mean normal force can be computed using probability density function (PDF) of the normal force. The PDF of this random variable is constructed using normal force data obtained from our 3D DEM simulations of homogeneous shear flows. In Fig. 7.6 we show the resulting force distribution $P(f)$ (where $f = f_n/\overline{f_n}$ is the normalized force). Figure 7.6 shows that about 70% of the contacts carries higher magnitude of normal forces than the average normal force. This PDF shows the generic feature of the force distribution in granular packing, i.e., it exhibits a peak (plateau) for force less than mean ($f < 1$) and exponential decay for large forces ($f > 1$).

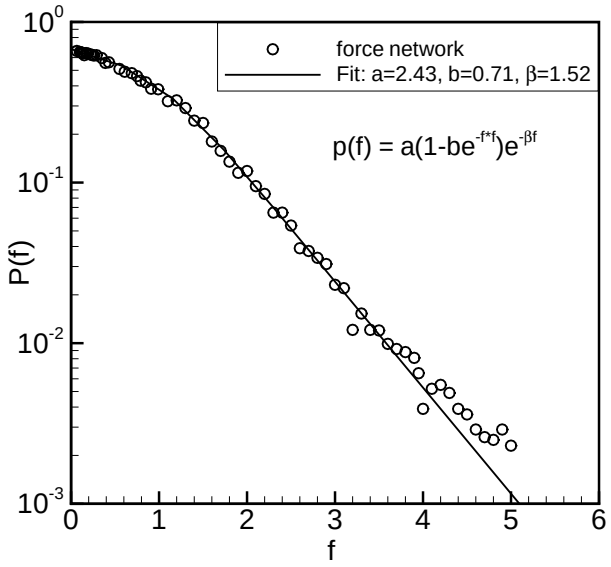

Figure 7.6 Probability density for normal contact forces fitted with Eq. 7.45.

Mueth et al. (1998) fitted their experimental data with an empirical function of the

form,

$$P(f) = a(1 - be^{-f^2})e^{-\beta f}, \tag{7.45}$$

and found $a = 3.0$, $b = 0.75$ and $\beta = 1.5$ for a static packing of glass spheres in a cylindrical container. To compare with this experimental data, we fit Eq. 7.45 to our computational data and find the function with $a = 2.43$, $b = 0.71$ and $\beta = 1.52$ aggress well with the force distribution in the force networks as shown in Fig. 7.6. We have extracted this force distribution profile for different values of solid volume fractions ν, particle friction coefficients μ and shear rates $\dot{\gamma}$, but none of these variations are found to significantly influence the shape of this force distribution and it remains robust. Mueth et al. (1998) also noticed that this force distribution is a robust property of these granular packings based on their experimental data.

After having all the required closures for the contact stress model, one can use Eq. 7.35 to predict stresses in the homogeneously sheared granular assembly. In the next section we perform assessment study of this proposed contact stress model by comparing its prediction for stresses against DEM data of homogeneous simple shear flow in different regimes.

7.5 Contact stress model assessment

In this section performance of proposed contact stress model (CSM) is assessed in different regimes (intermediate, quasi–static and inertial) of granular flow for a homogeneous shear problem. This task is achieved by comparing the magnitude of shear stress predicted using the proposed contact stress model (for range of solid volume fractions ν, particle friction coefficients μ and the shear rates $\dot{\gamma}$) against DEM data. As noted earlier, contact part of the stress contributes more than 95% to the total granular stress in the intermediate and quasi–static regime of granular flow (Vidyapati and Subramaniam, 2012a) . Hence predictive capability of the 'contact contribution' of stress is assessed in

the intermediate and quasi–static regimes. However, in the inertial regime the streaming contribution of the total granular stress could be significant (up to 15% for a solid volume fraction of 0.45 with a particle friction coefficient of 0.1), hence predictions for the total granular stress is required in this regime. Further, these test cases will determine if the proposed constitutive model is capable of predicting the correct power–law dependence of shear stress on the shear rate in the different regimes of granular flow.

7.5.1 Intermediate regime

Figure 7.7(a) shows a logarithmic plot of elastic scaling of the shear component of the contact stress as a function of the shear rate for a solid volume fraction of 0.58 with particle friction coefficient of 1.0. In this scaling, stress values in the intermediate regime where $\sigma \propto \dot{\gamma}^n$, with $0 < n < 2$. In this plot, stress variation for quasi–static flow will follow a horizontal line, and that in the inertial regime appears as a line with slope -1. However, lines with slope between 0 and -1 indicate the intermediate regime. In Fig. 7.7(a) the shear component of contact stress obtained from the contact stress model is shown by blank diamonds, whereas the filled squares are the data from DEM simulations of homogeneous simple shear flow. Figure 7.7(a) shows that the shear stress predicted using contact stress model closely follows the data obtained from the DEM simulations. The contact stress obtained from both, the proposed model and DEM follows the intermediate scaling ($\sigma \propto \dot{\gamma}^n$, where $0 < n < 2$) of the stress with the shear rate.

Figures 7.7(b) and 7.7(c) are the similar plots of contact contribution of shear stress with the shear rate, but for a solid volume fraction of 0.61 and 0.62, respectively, with a particle friction coefficient of 0.1. These specific simulation parameters are selected to ensure that they also correspond to the intermediate regime of flow. Both of these figures reveal that the proposed contact stress model is capable of capturing the correct scaling of stress with the strain rate ($\sigma \propto \dot{\gamma}^n$, where $0 < n < 2$). However, we notice

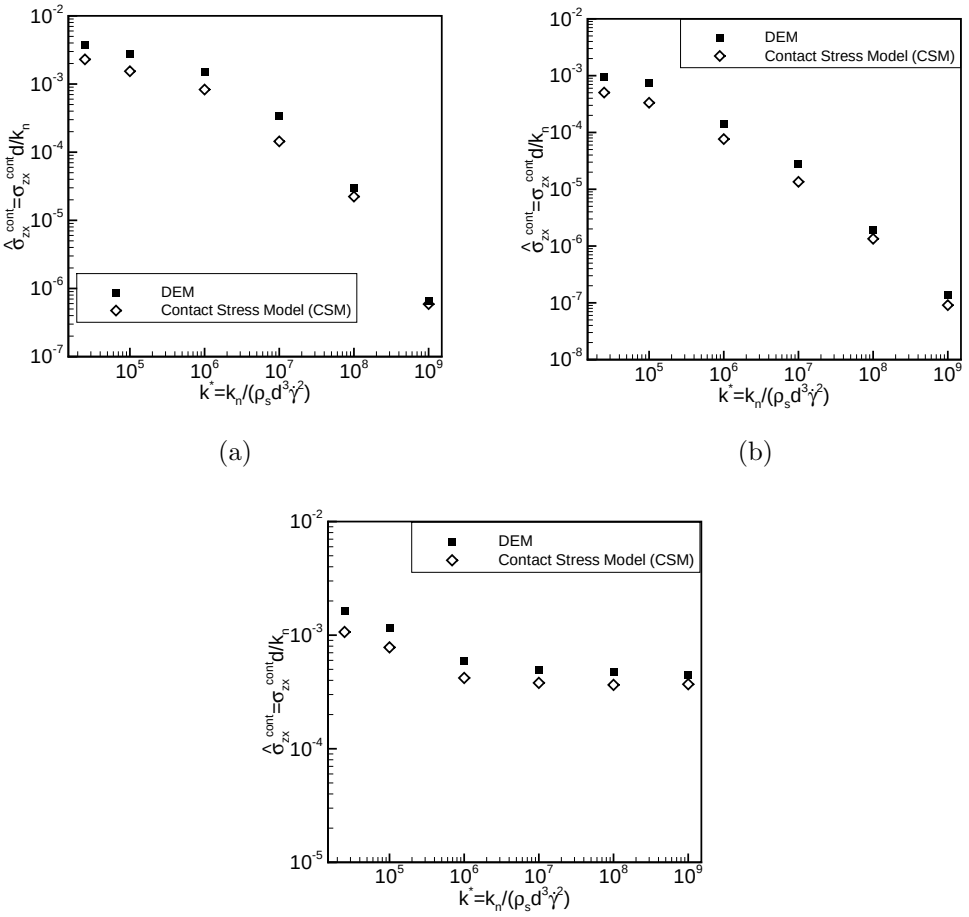

Figure 7.7 The shear component of contact stress as a function of shear rate $k^* = k_n/\left(\rho_s d^3 \dot{\gamma}^2\right)$ in the intermediate regime (a) For $\nu = 0.58$, $\mu = 1.0$, $e = 0.7$ (b) For $\nu = 0.61$, $\mu = 0.1$, $e = 0.7$ and (c) For $\nu = 0.62$, $\mu = 0.1$, $e = 0.7$.

a maximum quantitative difference of 25% in the higher shear rate regions (lower k^* values) when the model predictions are compare with the DEM data. Nevertheless, for higher values of solid volume fraction and k^* (lower shear rate), the model predictions seem to capture the correct quasi–static behavior (where stress remains independent of the shear rate) as seen in Fig. 7.7(c). From Figs. 7.7(a), 7.7(b) and 7.7(c), it is evident that the proposed contact stress model is capable of capturing the complex rheological behavior in the intermediate regime. The reason for the better performance of the proposed contact stress model is attributed to fact that unlike other models, this model incorporates mesoscale parameters (such as the coordination number and the fabric tensor) in constitutive modeling framework through relative acceleration concept which determines the structure dependent rheology.

7.5.2 Quasi–static regime

To assess the performance of the proposed contact stress model in the quasi–static regime, we selected two test cases with solid volume fraction of 0.60 and 0.62, with a interparticle friction coefficient of 1.0. As noted earlier in this regime too the contribution of streaming stress is negligible (less than 3%), hence we compare the contact stress predicted using proposed model against DEM data. In this regime, the stress remains independent of the shear rate ($\sigma \neq f(\dot{\gamma})$) as previously shown by Campbell (2002).

Figures 7.8(a) and 7.8(b) are the logarithmic plot of the elastic scaling of the shear component of contact stress as a function of the shear rate for a solid volume fraction of 0.60 and 0.62, respectively. The particle friction coefficient selected for both of these test cases is 1.0, which ensure that these test cases correspond to the quasi–static regime. The shear stress predictions obtained by contact stress model show a similar shear rate independent behavior (a behavior characteristic of quasi–static regime) as exhibit by the DEM data for both the solid volume fractions tested in this regime. Also there is a good quantitative agreement between shear stress predicted using contact stress model

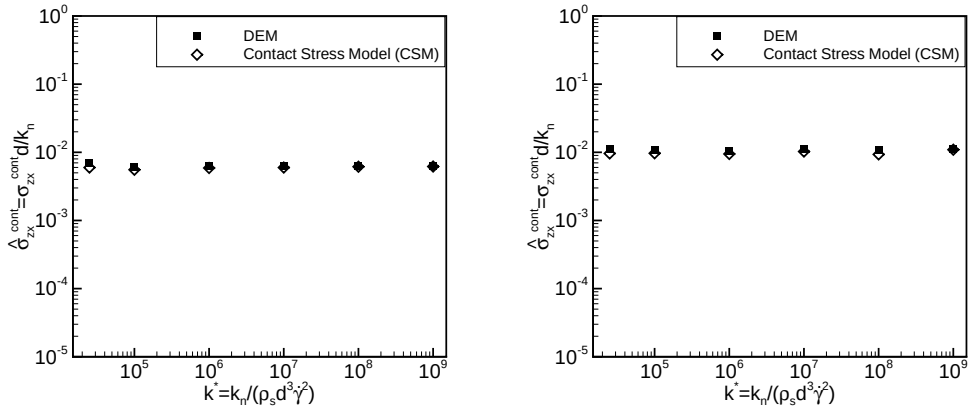

(a) (b)

Figure 7.8 The shear component of contact stress as a function of shear rate $k^* = k_n/\left(\rho_s d^3\dot{\gamma}^2\right)$ in the quasi–static regime (a) For $\nu = 0.60$, $\mu = 1.0$, $e = 0.7$ and (b) For $\nu = 0.62$, $\mu = 1.0$, $e = 0.7$.

and DEM data. These results verify that the proposed contact stress model can be used successfully to predict the granular rheology even in the quasi–static regime.

7.5.3 Inertial regime

The third granular regime is the inertial regime, where stress is dominated by binary or instantaneous collisions. In this regime, the streaming contribution of the total granular stress could be significant and cannot be neglected unlike other two regimes (intermediate and the quasi–static). For example streaming stress can contribute up to 15% for a solid volume fraction of 0.45. Hence accurate prediction of total granular stress is required in this inertial regime. However, the contact stress model proposed in this work can only predict the contact contribution of the stress. In order to predict the total granular stress in the inertial regime, we couple the contact stress model to the ROP (refined order parameter) model proposed in our earlier work (Vidyapati and Subramaniam, 2012a). Total granular stress can be obtained by solving ROP model as

follows (Vidyapati and Subramaniam, 2012a):

$$\sigma_{ij} = \frac{\sigma_0}{(1-\beta)}\left[\frac{\sigma_{ij}^{solid}}{\sigma_0} + \delta_{ij}(\beta+\alpha)\right], \tag{7.46}$$

where $\sigma_0 = \sigma_{ii}^s/3(1-\alpha)$ and α, β are the model coefficients which are functions of the order parameter (OP). Further, the OP can be obtained by solving Ginzburg–Landau equation as described in Vidyapati and Subramaniam (2012a). The other input required to obtain the total granular stress using ROP model is the solidlike stress σ_{ij}^{solid}, which can be obtained easily through the knowledge of contact stress contribution as follows (Volfson et al., 2003a):

$$\sigma_{ij}^{solid} = \rho\sigma_{ij}^{cont}, \tag{7.47}$$

where ρ is the order parameter obtained by solving Ginzburg–Landau equation. Once the order parameter ρ and the solidlike contribution of the stress σ_{ij}^{solid} is known, ROP model can predict the total granular stress for range of shear rates.

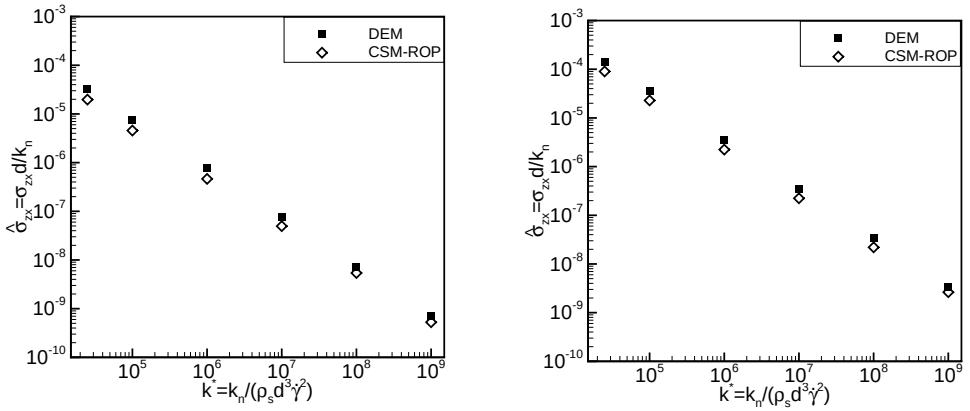

Figure 7.9 The shear component of the total granular stress as a function of shear rate $k^* = k_n/(\rho_s d^3\dot{\gamma}^2)$ in the inertial regime (a) For $\nu = 0.45$, $\mu = 0.5$, $e = 0.7$ and (b) For $\nu = 0.53$, $\mu = 0.5$, $e = 0.7$.

Figure 7.9(a) shows a logarithmic plot of the elastic scaling of the shear component of the total granular stress as a function of shear rate for a solid volume fraction of

0.45. In this scaling, stress values in the inertial regime where $\sigma \propto \dot{\gamma}^2$ corresponds to a line with slope -1. The shear component of the total granular stress obtained from the CSM–ROP model (where contact contribution of the stress is obtained using contact stress model proposed in this work) is shown by the black diamonds, whereas the filled squares show the date from DEM simulations. The total granular stress predicted using CSM–ROP model closely follows the DEM data. The total granular stress obtained from both the model and DEM follows the inertial scaling ($\sigma \propto \dot{\gamma}^2$) of the stress with the applied shear rate. Figure 7.9(b) is the similar plot which compares the total granular stress predicted by CSM–ROP model with data from DEM simulations. As observed in this figure the predictions obtained from CSM–ROP model follow both the scaling as well the magnitude of the DEM data.

7.6 Comparative assessment of different constitutive models in the intermediate regime

In order to show the competitive performance of the proposed contact stress model in the intermediate regime, we assess performance of other existing constitutive model in this regime along with the proposed contact stress model (CSM). In Fig. 7.10, the shear component of the stress is plotted with the shear rate for a solid volume fraction of 0.62 with interparticle friction coefficient of 0.1. The different constitutive models assessed are listed below:

1. Losert (2000): Losert et al. (2000) proposed a constitutive model with density–dependent viscosity. The shear stress in this model is given as,

$$\sigma_{xy} = \eta\dot{\gamma} \tag{7.48}$$

where viscosity is a function of the density as follows,

$$\eta = (\nu_{max} - \nu)^{-1.75}. \tag{7.49}$$

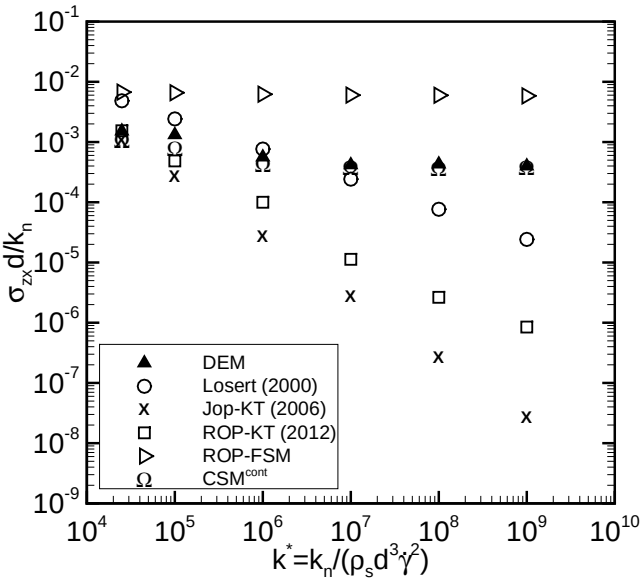

Figure 7.10 Shear component of the stress (different symbols represent result obtained with different constitutive models) plotted with shear rate $k^* = k_n/\left(\rho_s d^3 \dot{\gamma}^2\right)$. Simulation parameters: $\nu = 0.62$, $\mu = 0.1$, $e = 0.7$.

Figure 7.10 shows that the shear stress predicted using this model fails to capture the correct scaling of shear stress with shear rate in the intermediate regime. As noted earlier, the failure of this model is due the fact that this a viscosity based model. The viscosity is connected to the streaming contribution of the stress in the kinetic theory. However, this streaming part contributes less than 5% to the total granular stress in the intermediate and dense regime. Hence this model is not able to capture the correct scaling of stress with the strain–rate in this regime of granular flow. It should be noted that this model (Losert et al., 2000) was proposed based on the experimental data obtained from shear flow of granular material in a Couette geometry.

2. Jop (2006): Jop et al. (2006) described the granular material as an incompressible fluid with the stress tensor given by the following relations,

$$\sigma_{ij} = -P\delta_{ij} + \tau_{ij} \tag{7.50}$$

$$\tau_{ij} = \eta\left(|\dot{\gamma}|, P\right)\dot{\gamma}_{ij}, \tag{7.51}$$

where, P represents an isotropic pressure and η is an effective viscosity given by $\eta\left(|\dot{\gamma}|, P\right) = \mu\left(I\right)P/|\dot{\gamma}|$, where $\dot{\gamma}_{ij} = \partial u_i/\partial x_j + \partial u_j/\partial x_i$ is the strain rate tensor and $|\dot{\gamma}| = \left(0.5\dot{\gamma}_{ij}\dot{\gamma}_{ij}\right)^{0.5}$ is the second invariant of $\dot{\gamma}_{ij}$. The effective viscosity η is related to the friction coefficient $\mu\left(I\right)$ as follows:

$$\mu(I) = \mu_s + (\mu_2 - \mu_s)/(I_0/I + 1), \tag{7.52}$$

where $I = |\dot{\gamma}|d/\left(P\rho_s\right)^{0.5}$ is the inertia number.

However, the closure for the isotropic pressure P is not specified in this work because this model was intended for open surface flows (such as chute flow). If the closure for P is taken from kinetic theory (Lun et al., 1984), then the total granular stress is obtained using this model. As shown in Fig. 7.10 this model

coupled with the kinetic theory (Jop–KT (2006)) for the isotropic pressure fails to capture the correct trends of shear stress with shear rate in the intermediate regime. This model (Jop et al., 2006) was proposed for open chute flows whereas these constant volume DEM simulation of shear flows are more representative of silo and hopper flows where confining pressure at close packing plays an important role.

3. ROP–KT: This is the constitutive model proposed by Vidyapati and Subramaniam (2012a), where the ROP (refined order parameter) model is coupled with the kinetic theory of granular flows (KTGF) (Lun et al., 1984) for the fluidlike stress contribution of the total granular stress. As seen in Fig. 7.10 this model also fails to capture the correct trends of shear stress with shear rate in the intermediate regime. The reason for this failure is attributed to the fact that the ROP–KT model assumes that the fluidlike stress contribution follows the kinetic theory closure even in the intermediate regime of flow. However, it is found that this assumption does not hold in the intermediate regime where both collision and long–lasting frictional interaction between the particles are important.

4. ROP–FSM: A frictional stress model (FSM) is proposed by Srivastava and Sundaresan (2003) for the frictional part of the total granular stress. The FSM model is used to compute the solidlike stress contribution σ^s_{ij} and then the ROP model is solved to obtain the total granular stress as follows:

$$\sigma_{ij} = \frac{\sigma_0}{(1-\beta)}\left[\frac{\sigma^s_{ij}}{\sigma_0} + \delta_{ij}(\beta+\alpha)\right], \tag{7.53}$$

where $\sigma_0 = \sigma^s_{ii}/3(1-\alpha)$. One should note that Eq. 7.53 diverges as the order parameter goes to zero (its fluidlike limit), which reflects that the ROP–FSM model for the total stress does not contain any information about the fluidlike stress. This frictional stress model is based on the critical state theory of soil mechanics. At

the critical state the granular assembly deforms without any volume change and the frictional contribution of the stress is given by:

$$\frac{\boldsymbol{\sigma}^{fric}}{p_c(\nu)} = \mathbf{I} - \sqrt{2}\sin\phi\frac{\mathbf{S}}{\sqrt{\mathbf{S}:\mathbf{S}}}, \tag{7.54}$$

where the form for $p_c(\nu)$ (critical state pressure) is taken from Johnson and Jackson (1987)

$$p_c(\nu) = \begin{cases} F\frac{(\nu-\nu_{min})^r}{(\nu_{max}-\nu)^s} & \text{if } \nu > \nu_{min} \\ 0 & \text{if } \nu \leq \nu_{min} \end{cases} \tag{7.55}$$

where F, r and s are constants, taken from Srivastava and Sundaresan (2003). As shown in Fig. 7.10, this model (ROP–FSM) when coupled with the ROP model for the solidlike stress contribution predicts stresses that are independent of the shear rate (a behavior characteristic of the quasi–static regime). However, the data obtained from the DEM simulations show a dependency of shear stress on shear rate in this regime. The ROP–FSM results show that it is not simply a matter of modeling the fluidlike or solidlike parts of the total granular stress. Rather, what is lacking is a fundamental description of the dependence of stress on strain rate in the intermediate regime.

5. CSM (Contact Stress Model): This is constitutive model proposed in the present work, where stress is linked to the mesoscale flow descriptors such as the coordination number and the fabric tensor using relative acceleration concept, which is key to capturing the structure dependent rheology correctly. As seen in Fig. 7.10 this model is able to capture the correct scaling of the shear stress with the shear rate even in the intermediate regime of flow.

This study shows that only contact stress model proposed in the current work is able to predict the correct scaling of shear stress with strain rate in the intermediate regime of granular flow.

7.7 Discussions and conclusions

A constitutive model is developed to capture the complex rheological behavior of granular flows in the intermediate and dense regime. In the proposed modeling framework the statistical closure for the average contact stress is provided using relative acceleration concept between particle pairs, which is capable of capturing mesoscale descriptors such as the coordination number and the fabric tensor. In granular flows these mesoscale descriptors drive the microstructure, which is eventually responsible for the complex rheological behavior in different regimes. To complete the specification of the proposed contact stress model (CSM), we solve modeled evolution equation of the coordination number and fabric proposed by Sun and Sundaresan (2011). The steady state solution of these evolution equations are verified using DEM data of homogeneous simple shear flow. The closure for mean normal contact force is obtained by constructing probability distribution function (PDF) of the normal force data obtained from DEM simulations. In dense granular flows universal nature of the force PDF allows simplification, because the force distribution remains almost independent of particle (e.g., friction coefficient) and flow (e.g., shear rate) properties.

The predictive capability of the proposed contact stress model is verified by comparing its predictions for shear stress against DEM data for range of solid volume fractions and friction coefficients in the intermediate and quasi–static regime. It is shown that the contact stress model is capable of capturing the complex rheological behavior of granular flows in the intermediate and quasi–static regimes. It is also shown that this model can be successfully extended to inertial regime (where prediction of total granular stress is required) by coupling with the ROP model (Vidyapati and Subramaniam, 2012a) through the order parameter concept (Volfson et al., 2003b). The reason for this better prediction capability of the proposed contact stress model is attributed to the fact that, unlike other models this model include the mesoscale parameters (such as the

coordination number and the fabric tensor) of the problem in the constitutive modeling framework, which eventually drives the rheological behavior of granular flows.

CHAPTER 8. CONCLUSIONS AND FUTURE WORK

8.1 Conclusions

DEM (discrete element method) simulations and constitutive models have been used to understand the rheological behavior of dense granular flow and associated regime transition phenomenon from the quasi–static to inertial (rapid flow) regime. The principal findings of this research work is presented under different subcategories in the following.

8.1.1 Development of constitutive models

1. The refined order parameter (ROP) model proposed in chapter 5, enables a linear implementation of the objective form (coordinate system independent) of the OP model (Gao et al., 2005) through a simplification that allows inversion of the total granular stress from solidlike and fluidlike stress relations. The ROP model accurately predicts the total granular stress (to within 15%) up to a solid volume fraction of 0.57. However, beyond a solid volume fraction of 0.57 the flow transitions to the intermediate regime and the ROP model fails to capture the correct scaling of stress with the strain rate.

2. The contact stress model (CSM) proposed in chapter 7, relates the stress to the mesoscale descriptors such as the coordination number, the fabric tensor and the pair correlation function. The model predictions for shear stress reveal that the proposed contact stress model is capable of capturing the correct scaling of stress

with the shear rate ($\sigma \propto \dot{\gamma}^n, 0 < n < 2$) even in the intermediate regime. The reason for this better prediction capability of the proposed contact stress model is attributed to the fact that, unlike other models this model includes mesoscale parameters (such as the coordination number and the fabric tensor) that link microscale particle interactions to macroscopic constitutive behavior.

8.1.2 Granular flow physics from DEM simulations

1. DEM is a useful approach to characterize the granular rheology and phase transition through the order parameter (OP) dynamics. Existence of a third stable granular phase is discovered that is neither completely solid–like nor completely fluid–like as previously hypothesized by Aranson and Tsimring (2002). The proposed modified form of the free energy density function accurately accounts for this new third stable granular phase.

2. A comprehensive regime map is established using DEM data of homogeneously sheared granular assembly for wide range of solid volume fractions, particle friction coefficients and shear rates. This regime map will be helpful in quantifying the exact boundaries of different regimes of granular flow.

3. Decomposition of the DEM granular stress into contact and streaming parts reveals that the contact (virial) contribution to the stress dominates ($> 95\%$), and follows the same scaling ($\sigma \propto \dot{\gamma}^n, 0 < n < 2$) as the total granular stress in the intermediate regime. However, the streaming contribution always follows the inertial scaling ($\sigma \propto \dot{\gamma}^2$) even in the intermediate regime. The decomposition of the granular stress obtained from DEM into solidlike and fluidlike contributions (based on the OP) reveals that both these contributions follow the same scaling ($\sigma \propto \dot{\gamma}^n, 0 < n < 2$) as the total granular stress in the intermediate regime. This study indicates that

contact contribution of the granular stress plays a key role in capturing the correct rheological behavior in the intermediate regime.

8.1.3 Validated DEM with experiments

DEM simulations are the useful tool to qualitative predict the regime transition in granular flows. A transition from quasi–static ($\sigma \neq f(\dot{\gamma})$) to intermediate ($\sigma \propto \dot{\gamma}^n, 0 < n < 2$) behavior is identified when a secondary vertical flow is induced in the continuous mode operation of Couette shear cell. However, shear stress and shear–to–normal stress ratio were found to have quasi–static behavior ($\sigma \neq f(\dot{\gamma})$) in the batch mode operation of Couette shear cell. Nevertheless, there are quantitative differences in the magnitude of the stress predicted by DEM simulations and experiments.

8.1.4 Application of DEM to study practical flows

A three–dimensional (3D) flat–bottomed silo is studied using both discrete (DEM) and continuum methods. These simulations reveal that, all three different regimes of granular flow (inertial, intermediate and quasi–static) co–exist in this silo discharge problem. Further, the quantitative comparison study between DEM and different continuum models reveals that the traditionally used continuum models significantly over–predict the discharge rate from silo. It is also found that maximum error in the solid stress prediction is near the spatial locations where intermediate regime span.

8.2 Summary

In summary, DEM is a useful approach to understand the rheological behavior of dense granular flows, and to develop and assess constitutive models in different regimes. DEM's qualitative predictions and detailed information about the granular microstructure make it a valuable tool to develop constitutive models. Although the order pa-

rameter (OP) is capable of capturing the granular phase transition from solid–like to fluid–like behavior through its dependence on particle (particle friction coefficient) and flow (shear rate) properties, the assumption that the fluidlike stress can be modeled using kinetic theory of granular flows (KTGF) does not hold in the intermediate regime where both collisional and frictional (enduring) contacts between the particles are important. The discrete (DEM) and continuum simulations of the flat–bottomed silo reveal that intermediate regime poses a significant challenge for continuum models. The successful rheological prediction in this regime requires a constitutive model that can link microscale particle interactions to the macroscopic behavior. The contact stress model (CSM) proposed in this work is able to capture the correct scaling of stress with the strain rate even in the intermediate regime because, unlike other models, it does account for mesoscale descriptors such as the coordination number, the fabric tensor and the pair correlation function in a constitutive modeling framework.

8.3 Future work

This section summarizes the possible extension of this research work.

1. Quantification of third stable granular phase: In this research work (in chapter 5) the newly discovered third stable granular phase is quantified using structural quantities such as the fabric tensor, the coordination number and the pair correlation function. In order to further extend quantification of this third stable granular phase, an important quantity—the cluster size distribution, can be used. Following Lois et al. (2007) the length scale of the cluster can be used to characterize different flow regimes. Further, this length scale can be quantified using parameters such as radius of gyration of a cluster.

2. Extension of contact stress model to inhomogeneous flows: The proposed contact stress model can be extended to incorporate wall boundary effects in order to

solve inhomogeneous wall bounded shear problems. This requires specification of appropriate boundary conditions for the coordination number and the fabric tensor.

3. Quantification of stress fluctuations using CSM: One of the attractive features of the proposed contact stress model (CSM) is that we can quantify magnitude of the stress fluctuations. The expression for the average contact stress $\sigma_{\alpha\beta}^{cont}$ in CSM is as follows

$$\sigma_{\alpha\beta}^{cont} = \frac{1}{2V} N_{CN} \langle N(V) \rangle d \langle f_n^{(i)(j)} \rangle R_{\alpha\beta} \left(1 + \mu\right), \tag{8.1}$$

where V is sampling volume, N_{CN} is the coordination number, $\langle N(V) \rangle$ is the expected number of particles in volume V, d is the particle diameter, $\langle f_n^{(i)(j)} \rangle$ is the mean force between pair of contacting particles, $R_{\alpha\beta}$ is the fabric tensor and μ is the interparticle friction coefficient. The mean normal force $\langle f_n^{(i)(j)} \rangle$ can be related to PDF (probability density function) of normal force as follows

$$\langle f_n^{(i)(j)} \rangle = \int f P(f) df, \tag{8.2}$$

where PDF of normal force is given following function form (Mueth et al., 1998)

$$P(f) = a(1 - be^{-f^2})e^{-\beta f}, \tag{8.3}$$

with $a = 2.43$, $b = 0.71$ and $\beta = 1.52$. Using Eqs. 8.1 and 8.2, we can define the variance in contact stress as follows

$$var\left(\sigma_{\alpha\beta}^{cont}\right) = \frac{1}{2V} N_{CN} \langle N(V) \rangle d R_{\alpha\beta} \left(1 + \mu\right) \int f^2 P(f) df, \tag{8.4}$$

where

$$\int f^2 P(f) df = \left[\frac{-a}{\beta} e^{-\beta f} \left(f + \frac{1}{\beta} \right) + 1.2ab \left(\text{erf}(f + \frac{\beta}{2}) \right) + 0.5ab \left(e^{(-f^2 - \beta f)} \right) \right]. \tag{8.5}$$

This computed stress fluctuation using CSM can further be verified against DEM data.

In DEM (discrete element method) stress is computed in a given sampling volume or averaging in different bins. The average stress in DEM can be computed as follows

$$\{\sigma_{ij}\}_V = \frac{1}{N_{bin}} \sum_{k=1}^{N_{bin}} (\sigma_{ij})_k \tag{8.6}$$

where N_{bin} is the number of bins and $(\sigma_{ij})_k$ is the stress in the k^{th} bin. The stress fluctuations in DEM can be computed as follows

$$\{\sigma_{ij}\}' = (\sigma_{ij})_k - \{\sigma_{ij}\}_V. \tag{8.7}$$

Further one can compute the variance in the stress fluctuations from DEM as follows

$$var\,(\sigma_{ij}) = \frac{1}{N_{bin}} \sum_{k=1}^{N_{bin}} \{\sigma_{ij}\}'^2. \tag{8.8}$$

4. As a last but not the least note, validating the performance of proposed models with the experimental data is crucial step underlying all the developments.

APPENDIX A. VERIFICATION OF THE ORDER PARAMETER EXTRACTION

In order to verify our OP calculations with previously published results of Volfson et al. (2003b), we performed inhomogeneous wall–bounded shear simulations of granular particles. These inhomogeneous wall–bounded shear simulations are performed by shearing the granular material between two flat–frictional walls at $z = 0$ and $z = L$, whereas periodic boundary condition is imposed in the other two directions (x and y). The OP values extracted from these three–dimensional (3D) DEM simulations are verified by comparing them with similar calculations of Volfson et al. (2003b) for two–dimensional (2D) DEM. Following Volfson et al. (2003b), the OP values are averaged across the inhomogeneous direction to obtain a single value. For a meaningful comparison the 2D solid volume fraction reported in Volfson et al. (2003b) is converted to a corresponding 3D solid volume fraction by using the following relation (Wachem et al., 2001):

$$\nu_{3D} = \frac{2}{\sqrt{\pi\sqrt{3}}}\nu_{2D}^{3/2}. \tag{A.1}$$

Figure A.1 shows the variation of the OP with solid volume fraction for an inhomogeneous wall shear simulation. A maximum difference of about 15% is found in the OP at solid volume fraction of 0.60. Our results also verify the sudden increase in the OP as the solid volume fraction increases from 0.57 to 0.60 that is reported in Volfson et al. (2003b).

We also confirmed through DEM simulations of inhomogeneous wall–bounded shear flows that the OP is indeed capable of capturing the granular phase transition from solid-

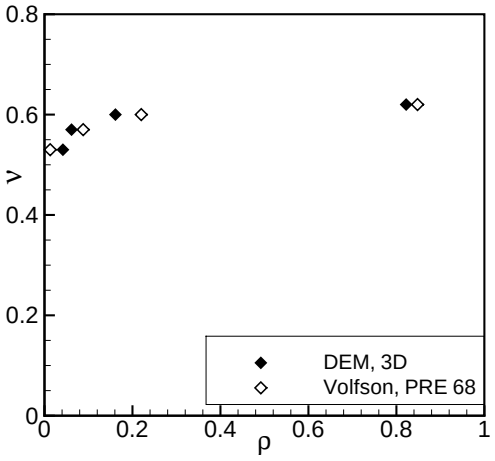

Figure A.1 The OP as a function of solid volume fraction for inhomogeneous wall shear simulation. The filled symbols represent the 3D DEM data, whereas blank symbols correspond to Volfson et al. (2003b). Simulation parameters: $\mu_p = \mu_w = 0.5$, $k^* = k_n/\rho_s d_0^3 \dot{\gamma}^2 = 10^5$ and $e = 0.7$.

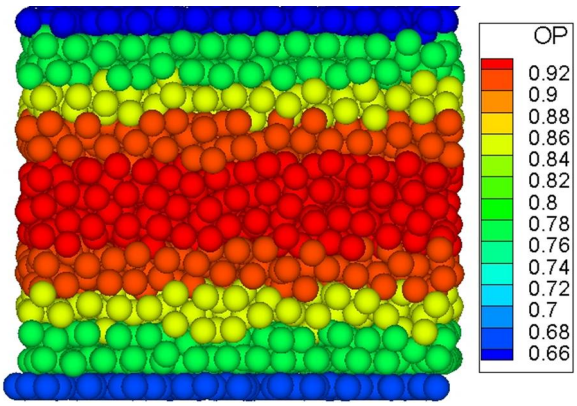

Figure A.2 Contour plot of the OP in an inhomogeneous wall–bounded shear flow, showing transition from fluidlike behavior (near the walls) to solidlike behavior (near centerline). Simulation parameters: $\nu = 0.62$, $\mu_p = \mu_w = 0.5$, $k^* = k_n/\rho_s d_0^3 \dot{\gamma}^2 = 10^5$ and $e = 0.7$.

like to fluidlike behavior. A contour plot of the OP for an inhomogeneous wall–bounded shear flow is shown in Fig. A.2. The OP is minimum near the wall and maximum near the centerline. This near–wall behavior is justified because the granular material will behave more like a liquid near the moving walls, than near the centerline.

BIBLIOGRAPHY

Aarons, L., and Sundaresan, S. (2006). Shear flow of assemblies of cohesive and non-cohesive granular materials. *Powder Technology*, 169:10–21.

Allen, M. P., and Tildesley, D. J. (1989). *Computer Simulation of Liquids*. Oxford: Oxford University Press.

Anand, A., Curtis, J. S., Wassgren, C. R., Hancock, B. C., and Ketterhagen, W. R. (2008). Predicting discharge dynamics from a rectangular hopper using the discrete element method (DEM). *Chemical Engineering Science*, 63:5821–5830.

Aranson, I. S., and Tsimring, L. S. (2002). Continuum theory of partially fluidized granular flows. *Physical Review E*, 65:061303.

Bagnold, R. A. (1954). Experiments on a gravity-free dispersion of large solid spheres in a Newtonian fluid under shear. *Proceedings of the Royal Society of London. Series A, Mathematical and Physical Sciences*, 225:49–63.

Bathurst, R. J., and Rothenburg, L. (1990). Observation on stress-force-fabric relationships in idealized granular material. *Mechanics of Materials*, 9:65–80.

Benyahia, S. (2008). Validation study of two continuum granular frictional flow theories. *Ind. Eng. Chem. Res.*, 47:8926–8932.

Beverloo, W. A., Leniger, H. A., and van de Velde, J. (1961). The flow of granular solids through orifices. *Chemical Engineering Science*, 15:243–250.

Brown, R. L., and Richards, J. C. (1960). Profile of flow of granules through apertures. *Transactions of the Institution of Chemical Engineering*, 38:260–269.

Campbell, C. S. (1990). Rapid granular flows. *Annu. Rev. Fluid Mech.*, 22:57–92.

Campbell, C. S. (2002). Granular shear flows at the elastic limit. *Journal of Fluid Mechanics*, 465:261–291.

Chialvo, S., Sun, J., and Sundaresan, S. (2011). Bridging the rheology of granular flows in three regimes. *http://meeting.aps.org/link/BAPS.2011.DFD.H25.10*

Corwin, E. I, Jaeger, H. M., and Nagel, R. S. (2005). Structural signature of jamming in granular media. *Nature*, 435:1075–1078.

Cowin, S. C. (2004). Anisotropic poroelasticity: fabric tensor formulation. *Mechanics of Materials*, 36:665–667.

Cundall, P., and Strack, O. (1979). A discrete numerical model for granular assemblies. *Geotech*, 29:47–65.

Daerr, A., and Douady, S. (1999). Two types of avalanche behavior in granular media. *Nature*, 399:241–243.

Donev, A., Torquato, S., and Stillinger, F. H. (2005). Pair correlation function characteristics of nearly jammed disordered and ordered hard–sphere packings. *Physical Review E*, 71:011105.

Engblom, N., Saxen, H., Zevenhoven, R., Nylander, H., and Enstad, G. G. (2011). Effect of material properties on segregation of binary and ternary powder mixtures in a small scale cylindrical silo. *Ind. Eng. Chem. Res.*, 50:11097–11108.

Evans, D. J. and Morriss, G. P. (1990). *Statistical mechanics of nonequillibrium liquids*. Academia Press.

Fenistein, D., and van Hecke, M. (2003). Kinematics: Wide shear zones in granular bulk flow. *Nature*, 425:256–256.

Forterre, Y., and Pouliquen, O. (2008). Flows of dense granular media. *Annu. Rev. Fluid Mech.*, 40:1–24.

Gao, D., Subramaniam, S., Fox, R. O., and Hoffman, D. K. (2005). Objective decomposition of the stress tensor in granular flows. *Physical Review E*, 71:021302.

G.D.R. MiDi (2004). On dense granular flows. *Eur. Phys. J. E.*, 14:341–365.

Goda, T. J., and Ebert, F. (2005). Three-dimensional discrete element simulations in hoppers and silos. *Powder Technology*, 158:58–68.

Goldhirsch, I. (2003). Rapid granular flows. *Annu. Rev. Fluid Mech.*, 35:267–293.

Hartley, R. R., and Behringer, R .P. (2003). Logarithmic rate dependence of force networks in sheared granular materials. *Nature*, 421:928–931.

Howell, D., Behringer, R. P., and Veje, C. (1999). Stress fluctuations in a 2D granular couette experiment: a continuous transition. *Physical Review Letters*, 82:5241-5244.

Jaeger, H. M., and Nagel, S. R. (1992). Physics of the granular state. *Science*, 225:1523–1531.

Jaeger, H. M., Nagel, S. R., and Behringer, R. P. (1996). Granular solids, liquids, and gases. *Rev. Mod. Phys.*, 68:1259–1273.

Jalali, P., and Hyppanen, T. (2010). Verification of continuum models for solids momentum transfer by means of discrete element method. *Ind. Eng. Chem. Res.*, 49:5270–5278.

Jasti, V., and Higgs, C. F. (2008). Experimental study of granular flows in a rough annular shear cell. *Physical Review E*, 78:041306.

Jenkins, J. T., and Savage, S. B. (1983). A theory for the rapid flow of identical, smooth, nearly elastic, spherical particles. *Journal of Fluid Mechanics*, 130:187-202.

Jenkins, J. T., and Richman, M. W. (1985). Kinetic theory for plane shear flows of a dense gas of identical, rough, inelastic, circular disks. *Phys. Fluids*, 28:3485–3494.

Ji, S., and Shen, H. (2008). Internal parameters and regime map for soft polydispersed granular material. *J. Rheol.*, 52:87–103.

Ji, S., Hanes, D. M., and Shen, H. H. (2009). Comparisons of physical experiment and discrete element simulations of sheared granular material in an annular shear cell. *Mechanics of Materials*, 41:764–776.

Johnson, P. C., and Jackson, R. (1987). Frictional Collisional Constitutive Relations for Granular Materials, with Application to Plane Shearing. *Journal of Fluid Mechanics*, 176:67–98.

Jop, P., Forterre, Y., and Pouliquen, O. (2006). A constitutive law for dense granular flows. *Nature*, 441(8):727-730.

Ketterhagen, W. R., Curtis, J. S., Wassgren, C. R., and Hancock, B. C. (2009). Predicting the flow mode from hoppers using the discrete element method. *Powder Technology*, 195:1–10.

Kheiripour Langroudi, M., Turek, S., Quazzi, A., and Tardos, G. I. (2010a). An investigation of frictional and collisional powder flows using a unified constitutive equation. *Powder Technology*, 197:91–101.

Kheiripour Langroudi, M., Sun, J., Sundaresan, S., and Tardos, G. I. (2010b). Transmission of normal stresses in un-sheared and sheared granular beds: the influence of particle size, shape, stiffness and cohesion. *Powder Technology*, 203:23–32.

Landau, L. D. and Lifshitz, E. M. (1980). *Statistical Physics*. Pergamon Press.

Landry, J. W., Gary, S. G., and Plimpton, S. J. (2004). Discrete element simulations of stress distribution in silos: crossover from two to three dimensions. *Powder Technology*, 139:223–239.

Lees, A. and Edwards, S. (1972). The computer study of transport process under extreme conditions. *J. Phys. C: Solid State Phyc.*, 5:1921–1929.

Lois, G., Lemaitre, A., and Carlson, M. J. (2005). Numerical test of constitutive laws for dense granular flows. *Physical Review E*, 72:051303.

Lois, G., Lemaitre, A., and Carlson, M. J. (2007). Spatial force correlations in granular shear flow. I. Numerical evidence. *Physical Review E*, 76:021302.

Losert, W., Bocquet, L., and Lubensky, T. C. and Gollub, J. P. (2000). Particle dynamics in sheared granular matter. *Physical Review Letters*, 85(7):1428-1431.

Luding, S., Hinirichsen, H., and Wolf, D. E. (2004). *The physics of granular media*. New York: Wiley-VCH Verlag.

Lun, C. K. K., Savage, S. B., Jeffrey, D. J., and Chepuriny, N. (1984). Kinetic theories for granular flow: inelastic particles in Couette flow and slightly inelastic particles in general flow fields. *Journal of Fluid Mechanics*, 140:223-256.

Majmudar, T. S., and Behringer, R. P. (2005). Contact force measurement and stres-induced anisotropy in granular materials. *Nature*, 453(23):1079-1082.

Majmudar, T. S., Sperl, M., Luding, S., and Behringer, R. P. (2007). Jamming Transition in Granular Systems. *Physical Review Letters*, 98(5):058001.

Markutsya, S. (2010). Modeling and simulation of nanoparticle aggregation in colloidal systems. *Phd Thesis, in Department of Mechanical Engineering. 2009, Iowa State University:Ames*.

Markutsya, S., Fox, R. O., and Subramaniam, S. (2012). Coarse–graining approach to infer mesoscale interaction potentials from atomistic interactions for aggragating systems. *In review with Ind. Eng. Chem. Res.*.

McCarthy, J. J., and Higgs, C. F. (2009). Granular flow in a rough annular shear, validating DEM simulations with experiments. *NETL 2009 Workshop on Multiphase Flow Science*.

McCarthy, J. J., Jasti, V., Marinack, M., and Higgs, C. F. (2010). Quantitative validation of the discrete element method using an annular shear cell. *Powder Technology*, 230:70–77.

Miller, B., Hern, C. O., and Behringer, R. P. (2003). Stress fluctuations for continuously sheared granular materials. *Physical Review Letters*, 77(15):3110–3113.

Mueth, D. M., Jaeger, H. M., and Nagel, S. R. (1998). Force distribution in a granular medium. *Physical Review E*, 57:3164–3169.

Mueth, D. M., Debregeas, F .G., Karczmar, G. S., Eng, P. J., Nagel, S. R., and Jeager, H .M. (2000). Signature of granular microstructure in dense granular flows. *Nature*, 406:385-389.

Nasuno, S., Kudrolli, A., Bak, A., and Gollub, J. P. (2000). Time-resolved studies of stick-slip friction in sheared granular layers. *Physical Review Letters*, 58(2):2161–2171.

Nedderman, R. M., Tuzun, U., Savage, S. B., and Houlsby, G. T. (1982). The flow of granular materials I: Discharge rate from hoppers. *Chemical Engineering Science*, 37:1597–1609.

Nedderman, R. M. (1992). *Static and kinematics of granular material*. Cambridge: Cambridge University Press.

Oda, M., Konishi, J., and Nemat–Nasser, S. (1980). Some experimentally based fundamental results on the mechanical behavior of granular materials. *Geotechnique*, 80:479–495.

Plimpton, S. J. (1995). Fast parallel algorithms for short-range molecular dynamics. *Journal of Computational Physics*, 117:1–19.

Radjai, F., Wolf, D., Jean, M. and Moreau, J. J. (1998). Bimodal character of stress transmission in granular packings. *Physical Review Letters*, 80(1):61–64.

Reynolds, O. (1885). On the dilatancy of media composed of rigid particles in contact. *Philos. Mag. Ser.*, 20:469–481.

Ristow, G. H. (1997). Outflow rate and wall stress for two–dimensional hoppers. *Physica A*, 235:319–326.

Rycroft, C. H., Grest, G. S., Landry, J .W., and Bazant, M. Z. (2006). Analysis of granular flow in a pebble-bed nuclear reactor. *Physical Review E*, 74:021306.

Savage, S. B. (1983). *Mechanics of granular materials: new models and constitutive relations*. Elsevier Ltd.

Savage, S. B., and Sayed, M. (1984). Stress developed by dry cohesionless granular materials sheared in an annular shear cell. *Journal of Fluid Mechanics*, 142:391–430.

Savage, S. B. (1998). Analyses of slow high-concentration flows of granular materials. *Journal of Fluid Mechanics*, 377:1–77.

Schaeffer, D. G. (1987). Instability in the Evolution Equations Describing Incompressible Granular Flow. *Journal of Differential Equations*, 66:19–50.

Schöllmann, S. (1999). Simulation of a two-dimensional shear cell. *Physical Review E*, 59:889-899.

Shundyak, K., van, H., and van, S. W. (2007). Force mobilization and generalized isostaticity in jammed packings of frictional grains. *Physical Review E*, 75:010301.

Silbert, L. E., Ertas, D., Grest, G. S., Halsey, T. C., Levine, D., and Plimpton, S. J. (2001). Granular flow down an inclined plane: Bagnold scaling and rheology. *Physical Review E*, 64:051302.

Silbert, L. E., Ertas, D., Grest, G. S., Halsey, T. C., and Levine, D. (2002). Geometry of frictionless and frictional sphere packing. *Physical Review E*, 65:031304.

Song, C., Wang, P., and Makse, H .A. (2008). A phase diagram for jammed matter. *Nature*, 453:629-632.

Srivastava, A., and Sundaresan, S. (2003). Analysis of a frictional-kinetic model for gas-particle flow. *Powder Technology*, 129:72–85.

Subhash, G., Nasser, S. N., Mehrabadi, M. M, and Shodj, H. M. (1991). Experimental investigation of fabric–stress relations in granular material. *Mechanica of Materials*, 11:87–106.

Subramaniam, S., and Vidyapati (2009). Rheological behavior of dense granular material: DEM simulations and Order Parameter model. *NETL 2009 Workshop on Multiphase Flow Science*.

Sun, J., Battaglia, F., and Subramaniam, S. (2006). Dynamics and structures of segregation in a dense, vibrating granular bed. *Physical Review E*, 74:061307.

Sun, J., and Sundaresan, S. (2010). A plasticity model with microstructure evolution for quasi-static granular flows. *Iutam-Isimm Symposium on Mathematical Modeling and Physical Instances of Granular flows*, 1227:280–289.

Sun, J., and Sundaresan, S. (2011). A constitutive model with microstructure evolution for flow of rate–independent granular materials. *Journal of Fluid Mechanics*, 682:590–616.

Sundaresan, S. (2001). Some outstanding questions in handling of cohesionless particles. *Powder Technology*, 115:2–7.

Syamlal, M., Rogers, W., and O'Brien, T. J. (1993). *MFIX Documentation: Theory Guide*. National Energy Technology Laboratory, Department of Energy.

Syamlal, M., Guenther, C., and Pannala, S. (2009). Advanced coal gasifier designs using large-scale simulations. *Journal of Physics: Conference Series*, 180:1–10.

Tardos, G. I., McNamara, S., and Talu, I. (2003). Slow and intermediate flow of a frictional bulk powder in the Couette geometry. *Powder Technology*, 131:23–39.

Tsai, J. C., and Gollub, J .P. (2004). Slowly sheared dense granular flows: crystallization and nonunique states. *Physical Review E*, 70:031303.

Vidyapati, V., Langroudi, M. K., Sun, J., Sundaresan, S., Tardos, G. I., and Subramaniam, S. (2012). Experimental and computational studies of dense granular flow: Transition from quasi-static to intermediate regime in a Couette shear device. *Powder Technology*, 220:7-14.

Vidyapati, V., and Subramaniam, S. (2012a). Granular rheology and phase transition: DEM simulations and order parameter based constitutive model. *Chemical Engineering Science*, 72: 20–34.

Vidyapati, V. and Subramaniam, S. (2012b). Granular flow in silo discharge: DEM simulations and model assessment. *Manuscript in preparation.*

Volfson, D., Tsimring, L. S., and Aranson, I. S. (2003a). Partially fluidized shear granular flows: Continuum theory and molecular dynamics simulations. *Physical Review E*, 68:021302.

Volfson, D., Tsimring, L. S., and Aranson, I. S. (2003b). Order Parameter Description of Stationary Partially Fluidized Shear Granular Flows. *Physical Review Letters*, 90(25):254301.

van Wachem, B. G. M., Schaaf, J., Schouten, J. C., Krishna, R., and Bleek, C. M. (2001). Experimental validation of Langrangian-Eluerian simulations of fluidized beds. *Powder Technology*, 116:115–165.

Zhang, H. P., and Makse, H. A. (2005). Jamming transition in emulsions and granular materials. *Physical Review E*, 72:011301.